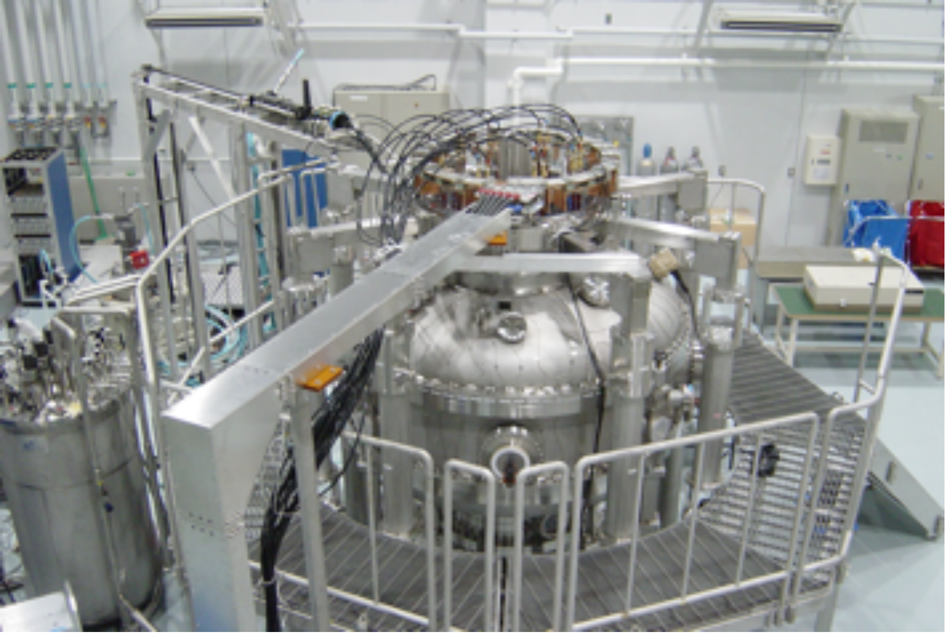

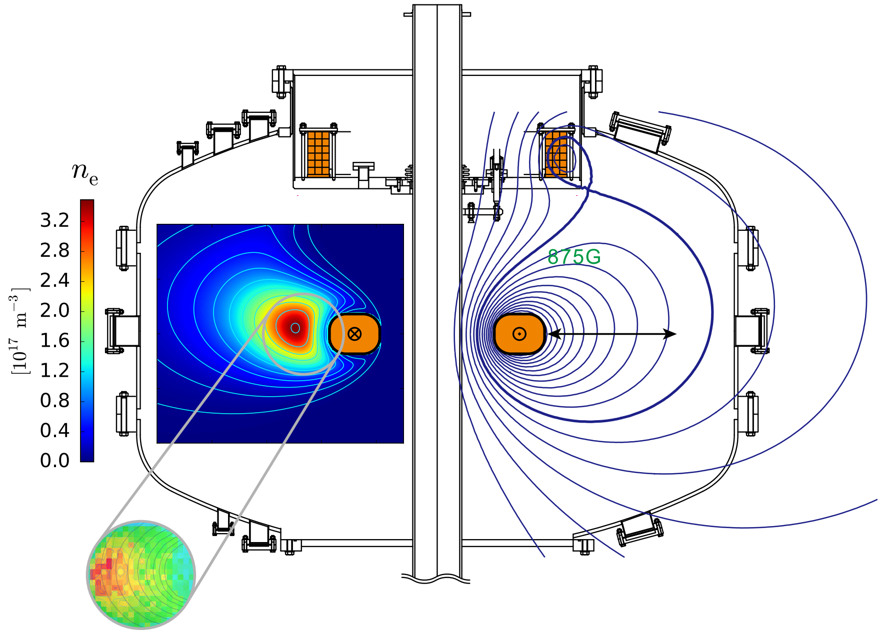

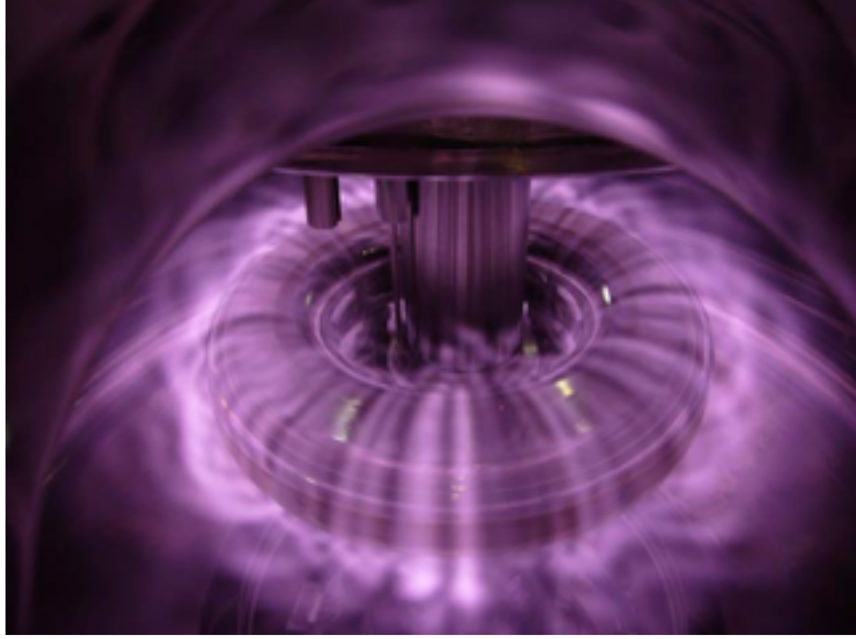

Particle acceleration in laboratory magnetosphere

RT-1 group

Y. Kawazura, Z. Yoshida, M. Nishiura, H. Saitoh, N. Sato, T. Nogami, N. Takahashi, Y. Yano, M. Yamasaki, A. Kashyap, T. Mushiake, and M. Nakatsuka

Graduate School of Frontier Sciences, The University of Tokyo

East-Asia School and Workshop on Laboratory, Space, and Astrophysical Plasmas,
Tsukuba, Japan, 14 July 2016

THE UNIVERSITY OF TOKYO

GRADUATE SCHOOL OF FRONTIER SCIENCES
THE UNIVERSITY OF TOKYO

Magnetosphere : the most natural magnetic confinement device

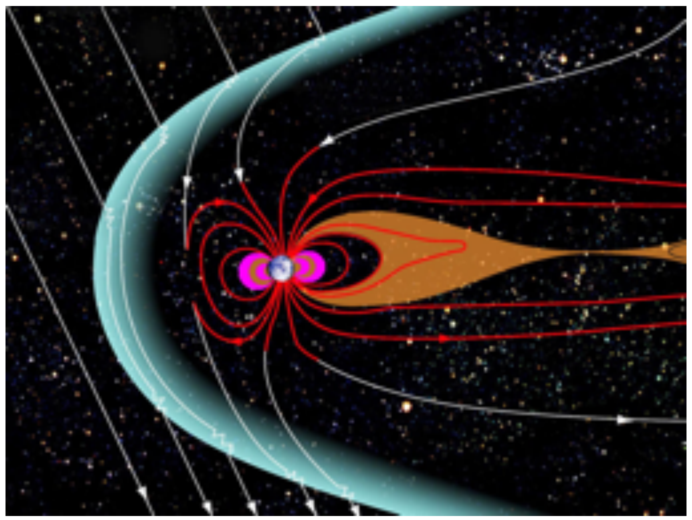

Earth's magnetosphere

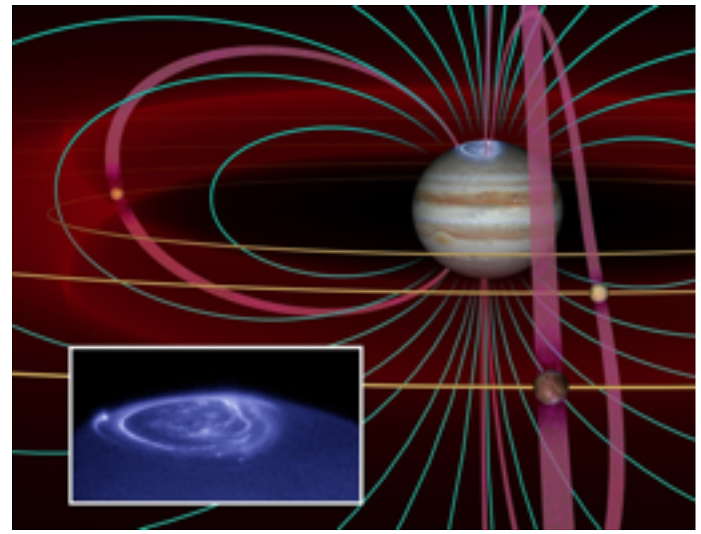

Jovian magnetosphere

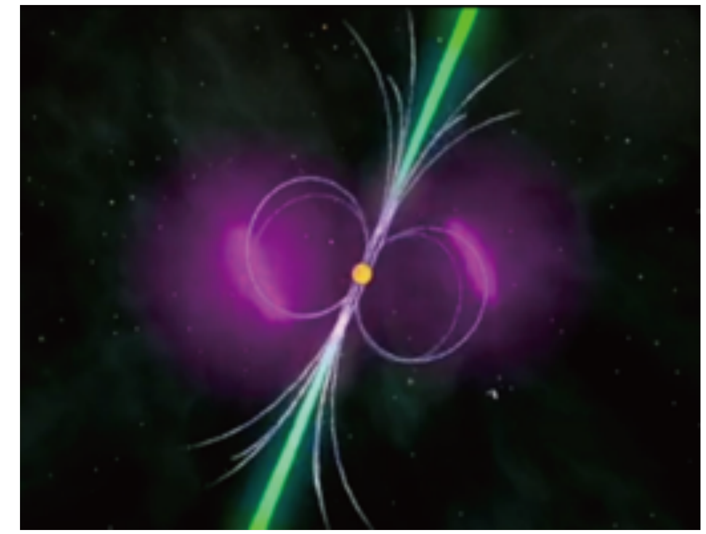

pulser magnetosphere

- ✓ Dipole field is the simplest magnetic field configuration
- ✓ Magnetospheres are commonly seen objects in the universe
- ✓ Totally different confinement method from the sun
- ✓ Magnetic field does not work on charged particle ⇔ Gravitational force does work

How come particles are attracted to a dipole field?

- ✓ Radiation belt = clump of highly energized plasma

How are energized particles supplied to a radiation belt?

[1] http://www.nasa.gov

Outline

- ✓ Self-organization of plasma in a magnetosphere: inward diffusion
  - Empirical diffusion model
  - Modern theory for self-organization in a magnetosphere: Casmir leaves
  - Boltzmann distribution on a Casmir leaf
  - Rigorously formulated diffusion equation
  - Introduction to a Laboratory magnetosphere: overview of RT-1 experiment
  - Experimental observation of inward diffusion
- ✓ Particle acceleration in a magnetosphere
  - Adiabatic acceleration: betatron and Fermi accerelations
  - Experimental observation of particle acceleration
  - Numerical simulation of the diffusion equation showing adiabatic accelerations
- ✓ Summary

Theoretical studies on self-organization of magnetospheric plasma

Self-organized magnetospheric plasma

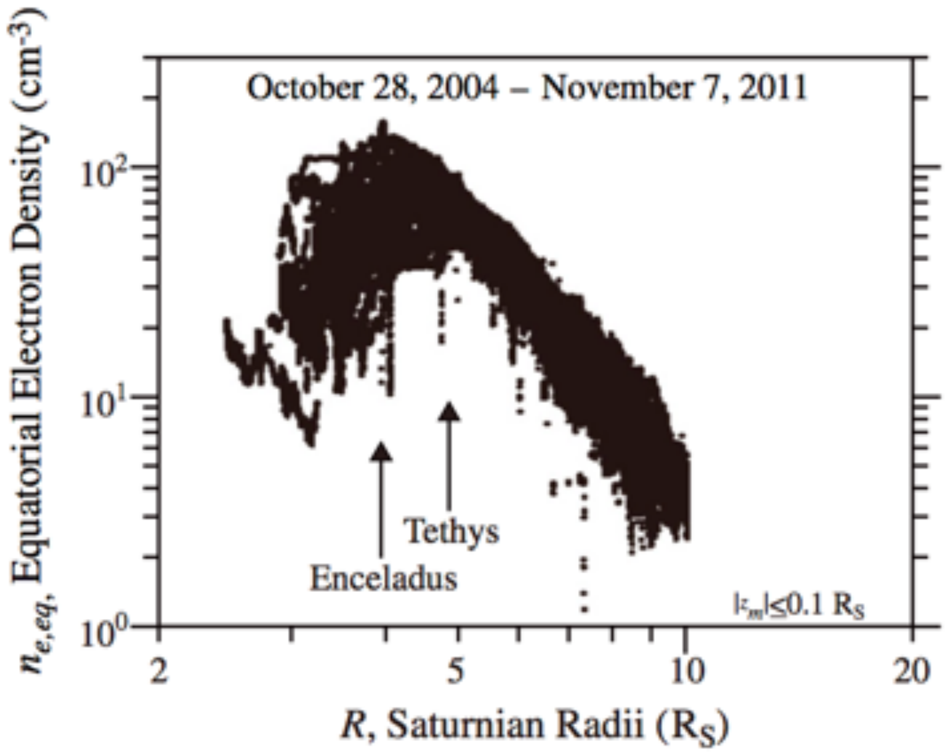

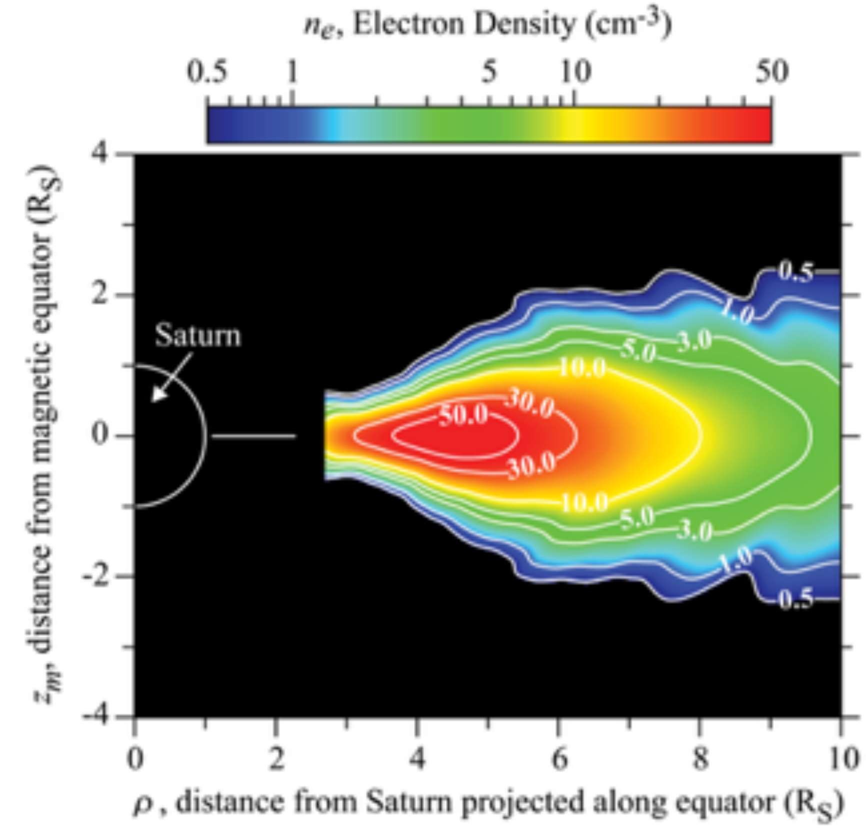

Space craft (Cassini) exploration [1]

- ✓ Plasma in a magnetosphere has planet-ward density gradient
- ✓ Plasma is spontaneously attracted to a planet
  - ➡ Inward diffusion (or radial diffusion, or up-hill diffusion) [2]
- ✓ Seemingly contradicting to the maximum entropy principle
  - Diffusion should diminishes a “gradient”

[1] A. M. Persoon et al. J. Geophys. Res.: Space Phys. **118** 2970-2974 (2013)
[2] M. Schulz and L. J. Lanzerotti, Particle Diffusion in the Radiation Belts, (Springer, 1974).

Scale hierarchy of a charged particle

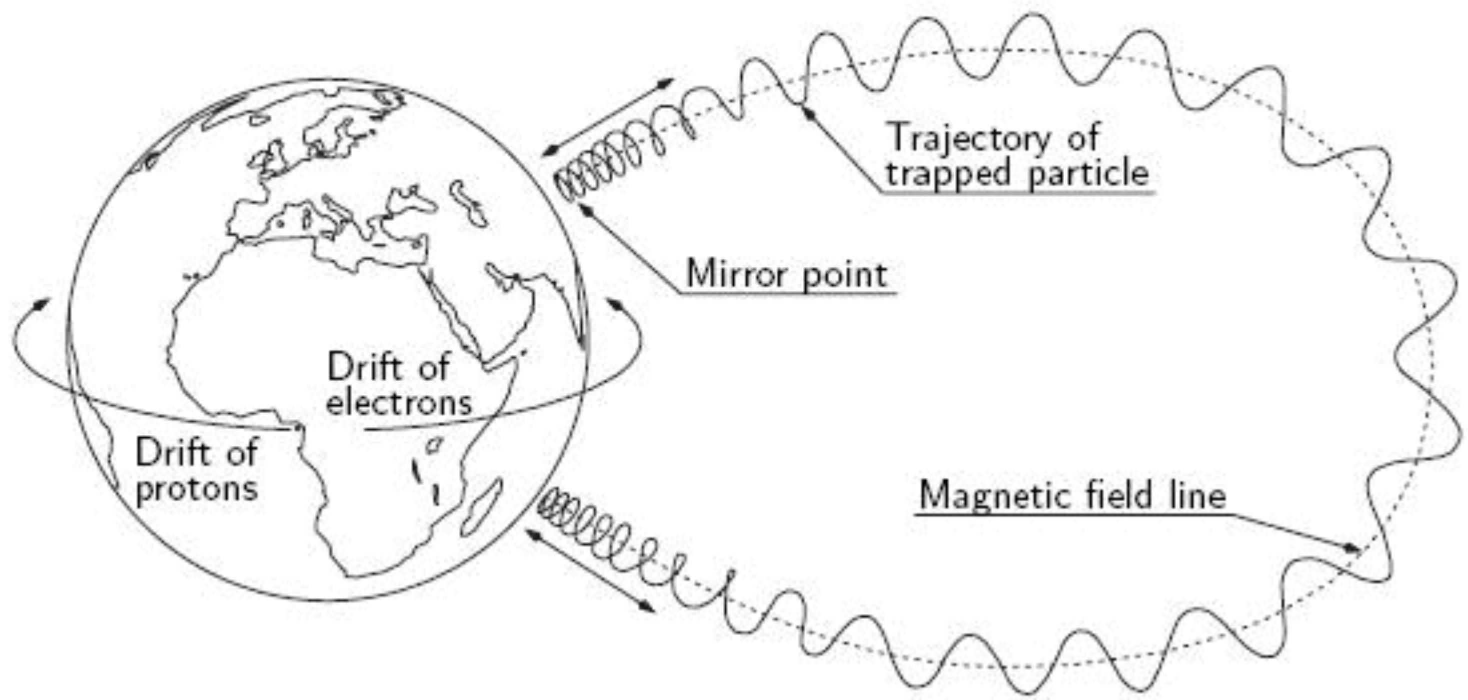

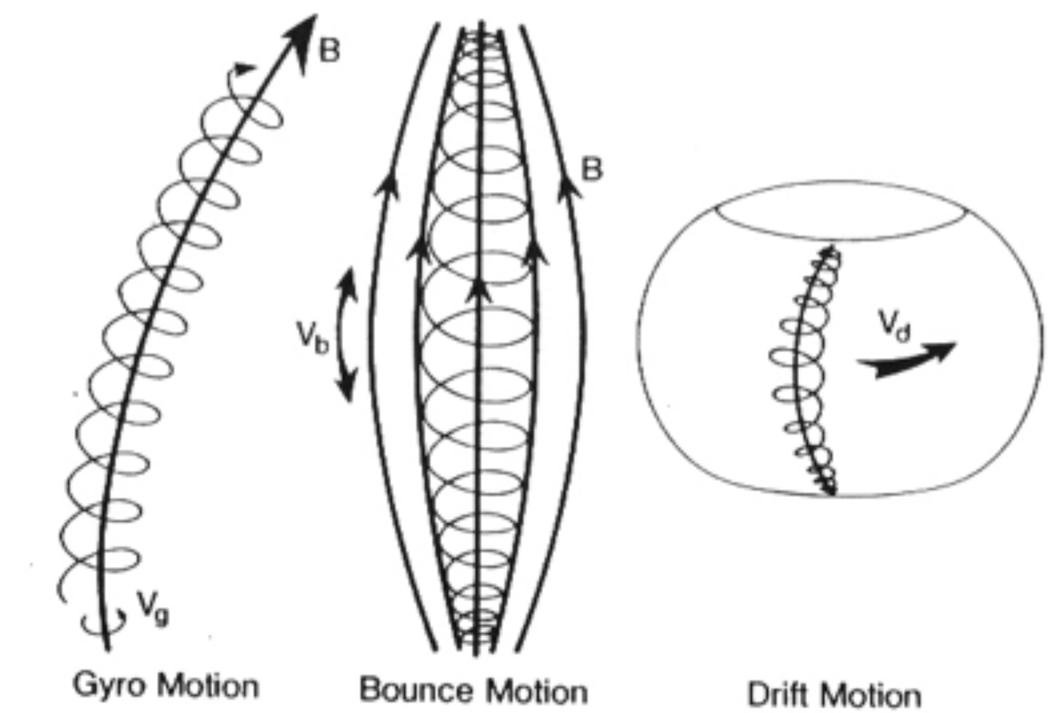

- ✓ Particle motion in a magnetosphere is divided into three periodic motions
- ✓ Three corresponding adiabatic invariants (AIs)

First invariant $\mu = \dfrac{mv_\perp^2}{2B}$: cyclotron motion

Second invariant $J = \oint p_\parallel \, \mathrm{d}l$: bounce motion

Third invariant $\Phi = \oint \boldsymbol{B} \cdot \mathrm{d}S$: drift motion

$\omega_\mathrm{c} \gg \omega_\mathrm{b} \gg \omega_\mathrm{d}$
scales hierarchy

- ✓ Particle motion is integrable if all AIs are conserved, and there is no cross field transport

[1] M. Walt, Introduction to Geomagnetically Trapped Radiation, (Cambridge Univ. Press, 1994.).

Empirical equation of inward diffusion

- ✓ AI conservation is violated when fluctuation time scale < periodic motion time scale
- ✓ The third AI (Φ) is the most fragile, and inward diffusion is triggered by violation of Φ maintaining the other AIs.
- ✓ Let the distribution function as a function of three AIs $f = (\mu,\ J,\ \Phi)$
- ✓ Evolution of f is modeled by $\dfrac{\partial f}{\partial t} = \sum_{i,j} \dfrac{\partial}{\partial J_i}\left(D_{J_i J_j}\dfrac{\partial f}{\partial J_i}\right)$, $(J_1,\ J_2,\ J_3) = (\mu,\ J,\ \Phi)$ [1]
- ✓ When the first and second AIs are conserved, this is 1D equation with respect to Φ
- ✓ For point dipole configuration $\Phi \sim L^{-1}$ (L : L-shell)

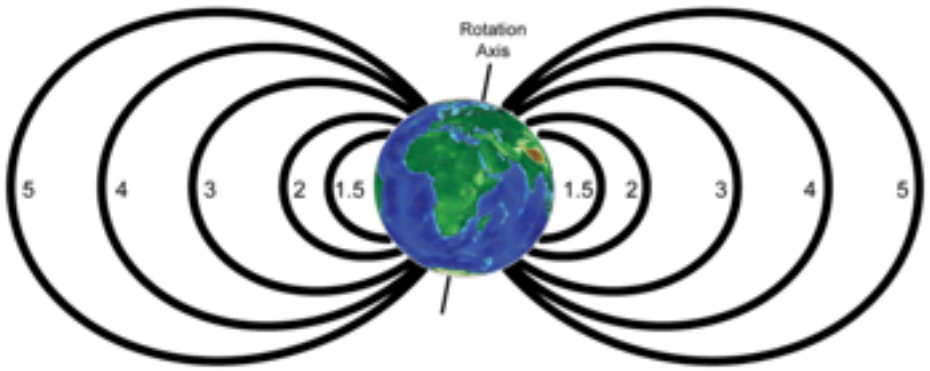

$$\frac{\partial f}{\partial t} = L^2 \frac{\partial}{\partial L}\left(\frac{D_{LL}}{L^2}\frac{\partial f}{\partial L}\right) - \frac{1}{\tau}$$

loss term:
pitch angle scattering,
charge exchange…

- ✓ Diffusion coefficient is $D_{LL} = \left\langle (\Delta L)^2 \right\rangle / 2$ [2]
- ✓ Particle numbers within flux tubes will be equalized

= non-uniform density in the Cartesian coordinates

[1] M. Schulz and L. J. Lanzerotti, Particle Diffusion in the Radiation Belts, (Springer, 1974).
[2] M. Walt, Introduction to Geomagnetically Trapped Radiation, (Cambridge Univ. Press, 1994).
[3] A. Hasegawa, Phys. Scr. **T116** 72 (2005)

Empirical equation of inward diffusion

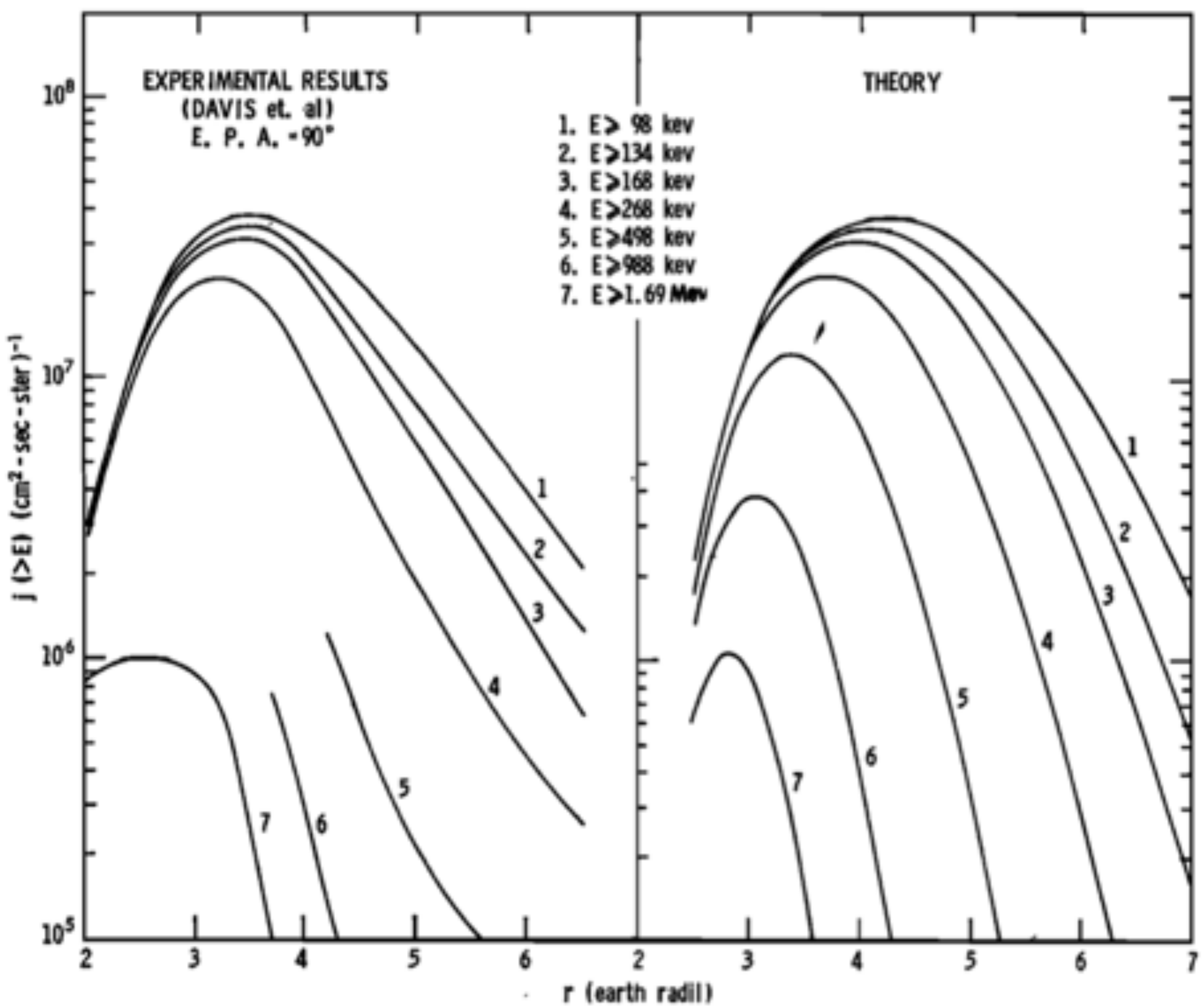

Fig. 8. Comparison of integral fluxes as measured by *Davis et al.* [1964] and calculated integral fluxes. The calculated curves are normalized to the same peak flux for the lowest energy threshold. More recent information (Davis, private communication) indicates that all the experimental fluxes should be increased uniformly by approximately 25%. There is also evidence that the energy 7 curve ($E \geq 1.69$ Mev) is too low in the 2–3 earth radii region, owing to saturation of the detector. The incomplete curves for energies 5 and 6 are due to detector saturation.

Diffusion coefficient

$$\left\langle \frac{(\Delta r)^2}{\Delta t} \right\rangle = 0.031 r_{b0}^2 \left(\frac{r}{r_{b0}}\right)^{10} \qquad \frac{(\text{earth radii})^2}{\text{day}}$$

Comparison of a flux by the observation and the theoretical prediction

✓ Good agreement with observational results [1]

[1] M. P. Nakada, and G. D. Mead, J. Geophys. Res. **70** 4777 (1965).

Empirical equation of inward diffusion

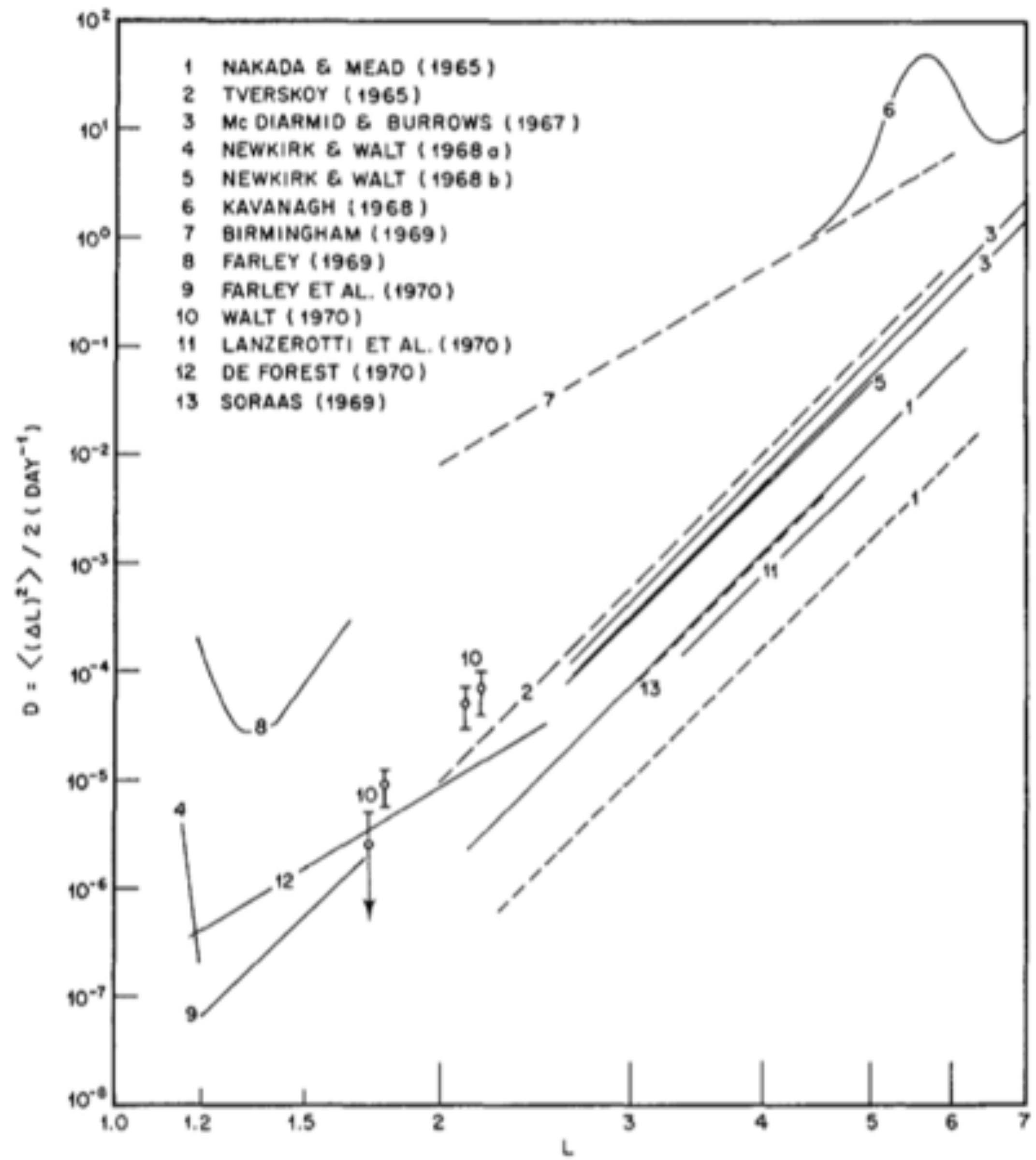

Fig. 18. Experimental (solid lines) and theoretical (dashed lines) values of the radial diffusion coefficient.

Diffusion coefficient: theoretical and observational value

- ✓ Good agreement with observational results [1]
- ✓ Diffusion coefficient has been improved to reproduce observations more precisely

[1] M. P. Nakada, and G. D. Mead, J. Geophys. Res. **70** 4777 (1965).
[2] M. Walt, Introduction to Geomagnetically Trapped Radiation, (Cambridge Univ. Press, 1994.)

Modern theory of self-organization in a magnetosphere

- ✓ Adiabatic invariant is regarded as **a topological constraint in a phase space** [1]

  What is the topological constraint?

- ✓ Let us go back to Hamiltonian mechanics of a particle

$$\frac{\mathrm{d}z}{\mathrm{d}t} = \mathcal{J}_{\mathrm{c}} \frac{\partial H}{\partial z} , \quad \mathcal{J}_{\mathrm{c}} = \begin{pmatrix} J_{\mathrm{c}} & 0 & 0 \\ 0 & J_{\mathrm{c}} & 0 \\ 0 & 0 & J_{\mathrm{c}} \end{pmatrix}, \quad J_{\mathrm{c}} = \begin{pmatrix} 0 & I \\ -I & 0 \end{pmatrix}$$

- ✓ Boltzmann distribution of particles governed by this equation of motion is

$$f = Z^{-1} \mathrm{e}^{-\beta H}$$

- ✓ H does not include $\boldsymbol{B}$. But f is dramatically changed under the presence of $\boldsymbol{B}$
- ✓ Instead of changing H (energy), we change $\mathcal{J}_{\mathrm{c}}$ (geometry)
- ✓ Microscopic variables are separated by coarse-graining

$$\mathcal{J}_{\mathrm{c}} \quad \rightarrow \quad \mathcal{J}_{\mathrm{nc}} = \begin{pmatrix} 0 & 0 & 0 \\ 0 & J_{\mathrm{c}} & 0 \\ 0 & 0 & J_{\mathrm{c}} \end{pmatrix} \qquad z = (\mu, \vartheta_{\mathrm{c}}; J_{\|}, \vartheta_{\mathrm{b}}; \psi, \theta)$$

[1] Z. Yoshida and S.M. Mahajan, Prog. Theor. Exp. Phys. **2014**, 073J01 (2014);
Z. Yoshida et al., Plasma Phys. Control. Fusion **55** 014018 (2013)

Casimir leaves

- ✓ $\mathcal{J}_{\rm nc}$ has a kernel → Casmir invariant $\mathcal{J}_{\rm nc}\dfrac{\partial C}{\partial z} = 0$
- ✓ 1st adiabatic invariant gives $C = g(\mu)$
- ✓ Particle is constrained on $C = \text{constant}$ surface; Casimir invariant foliates a phase space
- ✓ Further foliation by $J_{||}$ $\begin{pmatrix} 0 & 0 & 0 \\ 0 & J_{\rm c} & 0 \\ 0 & 0 & J_{\rm c} \end{pmatrix} \rightarrow \begin{pmatrix} 0 & 0 & 0 \\ 0 & 0 & 0 \\ 0 & 0 & J_{\rm c} \end{pmatrix}$

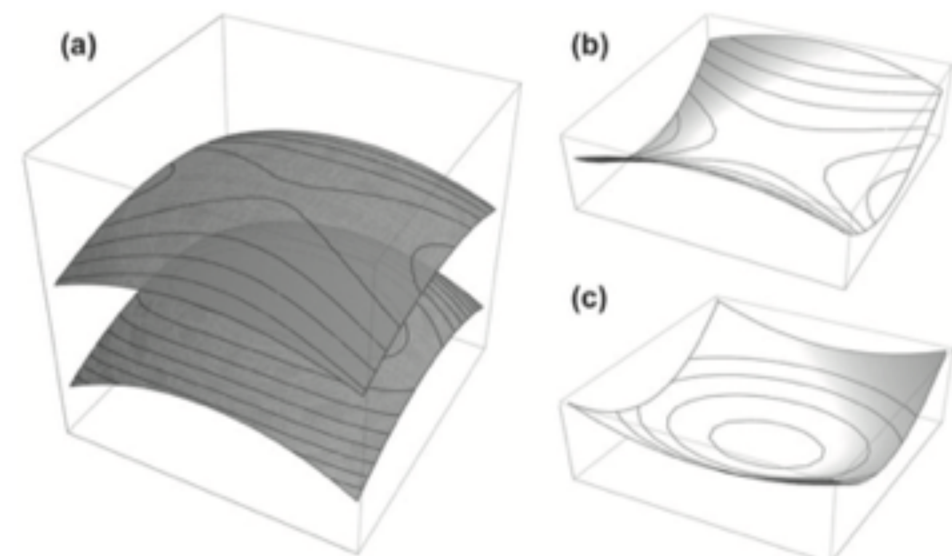

- ✓ We then consider a grand canonical distribution on the foliated phase space
  - μ-foliation $\delta(S - \alpha N - \beta E - \gamma M_1) = 0$

$$\downarrow$$

$$f_\gamma = Z^{-1} \mathrm{e}^{-(\beta H_{\rm gc} + \gamma\mu)}$$

$$E = \int H_{\rm gc} f \mathrm{d}^6 z, \quad H_{\rm gc} = \omega_{\rm c}\mu + \omega_{\rm b} J_{||} + q\phi$$

Guiding center Hamiltonian

  - μ & J||-foliation $\delta(S - \alpha N - \beta E - \gamma_1 M_1 - \gamma_2 M_2) = 0$

$$\downarrow$$

$$f_{\gamma_1,\gamma_1} = Z^{-1} \mathrm{e}^{-(\beta H_{\rm gc} + \gamma_1\mu + \gamma_2 J_{||})}$$

$$S = -\int f \ln f \mathrm{d}^6 z, \quad N = \int f \mathrm{d}^6 z$$

$$M_1 = \int \mu f \mathrm{d}^6 z, \quad M_2 = \int J_{||} f \mathrm{d}^6 z$$

[1] Z. Yoshida and S.M. Mahajan, Prog. Theor. Exp. Phys. **2014**, 073J01 (2014);
Z. Yoshida et al., Plasma Phys. Control. Fusion **55** 014018 (2013); Z. Yoshida, Adv. Phys. X **1** 2 (2016)

Boltzmann distribution on a Casimir leaf

- μ-foliation

$$f_\gamma = Z^{-1}\mathrm{e}^{-(\beta H_{\mathrm{gc}}+\gamma\mu)}$$

$$\longrightarrow \quad \rho = \int f_\gamma \frac{2\pi\omega_{\mathrm{c}}}{m}\mathrm{d}\mu\mathrm{d}v_{\|}$$

- μ & $J_{\|}$-foliation

$$f_{\gamma_1,\gamma_1} = Z^{-1}\mathrm{e}^{-(\beta H_{\mathrm{gc}}+\gamma_1\mu+\gamma_2 J_{\|})}$$

$$\longrightarrow \quad \rho = \int f_{\gamma_1,\gamma_2} \frac{2\pi\omega_{\mathrm{c}}\mathrm{d}\mu}{m}\frac{\mathrm{d}J_{\|}}{mL_{\|}}$$

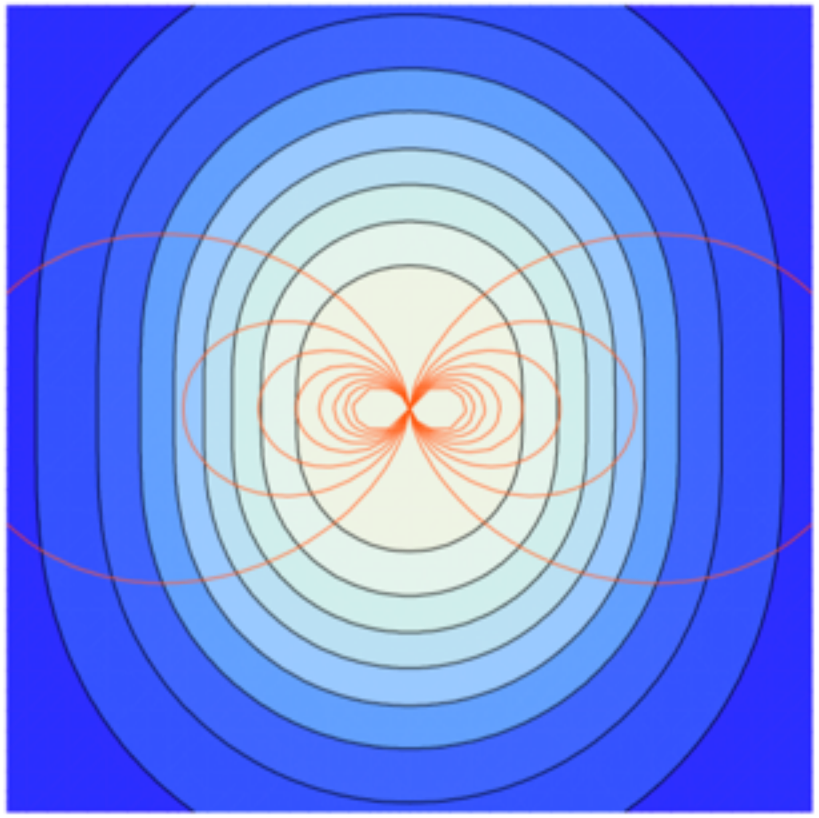

μ-foliation

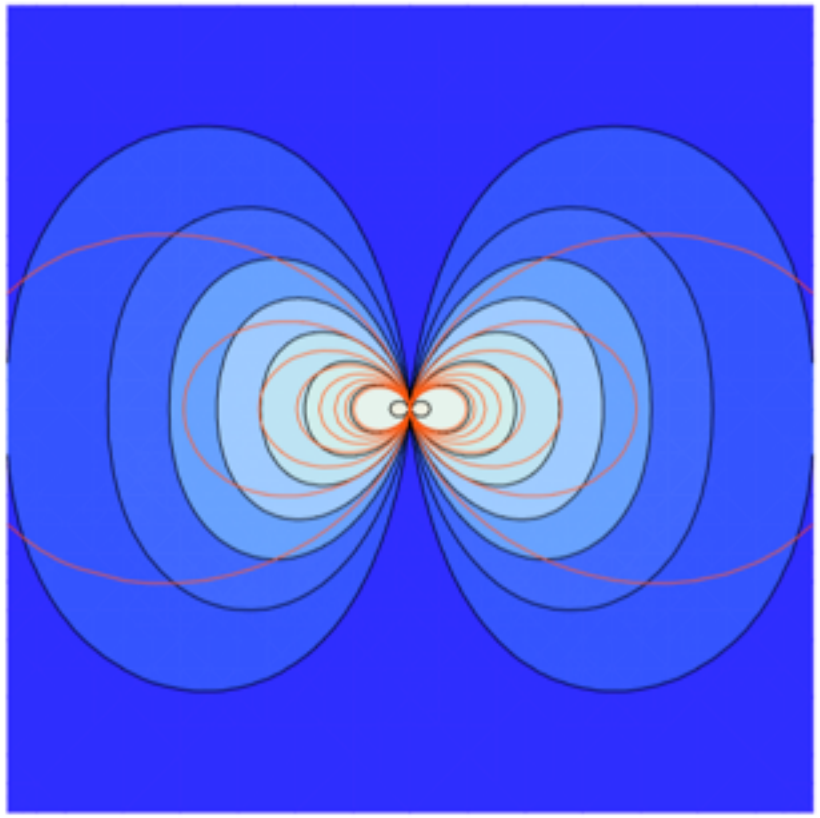

μ & $J_{\|}$-foliation

Statistical equilibrium on a Casimir leaf gives a self-organized density profile

[1] Z. Yoshida and S.M. Mahajan, Prog. Theor. Exp. Phys. **2014**, 073J01 (2014)

Diffusion on a Casimir leaf

- How do we describe a transient state equilibrating toward such equilibrium?
  - ➡ Rigorous diffusion equation on the foliated phase space was formulated recently [1]

$$\frac{\partial f}{\partial t} = \sum \frac{\partial}{\partial \Phi}\left(D_{\Phi\Phi} \frac{\partial f}{\partial \Phi} \right)$$

conventional diffusion equation

$$\longrightarrow$$

$$\begin{aligned}
\frac{\partial P}{\partial t} = & -v_\parallel \frac{\partial P}{\partial \ell} + \frac{\partial}{\partial v_\parallel}\left[\left(\frac{\langle \mu \rangle_v}{m} \frac{\partial B}{\partial \ell} + \gamma v_\parallel \right) P \right] \\
& - \left(\frac{1}{2} - \alpha \right) D_\perp \frac{\partial}{\partial \psi} \left\{ \left[\left(\mathfrak{q} \frac{\partial}{\partial \ell} + \frac{\partial}{\partial \psi} \right) \ln(rB) \right] P \right\} \\
& - \left(\frac{1}{2} - \alpha \right) D_\perp \frac{\partial}{\partial \ell} \left\{ \left[\mathfrak{q} \left(\mathfrak{q} \frac{\partial}{\partial \ell} + \frac{\partial}{\partial \psi} \right) \ln(rB) \right] P \right\} \\
& - \frac{1}{2} D_\perp \frac{\partial}{\partial \ell} \left\{ \left[\left(\mathfrak{q} \frac{\partial}{\partial \ell} + \frac{\partial}{\partial \psi} \right) \mathfrak{q} \right] P \right\} \\
& + \frac{1}{2} D_\perp \frac{\partial^2}{\partial \ell^2} \left(\mathfrak{q}^2 P \right) + D_\perp \frac{\partial^2}{\partial \ell \partial \psi} (\mathfrak{q} P) \\
& + \frac{1}{2} D_\perp \frac{\partial^2 P}{\partial \psi^2} + \frac{1}{2} D_\parallel \frac{\partial^2 P}{\partial v_\parallel^2}.
\end{aligned}$$

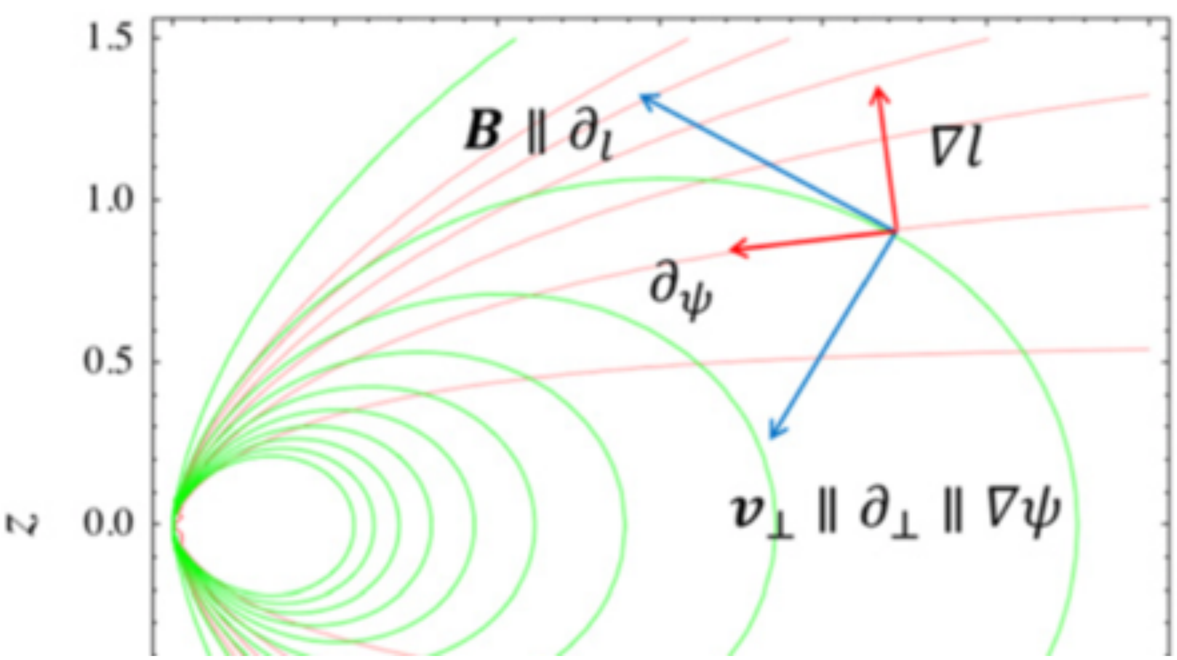

ψ : magnetic flux function

ℓ : magnetic field line length

$\mathfrak{q}$: geometrical factor
(magnetic coordinate is non-orthogonal coordinate system $\nabla \ell \cdot \partial_\perp \neq 0$)

α : phase difference between a perturbation and a resulting motion

[1] N. Sato and Z. Yoshida, J. Phys. A: Math. Theor. 48 (2015) 205501.

Numerical simulation of the new diffusion equation

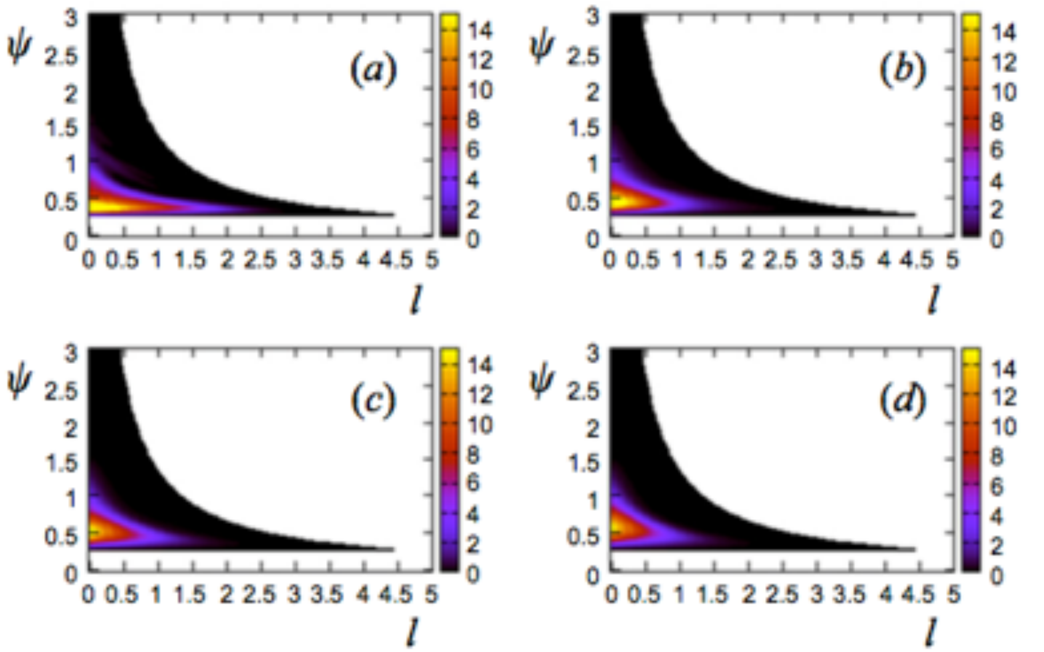

Figure 4. Time evolution of the proper-frame density u. (a): $t = 0.24$. (b): $t = 0.96$. (c): $t = 1.68$. (d): $t = 2.4$.

density evolution on the magnetic coordinate

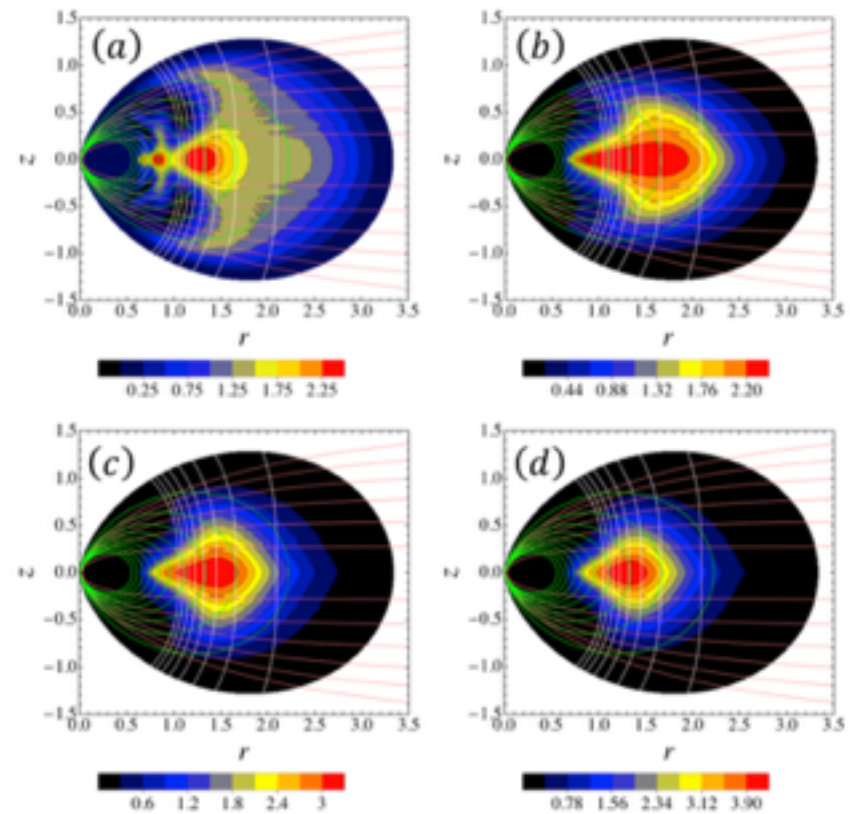

Figure 5. Time evolution of the laboratory frame density ρ. (a): $t = 0.24$. (b): $t = 0.96$. (c): $t = 1.68$. (d): $t = 2.4$.

density evolution on the laboratory coordinate

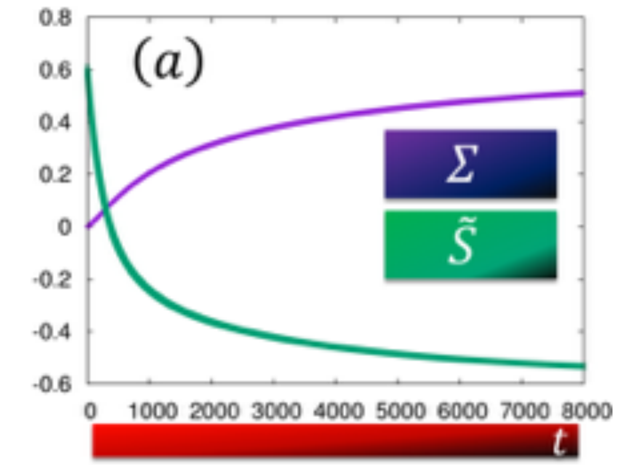

entropy evolution

$\tilde{S}$: defined by a proper measure

Σ : defined by a “familiar” measure

- ✓ Density is flattened on the magnetic (proper) coordinate
- ✓ Density becomes inhomogeneous on the laboratory coordinate [1]
- ✓ Properly defined entropy increases while “familiar” entropy decreases [2]

[1] N. Sato and Z. Yoshida, J. Phys. A: Math. Theor. 48 (2015) 205501.
[2] N. Sato and Z. Yoshida, Phys. Rev. E **93** 062140 (2016).

Experimental studies on inward diffusion

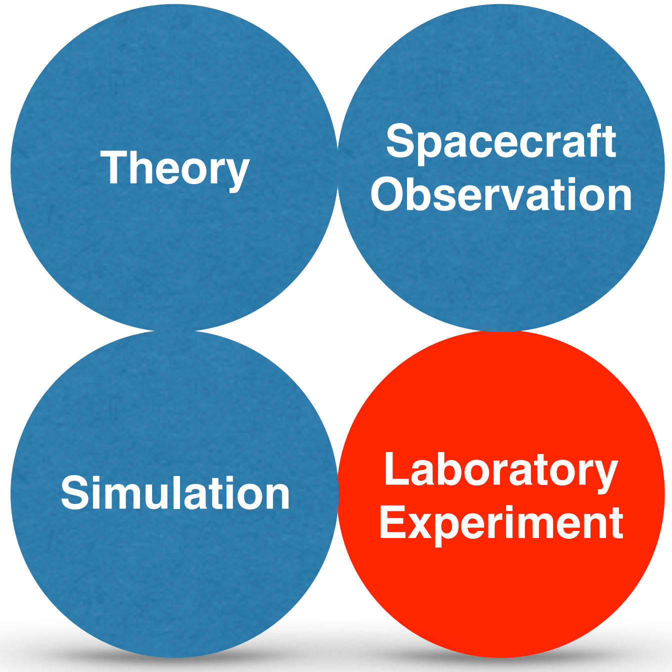

Laboratory magnetosphere devices

Ring trap 1 (RT-1) @The University of Tokyo

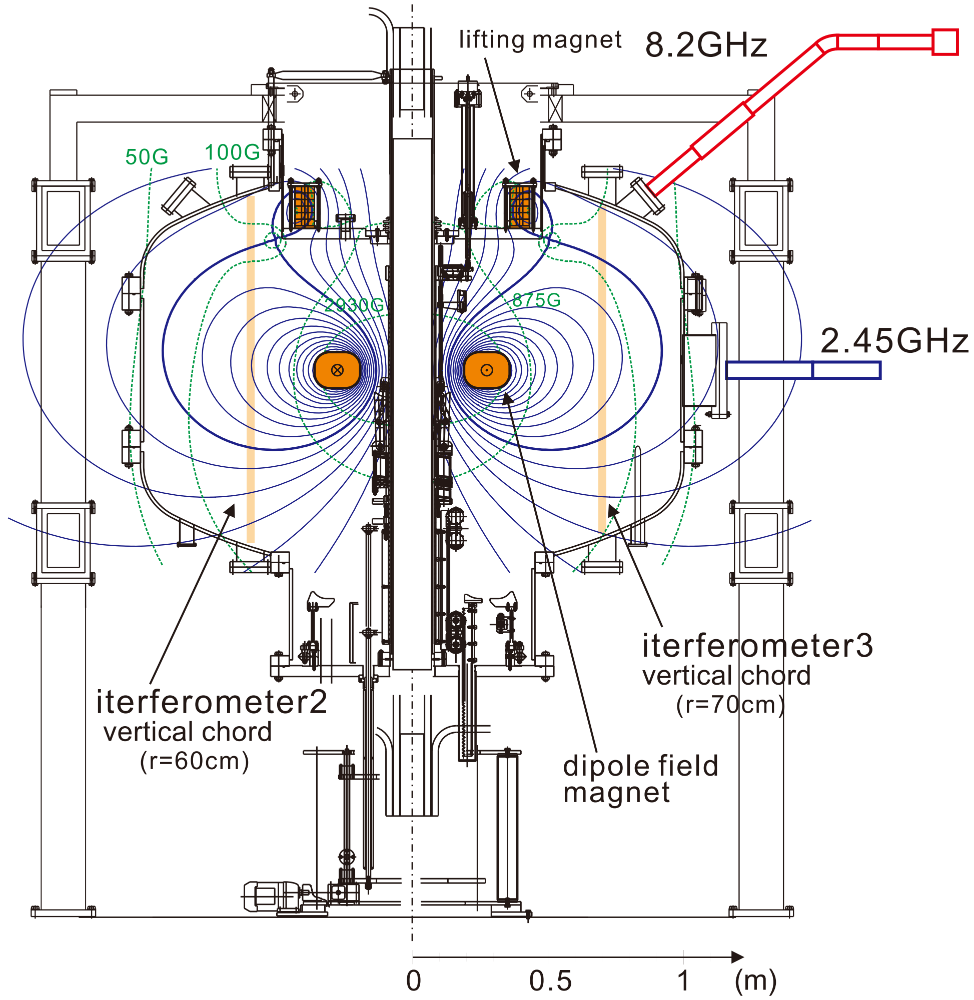

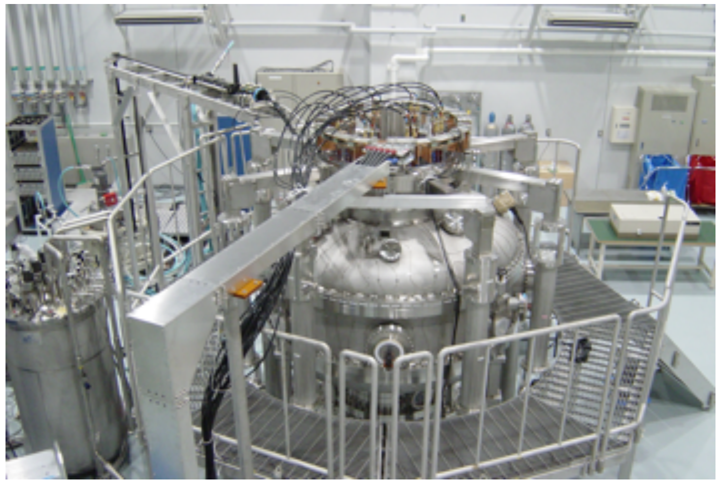

Levitated Dipole Experiment (LDX) @MIT

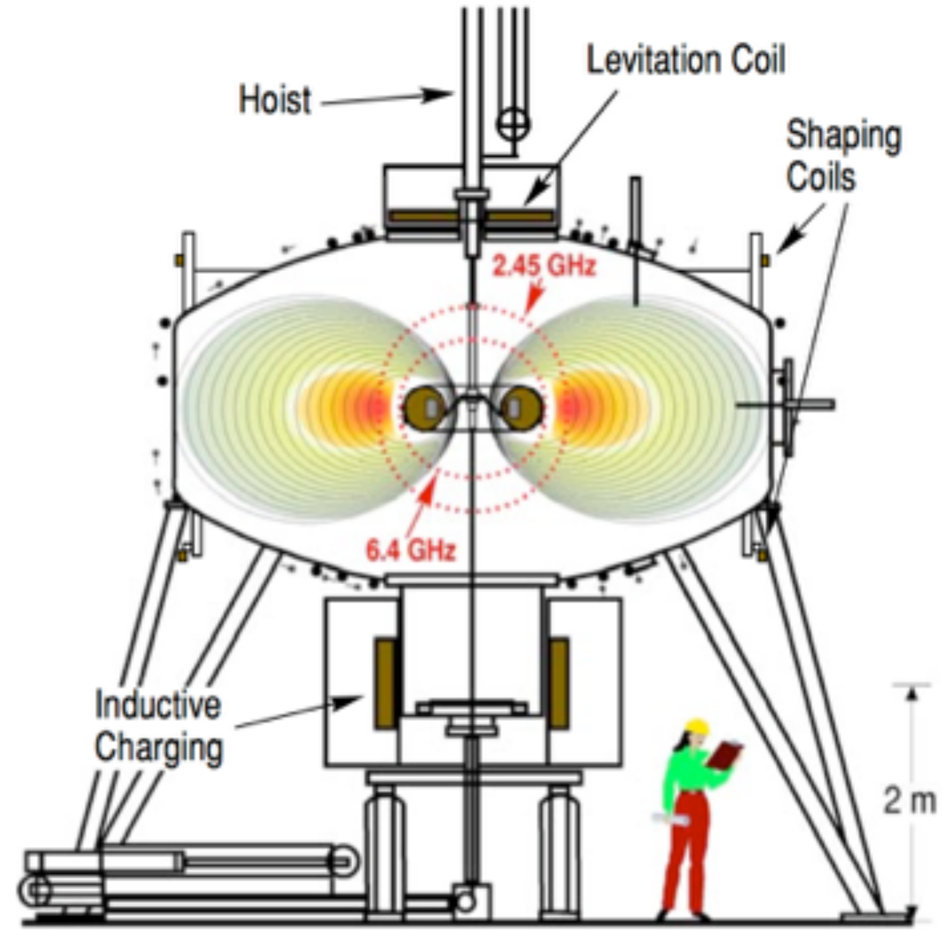

[1] Z. Yoshida, et al., Plasma Fusion Res. **1**, 008 (2006). [2] D.T. Garnier, et al., Fusion Engineering and Design **81** 2371–2380 (2006).

Laboratory magnetosphere devices

Ring trap 1 (RT-1) @The University of Tokyo

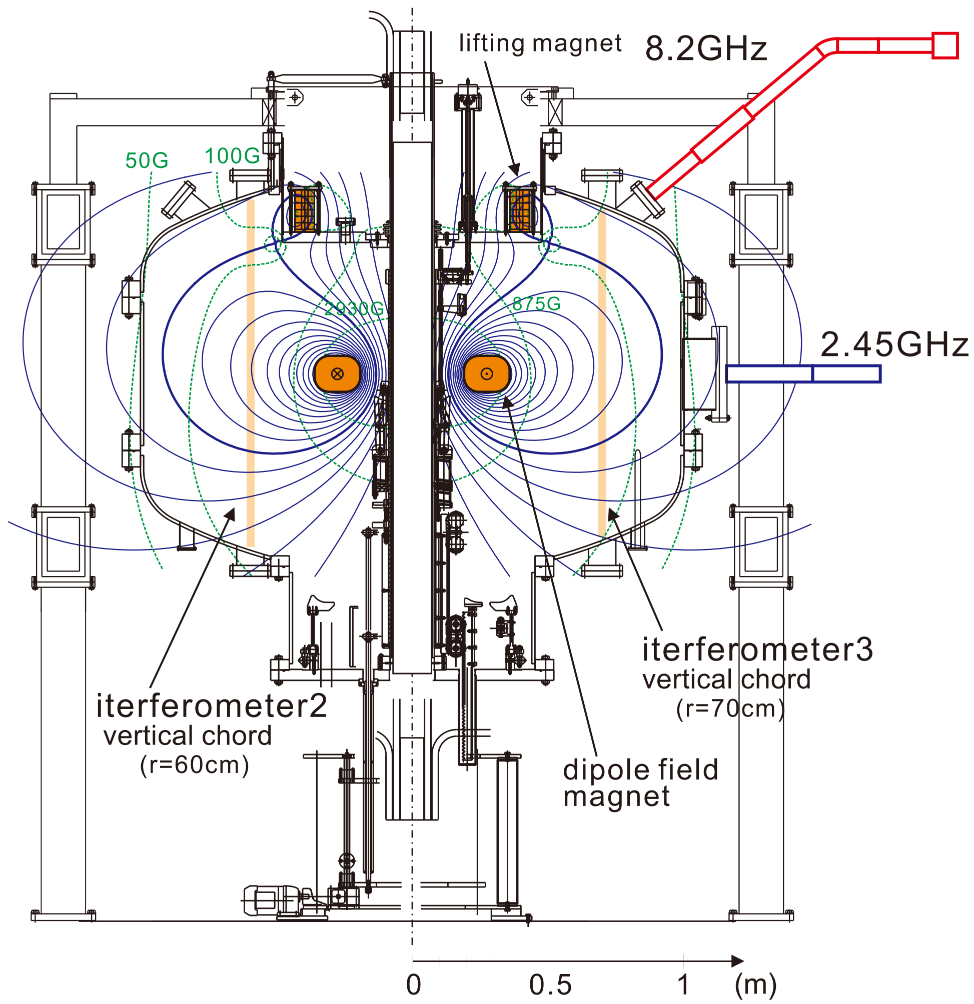

Levitated Dipole Experiment (LDX) @MIT

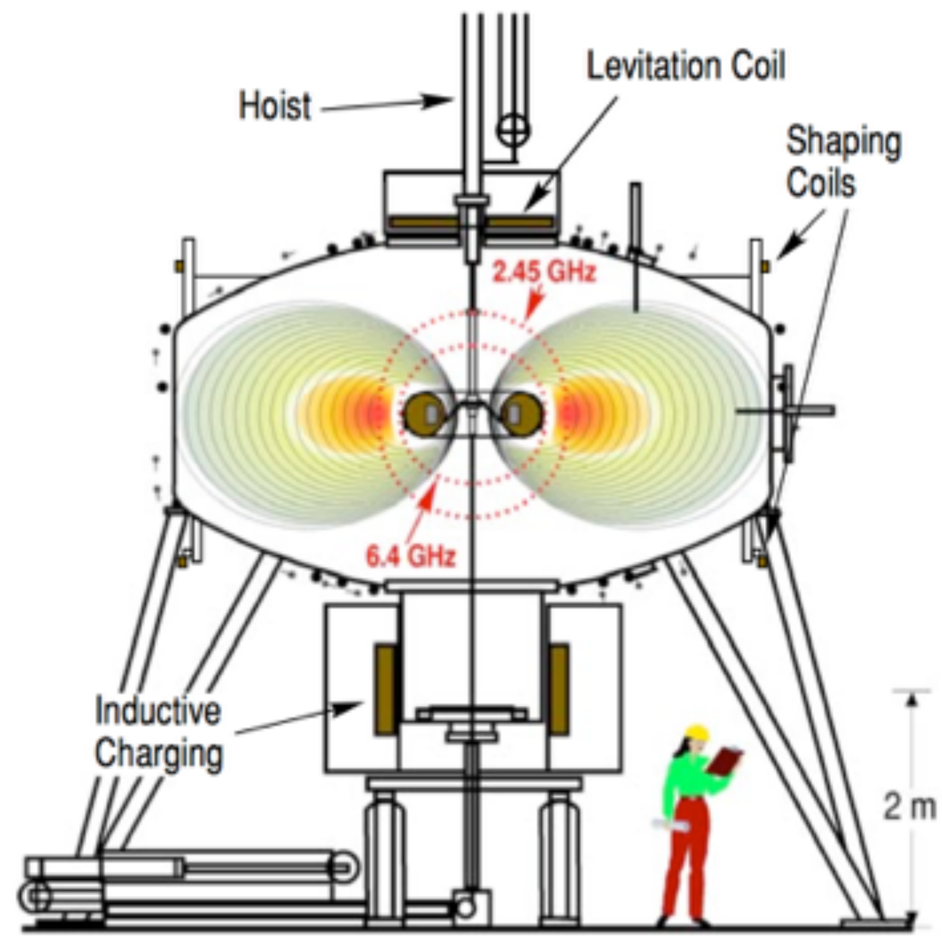

- ✓ A levitated superconducting magnet simulates artificial magnetosphere
- ✓ “Testing ground” of planetary plasma
- ✓ Possibility of an advanced fusion [2] (local $\beta_e > 1$ in recent RT-1 plasma) [1]

[1] Z. Yoshida, et al., Plasma Fusion Res. **1**, 008 (2006). [2] D.T. Garnier, et al., Fusion Engineering and Design **81** 2371–2380 (2006).
[2] A. Hasegawa, et al., Nucl. Fusion **30**, 2405 (1990). [3] M. Nishiura, et al., Nucl. Fusion **55** 053019 (2015).

RT-1 : Levitation

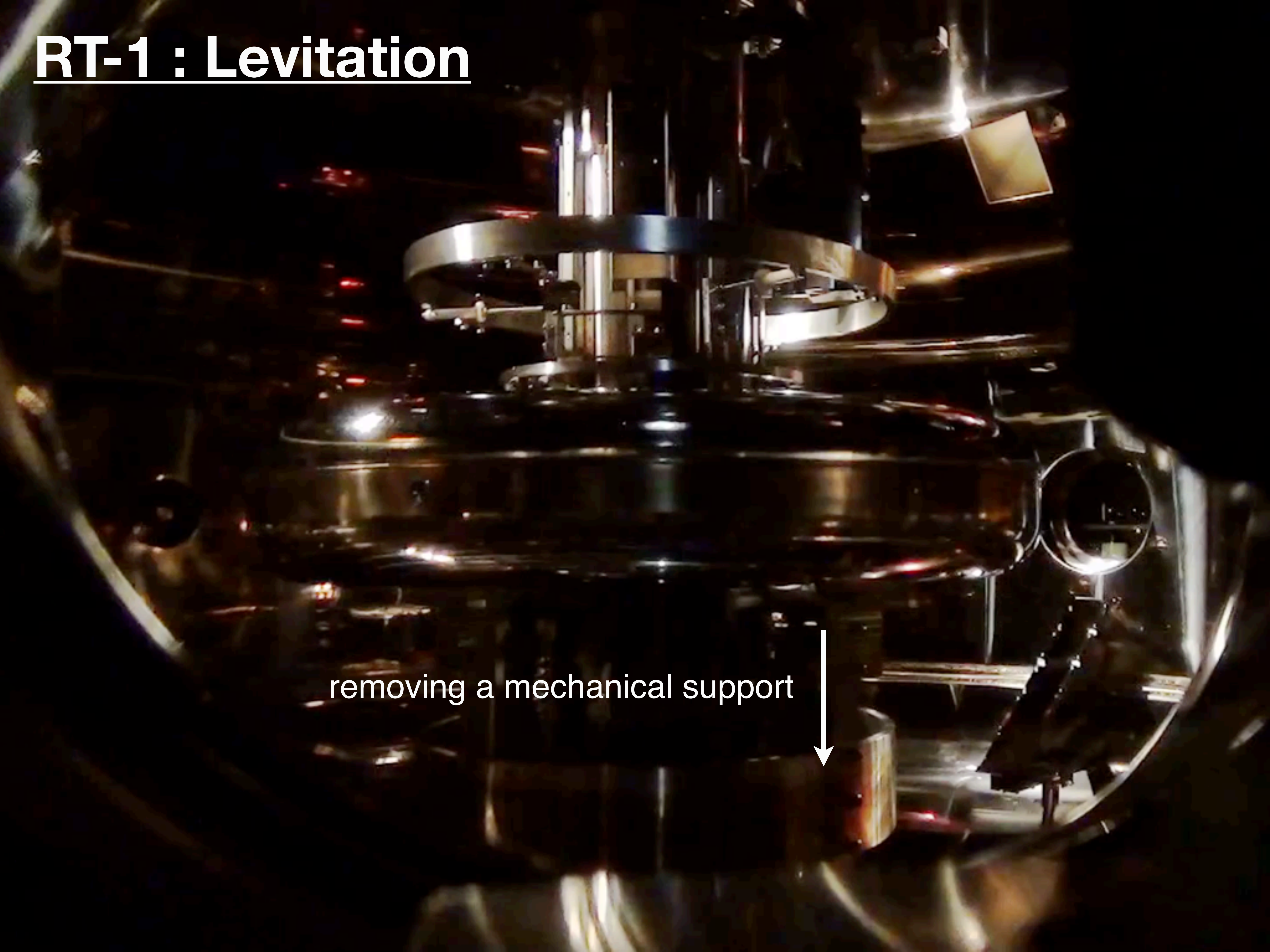

RT-1 : Position control

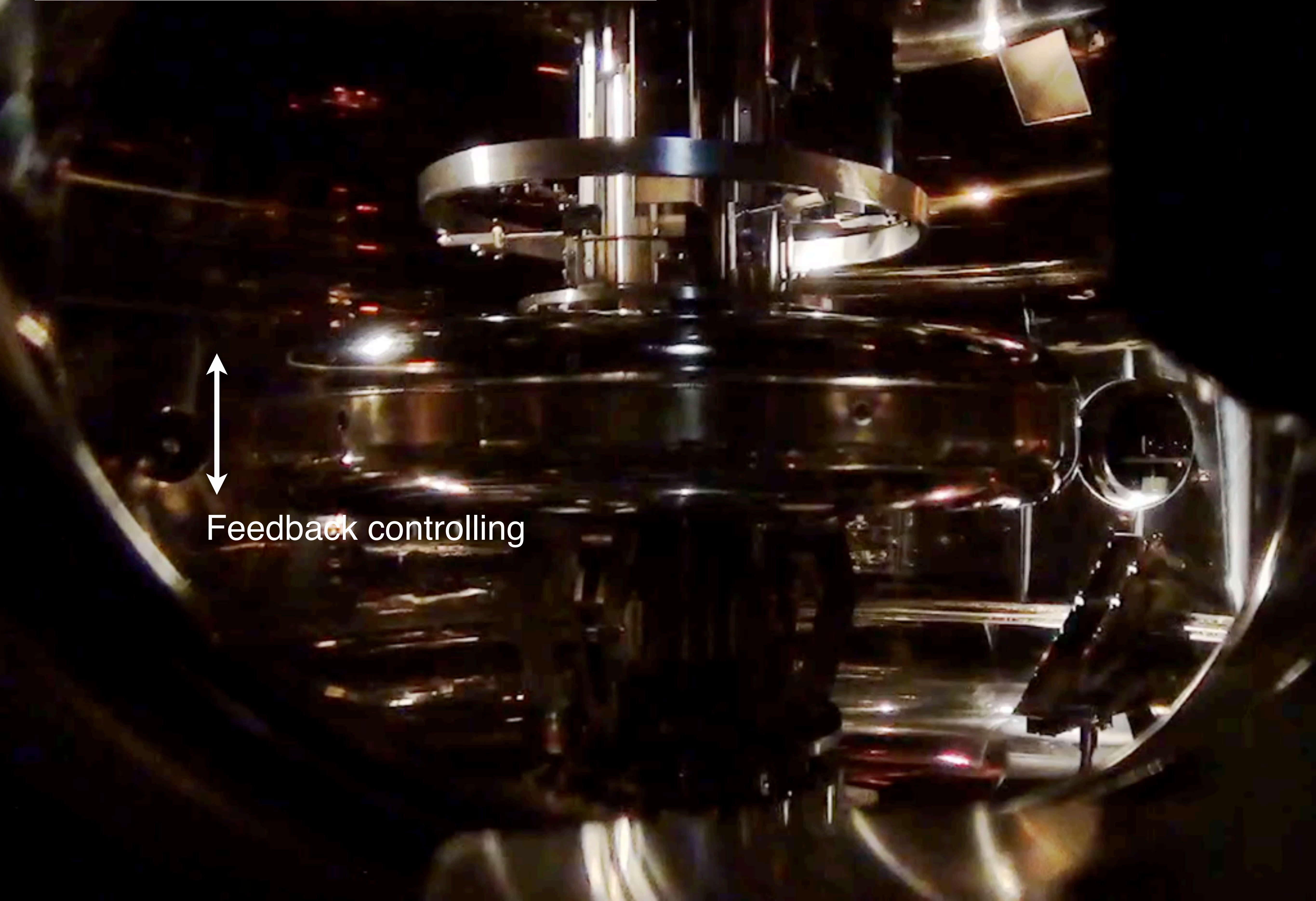

RT-1 : Plasma shot

Overview of RT-1 device

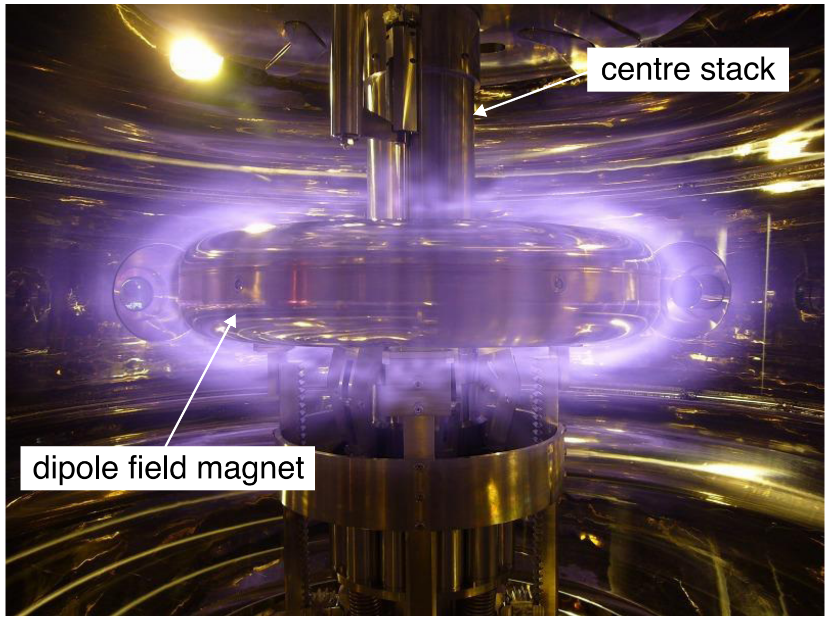

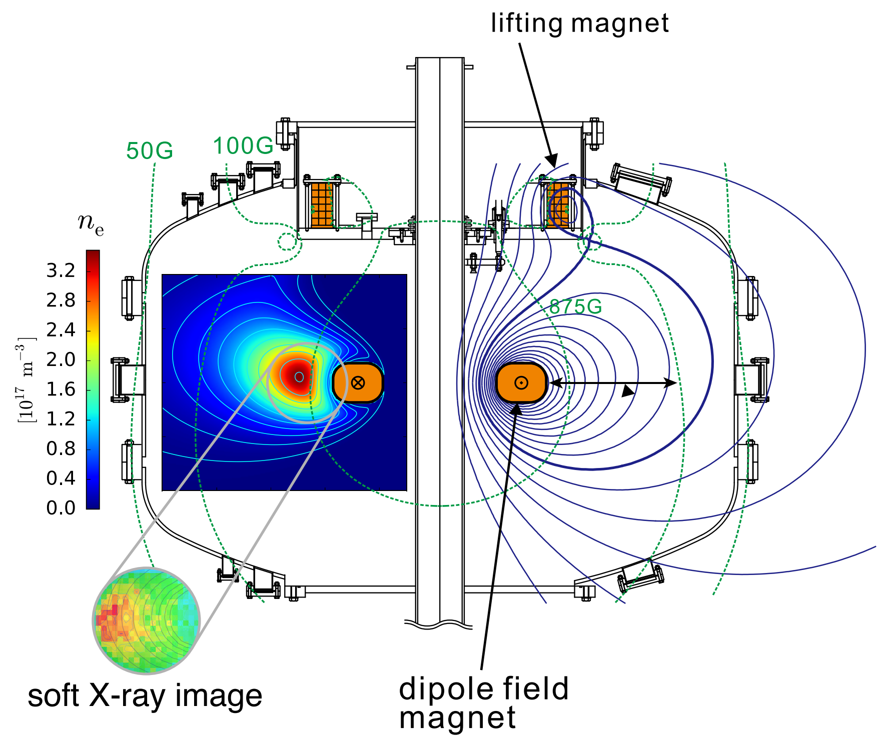

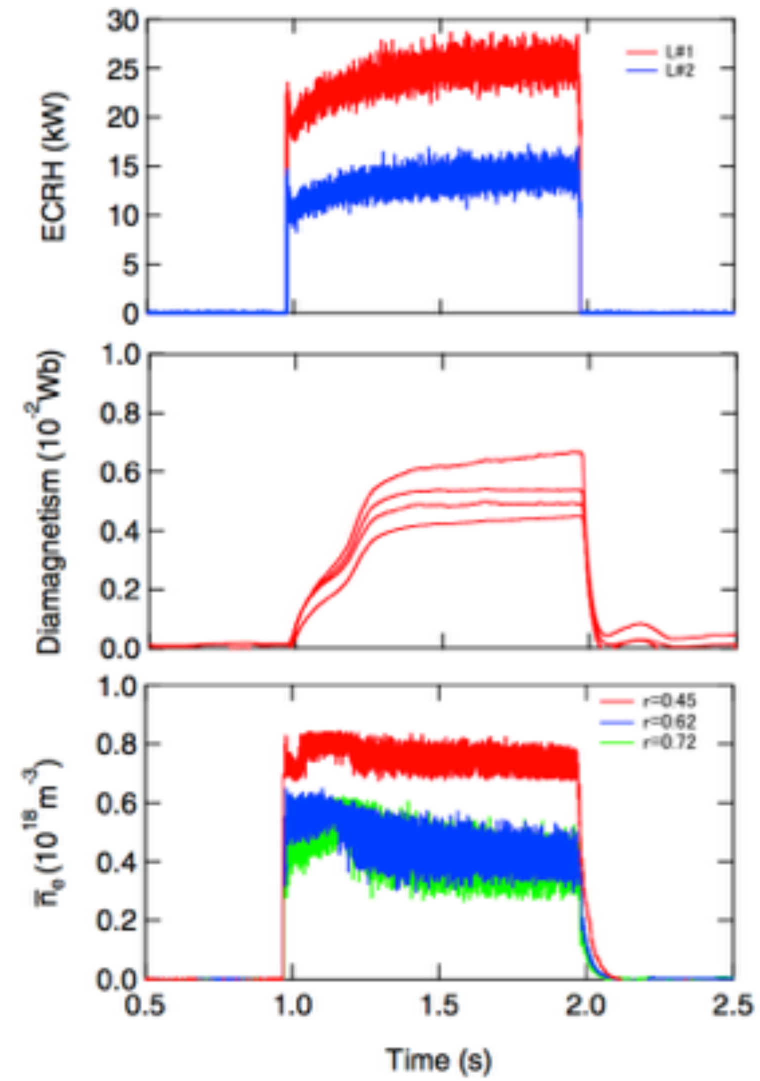

Figure 2. Discharge waveforms for a high-β deuterium plasma. (*a*) ECRH power, (*b*) diamagnetic signal and (*c*) line-averaged densities measured by interferometers.

- ✓ “Loss-cone-less” mirror confinement
- ✓ Plasma is generated by ECH (8.2G, 50kW)
  - dischage duration : 1s
  - n_e : 10^{17}~10^{18} m^{-3} (hot/cold ~ 1) [1]
  - T_e ≧10 keV (hot), ~100 eV (cold)
  - T_i ~ 50 eV
- ✓ Recently ICH was succeeded [2]
- ✓ Non-neutral plasma confinement has been also studied [3]

[1] H. Saitoh, et al., Nucler Fusion **51**, 063034 (2011).
[2] M. Nishiura, et al., Plasma Fusion Res. **11**, 2402054 (2016).
[3] H. Saitoh, et al., Phys. Plasmas **18**, 056102 (2011)

High β plasma in RT-1

scaling of β [1]

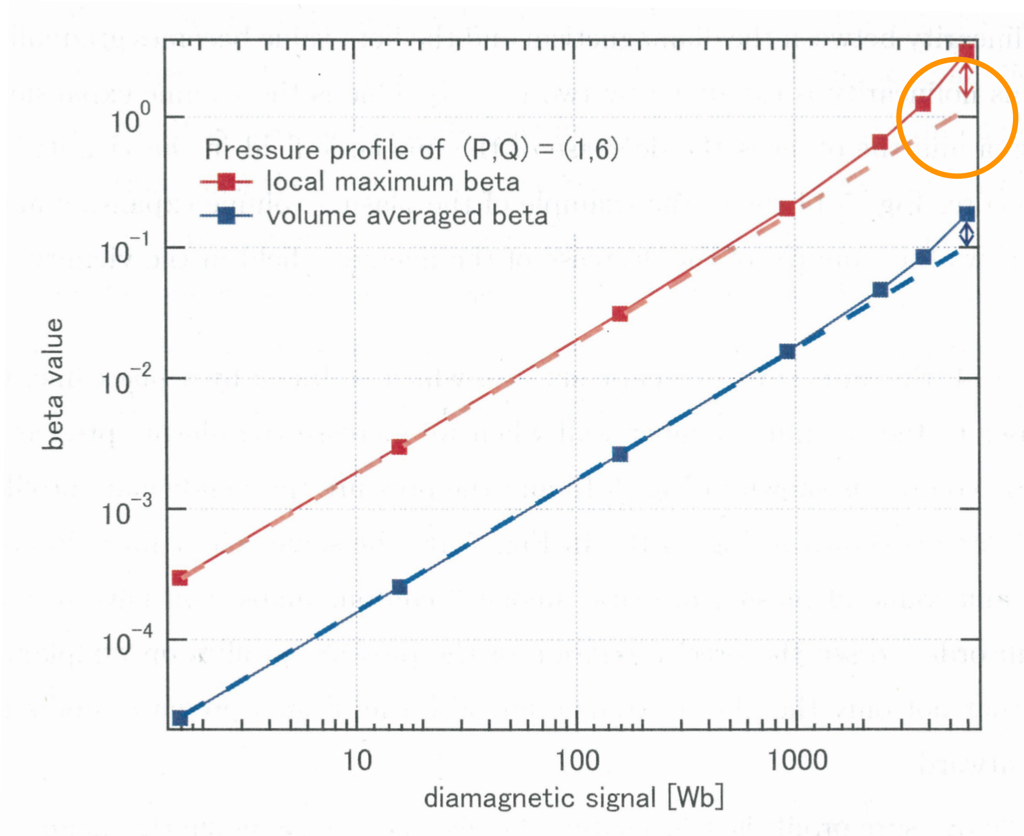

RT-1 plasma parameter region [2]

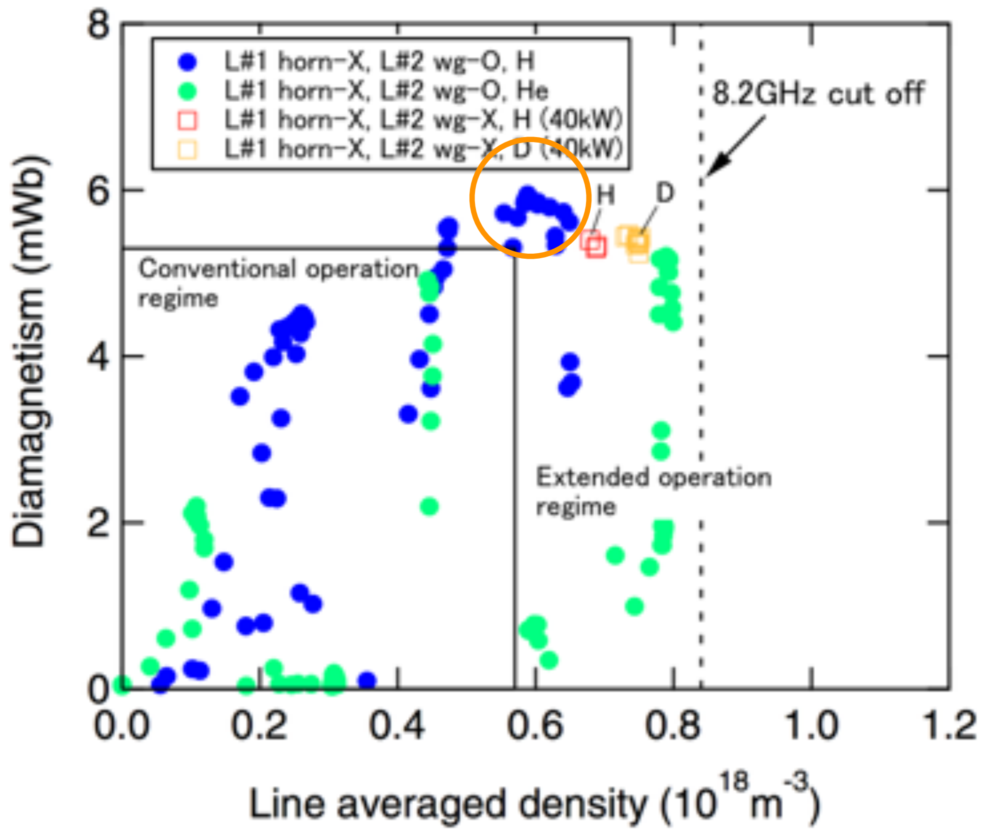

Flux loops outside the chamber

Hall probes inside the chamber → estimate β

numerical solution of Grad–Shafranov equation [4]

✓ Latest RT-1 plasma achieved local maximum β > 1 [3]

[1] Y. Yano, PhD dissertation (The University of Tokyo) (2010). [2] M. Nishiura, et al., Nucl. Fusion **55** 053019 (2015).
[3] M. Furukawa, Phys. Plasmas **21** 012511 (2014).

Observation of the inward diffusion in RT-1

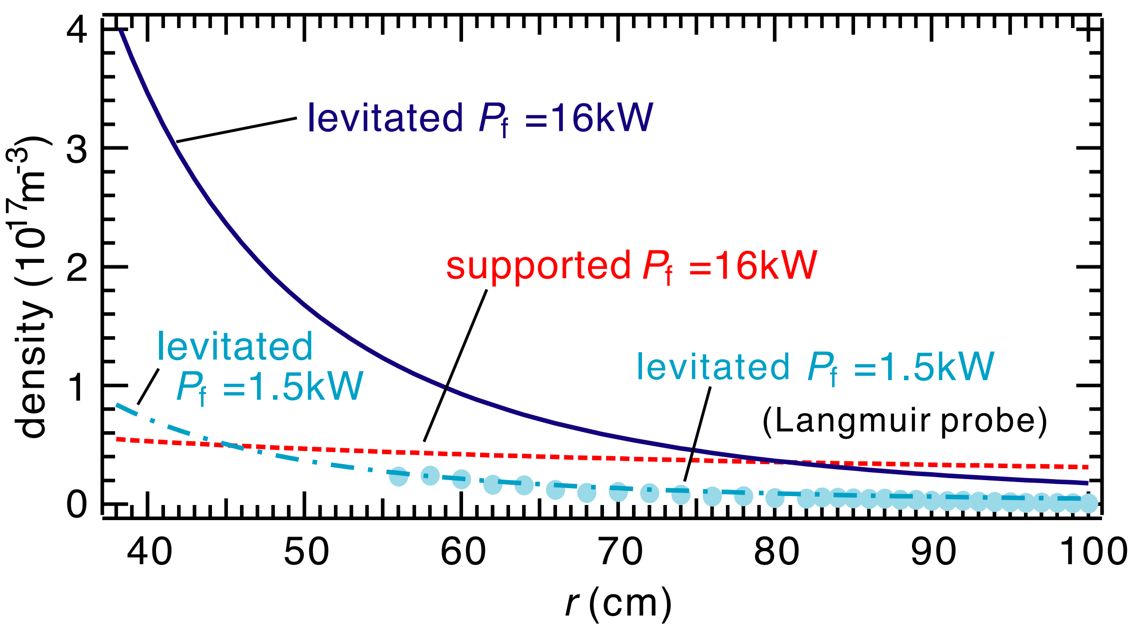

Radial profile of n_e on equatorial plane reconstructed from interferometer data

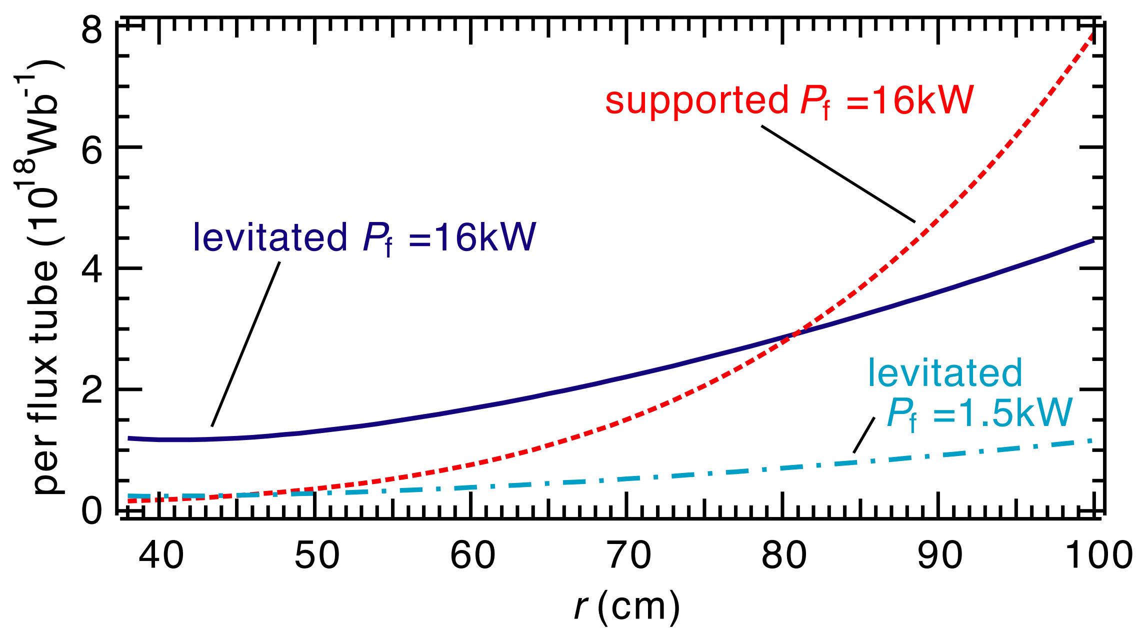

Particle number per a flux tube

- ✓ Density dramatically increases when the dipole magnet is levitated
- ✓ Highly peaked density resembling a magnetosphere

[1] H. Saitoh, et al., Nucler Fusion **51**, 063034 (2011).

Observation of the inward diffusion in RT-1

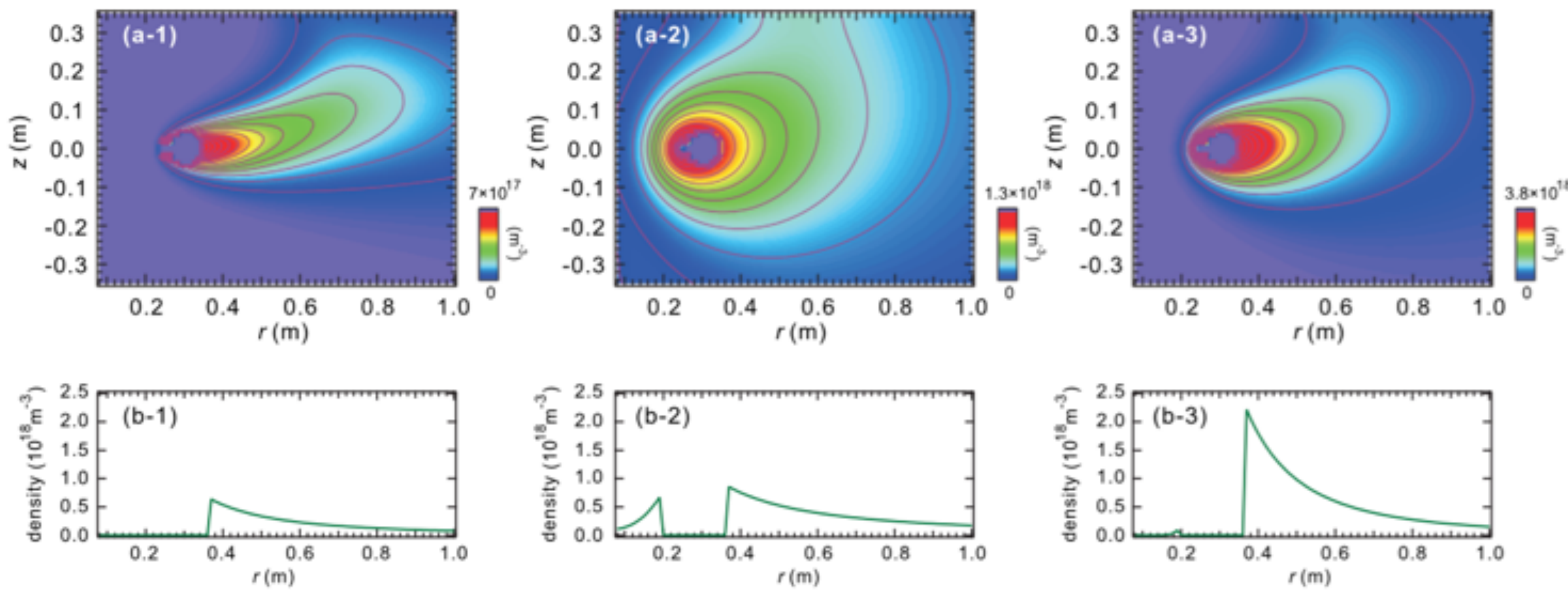

FIG. 7. Electron density profiles corresponding to Table I. (a) Two dimensional contour maps and (b) radial profiles on the $z = 0$ m plane of electron density in cases with (1) high-β and low-n_e, (2) low-β and high-n_e, and (3) high-β and high-n_e states. On the $z = 0$ m plane, the dipole field magnet surface is located at $r = 0.18$ and 0.375 m.

✓ 2D density profile reconstructed from the interferometer data

→ Radially elongated & vertically thin structure due to a mirror effect

[1] H. Saitoh, et al., Phys Plasmas **21**, 082511 (2014).

Observation of the inward diffusion in LDX

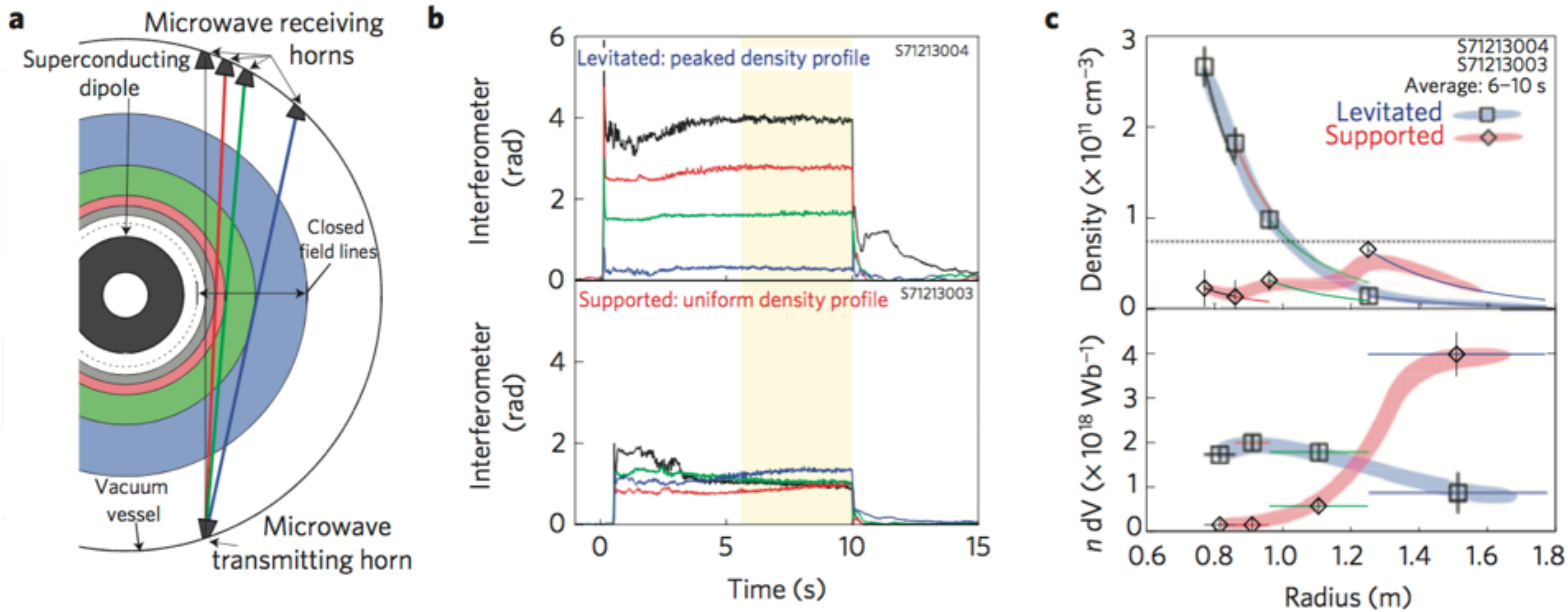

✓ Inward diffusion was also observed in LDX

[1] A. C. Boxer, et al., Nat. Phys. **6**, 207 (2010).

Observation of the inward diffusion in LDX

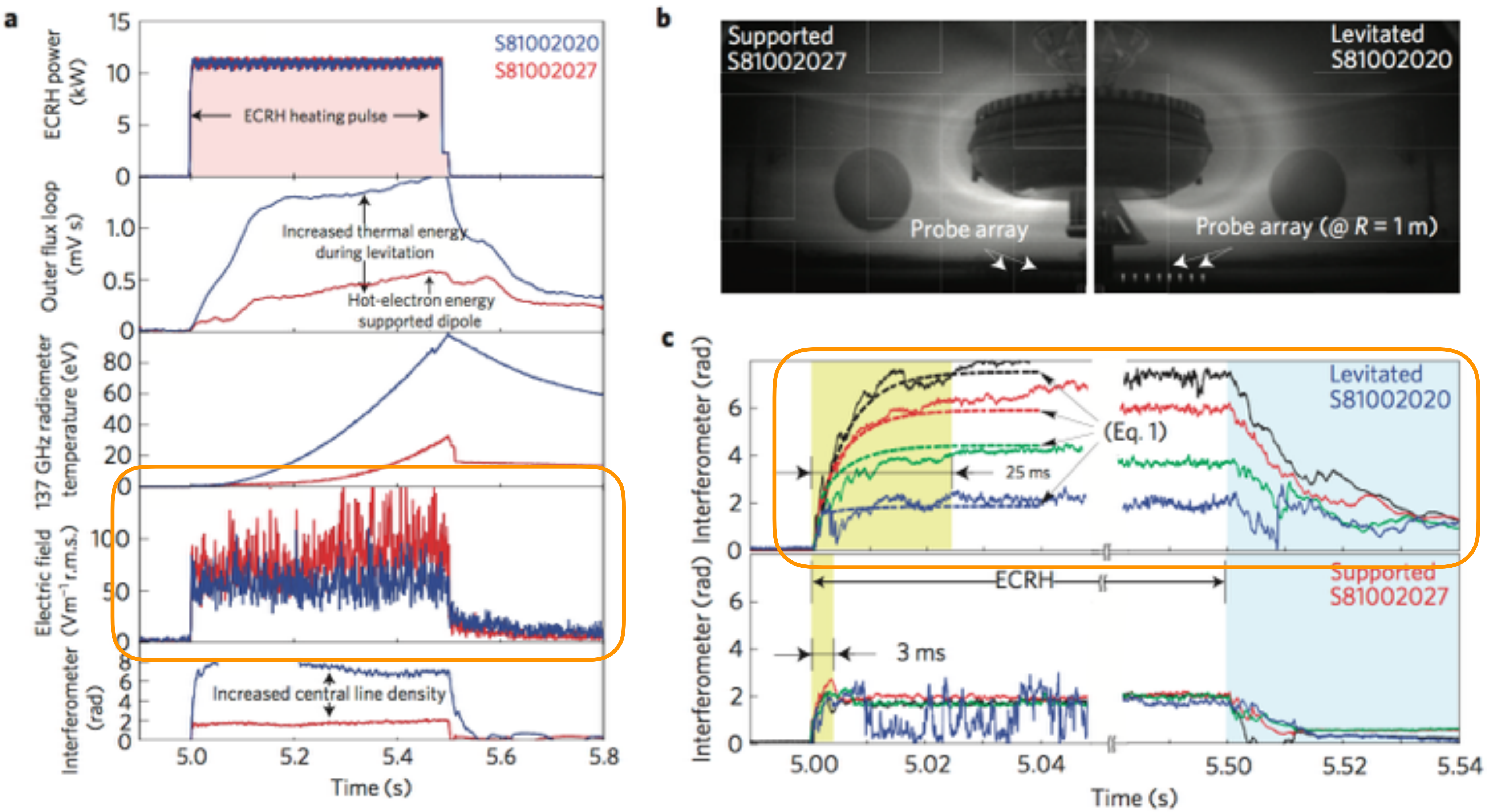

- ✓ Fluctuation of E_θ at the edge was measured to estimate the diffusion coefficient

$$\frac{\partial N}{\partial t} = \langle S \rangle + \frac{\partial}{\partial \psi} D \frac{\partial N}{\partial \psi} \qquad (1)$$

- ✓ Empirical diffusion equation reproduced the interferometer data

[1] A. C. Boxer, et al., Nat. Phys. **6**, 207 (2010).

Interim summary

- ✓ Plasma supplied from solar wind is spontaneously attracted to a planet
- ✓ Such a self-organization is explained by inward diffusion
- ✓ A violation of a third AI while the other two AIs are kept constant triggers inward diffusion
- ✓ Scale hierarchies of AIs (Casimir invariants) induce a foliated phase space
- ✓ Statistic equilibrium on the foliated phase space = self-organization in laboratory
- ✓ A rigorously formulated diffusion equation revealed transient relaxation on the foliated phase space and self-organization in the laboratory space
- ✓ Laboratory magnetosphere experiments has been progressed during the last decade
- ✓ A new “platform” of astrophysics research is provided
- ✓ Inward diffusion was experimentally verified in the laboratory magnetospheres

Particle acceleration in laboratory magnetosphere

Planetary Van Allen radiation belts

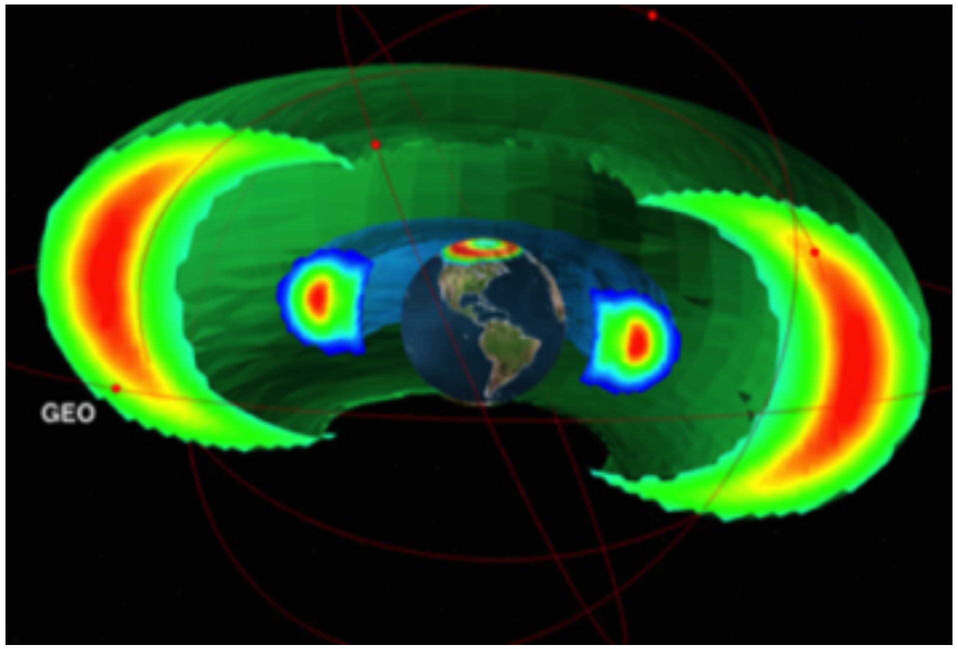

Earth's radiation belt

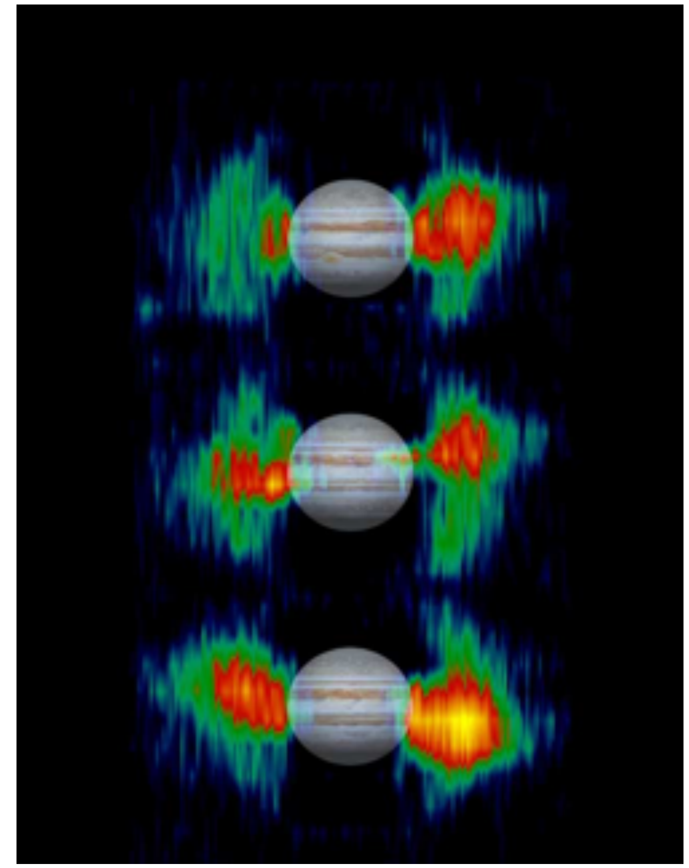

synchrotron emission from ultra-relativistic electrons in Jovian radiation belt

- ✓ Particles are not only attracted to a planet but also accelerated
  - ➡ Another self-organization in a magnetosphere
- ✓ Wide-ranged energy (100keV ~ 10MeV)

[1] R.V. Hilmer, Air Force Research Laboratory
[2] http://www.nasa.gov

Acceleration mechanisms

- ✓ Adiabatic acceleration: concomitant with inward diffusion
- ✓ Inward (toward a strong B and short bounce length region) transport
  - ➡ conservation of the first and second AIs → increase in particle's kinetic energy
- ✓ A primary generator of radiation belts [1]

$$\omega_{\mathrm{c}} \gg \omega_{\mathrm{bounce}} \gg \omega_{\mathrm{drift}}$$

$$\boxed{\mu = \frac{mv_\perp^2}{2B}} \qquad \boxed{J = \oint p_{\parallel}\, \mathrm{d}l} \qquad \cancel{\boxed{\Phi = \oint \boldsymbol{B} \cdot \mathrm{d}S}}$$

inward transport

$T_\perp$ increase (Betatron acceleration)

inward transport

$T_{\parallel}$ increase (Fermi accrelation)

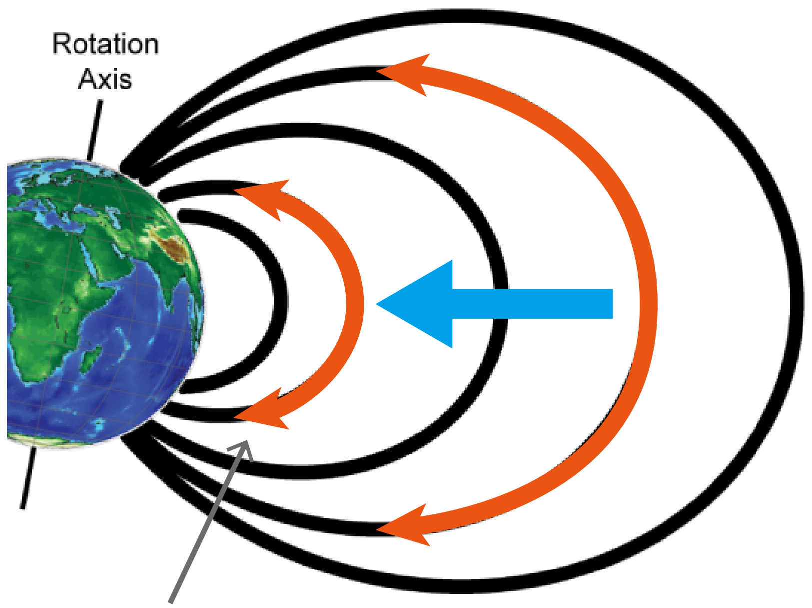

- stronger magnetic filed
- shorter bounce length

[1] A. J. Dessler, ed. Physics of the Jovian magnetosphere., 3. (Cambridge University Press, 2002).
[2] A. M. Persoon, et al., J. Geophys. Res. 114, A0421 (2009).

Acceleration mechanisms

✓ Adiabatic acceleration creates particle energy anisotropy [1]

- For point dipole configuration,

$$B \propto r^{-3} \qquad\qquad L\ \text{(bounce length)} \propto r^{1}$$

$$\downarrow \qquad\qquad\qquad\qquad \downarrow$$

$$v_\perp^2 = \frac{2\mu B}{m} \propto r^{-3} \qquad\qquad v_\parallel^2 \sim \left(\frac{J}{mL}\right)^2 \propto r^{-2}$$

✓ $T_\perp$ glows faster than $T_\parallel$ $\rightarrow$ $T_\perp > T_\parallel$

✓ Such an anisotropy has been observed in the planetary radiation belts [2]

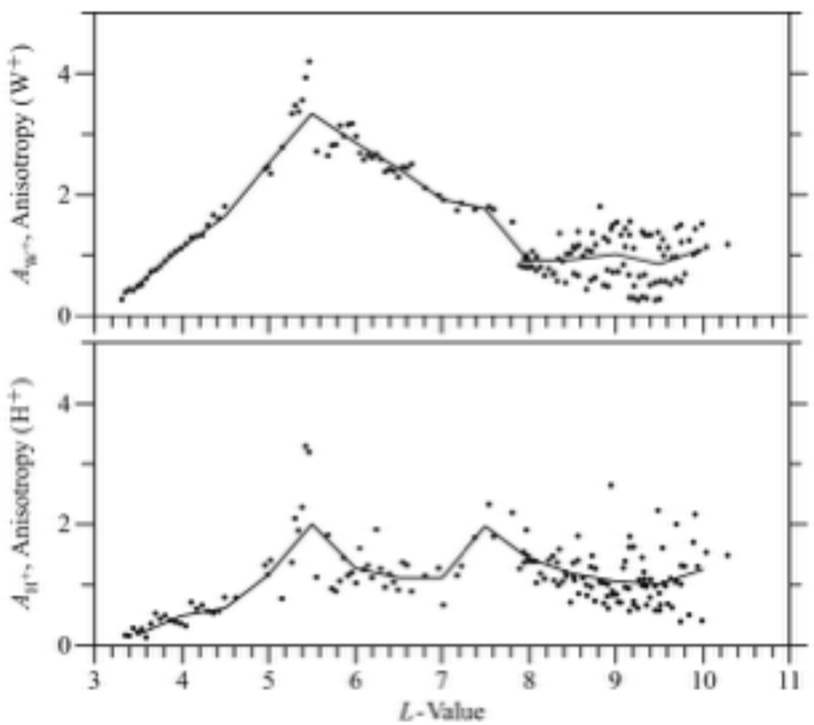

- stronger magnetic filed
- shorter bounce length

[1] A. J. Dessler, ed. Physics of the Jovian magnetosphere., 3. (Cambridge University Press, 2002).
[2] A. M. Persoon, et al., J. Geophys. Res. 114, A0421 (2009).

Acceleration mechanisms

- ✓ Non-adiabatic acceleration, wave-particle interaction, is also important

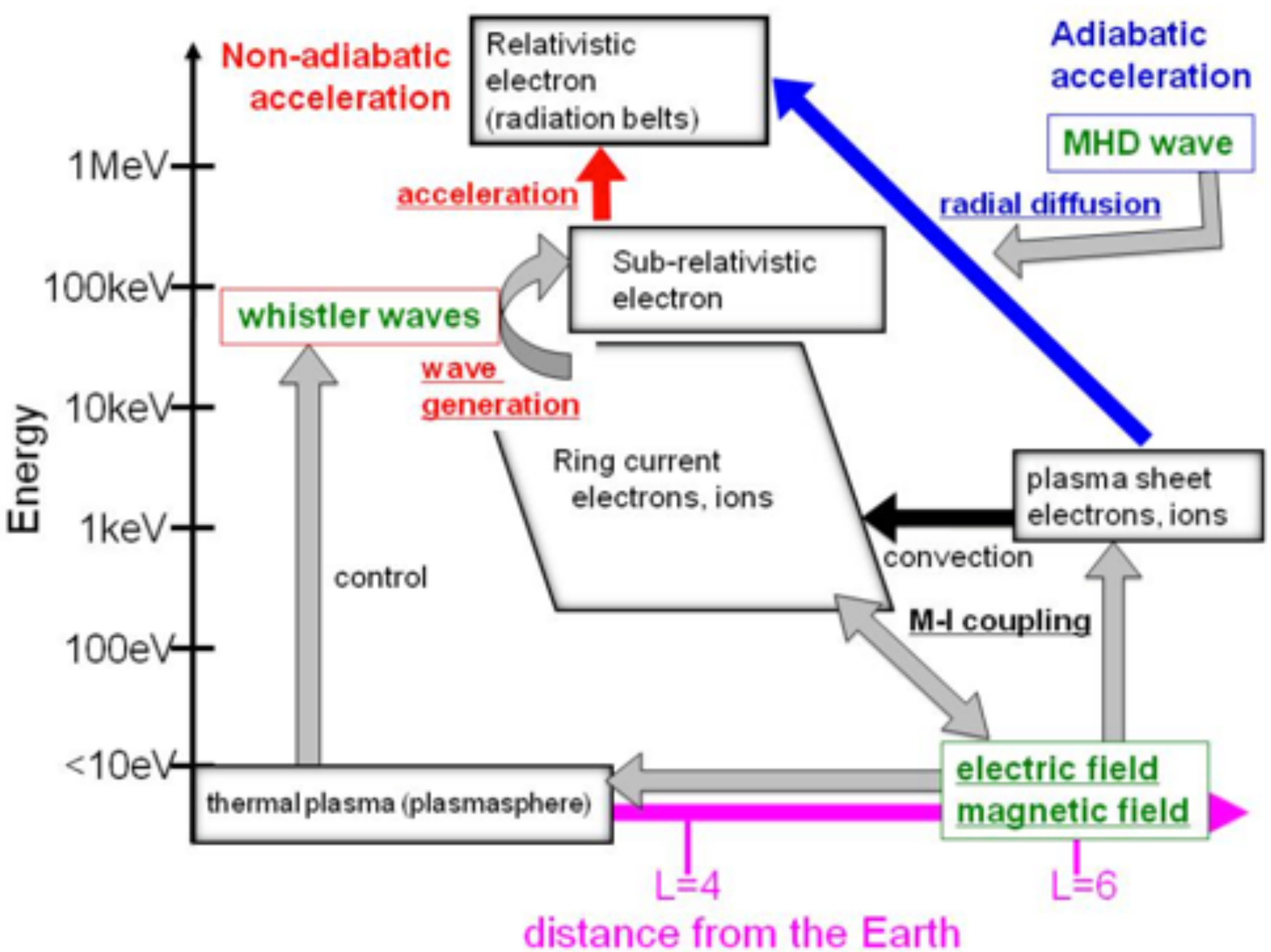

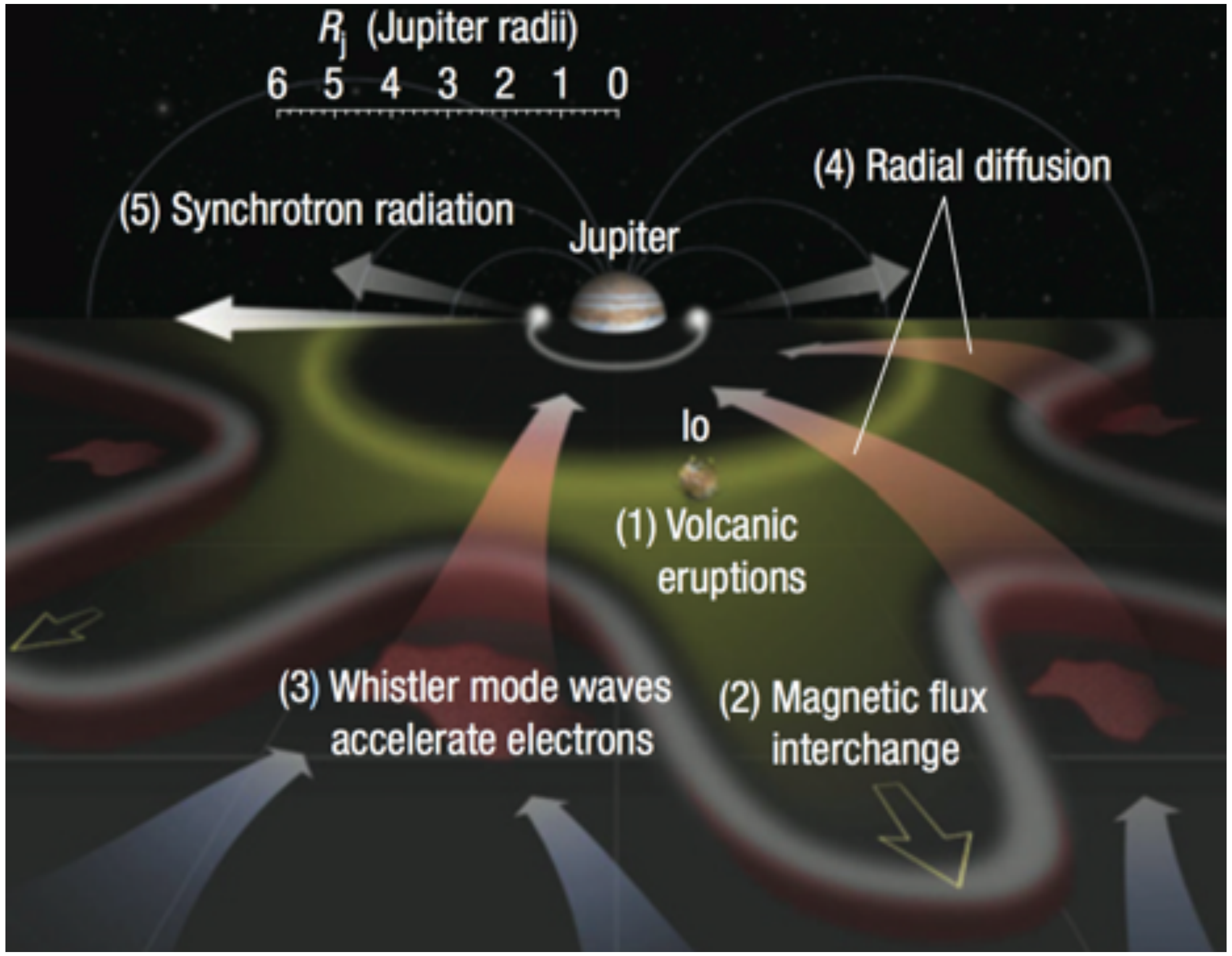

[1] Y. Ebihara and Y. Miyoshi, Dynamic inner magnetosphere: A tutorial and recent advances, in *The Dynamic Magnetosphere*, IAGA Special Sopron Book Series 3, (Springer Science+Business Media B.V., 2011).
[2] R. B. Horne, et al., Nature Phys. 4, 301 (2008).

Observation of particle acceleration in RT-1

Ion temperature measurement in RT-1

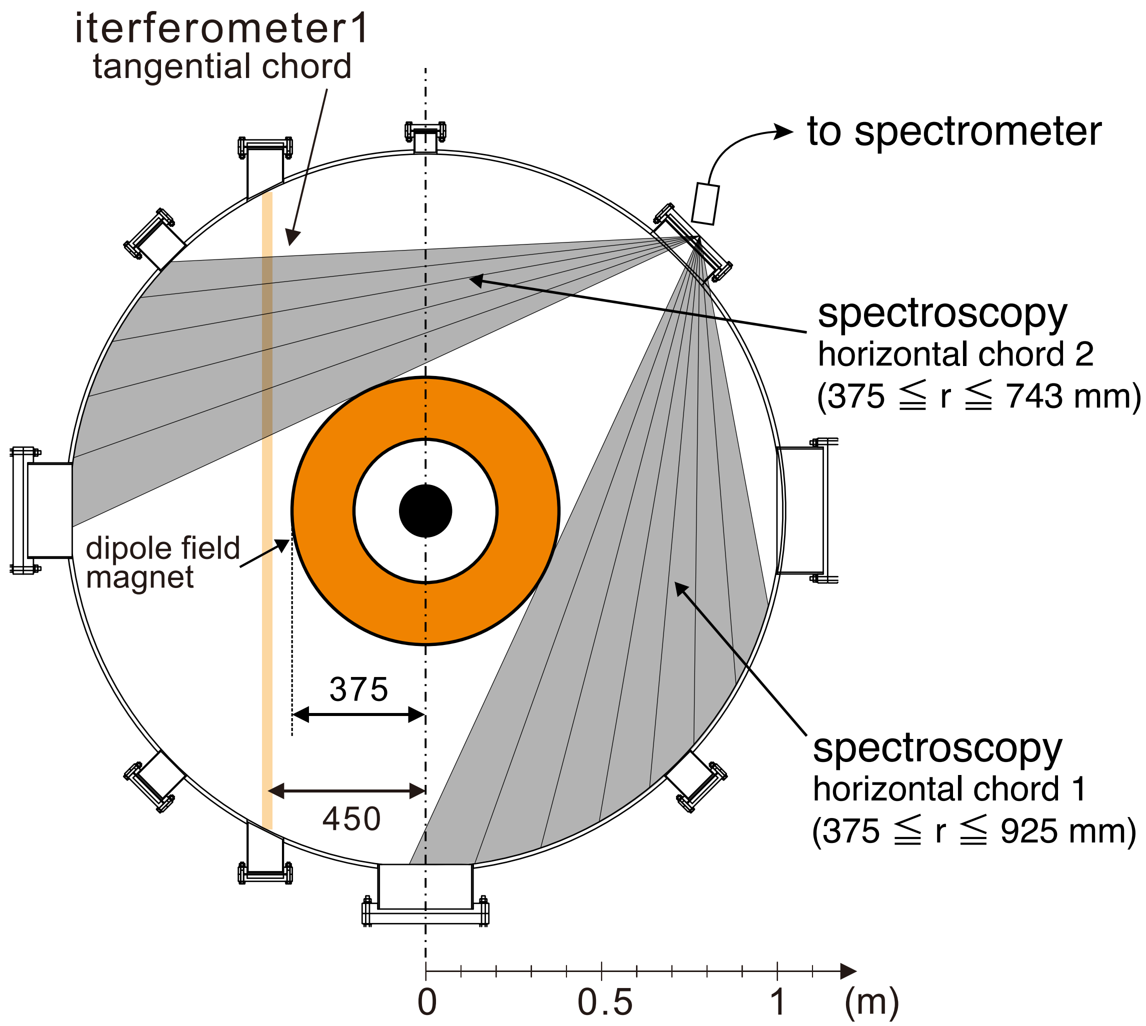

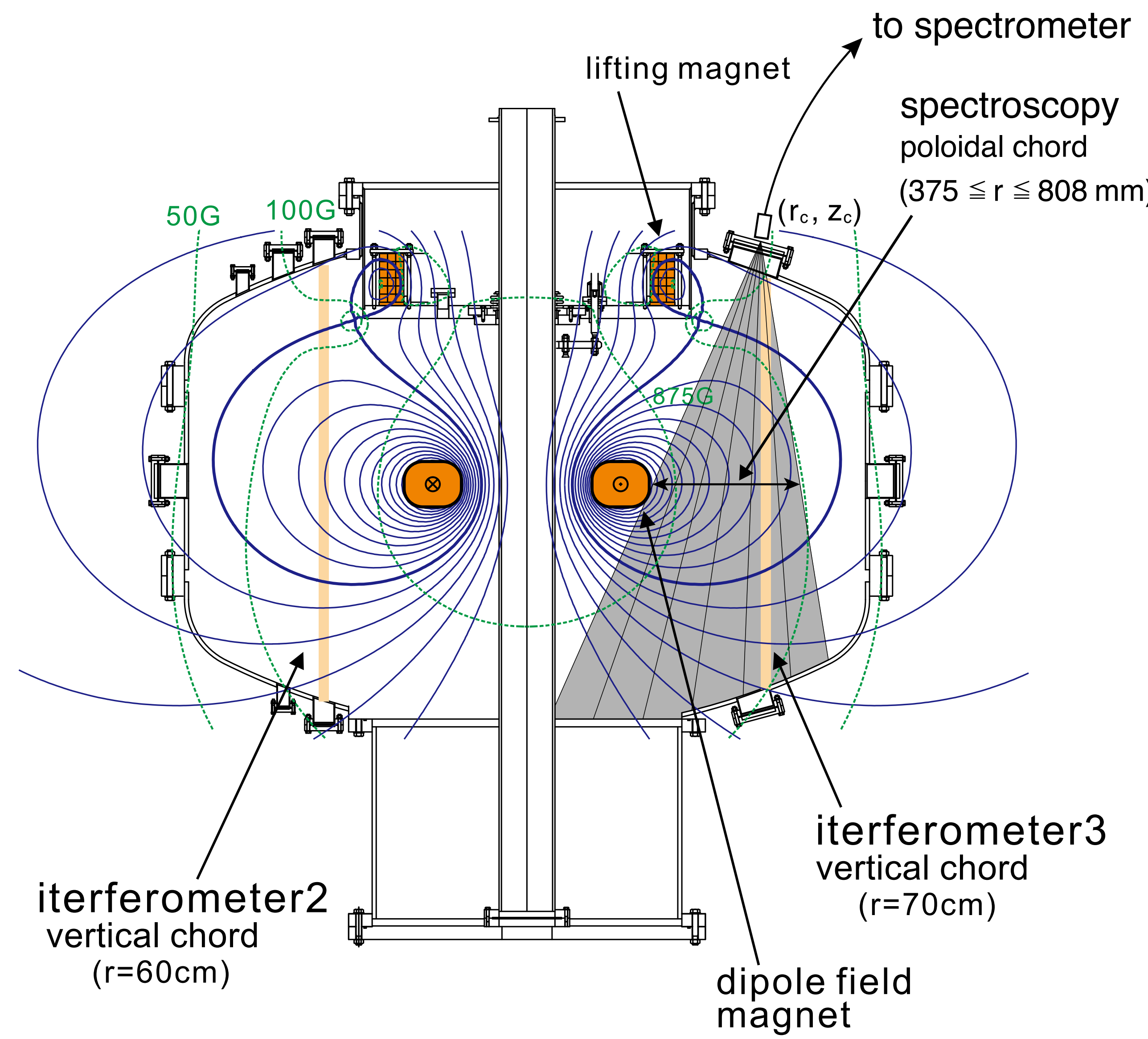

- ✓ In RT-1, electrons are heated by ECH → electron is not a good measure of anisotropy
- ✓ We measure ion temperature by Doppler spectroscopy
- ✓ RT-1 does not have toroidal field

➡ Horizontal line of sight → $T_\perp$, Vertical line of sight → $\sqrt{(T_\parallel^2 \cos^2\theta + T_\perp^2 \sin^2\theta)}$

(θ: angle between a magnetic field line and a line of sight)

Observation of ion temperature anisotropy

✓ Doppler broadening of He II (468.56nm) spectrum was measured to estimate T_{He+}

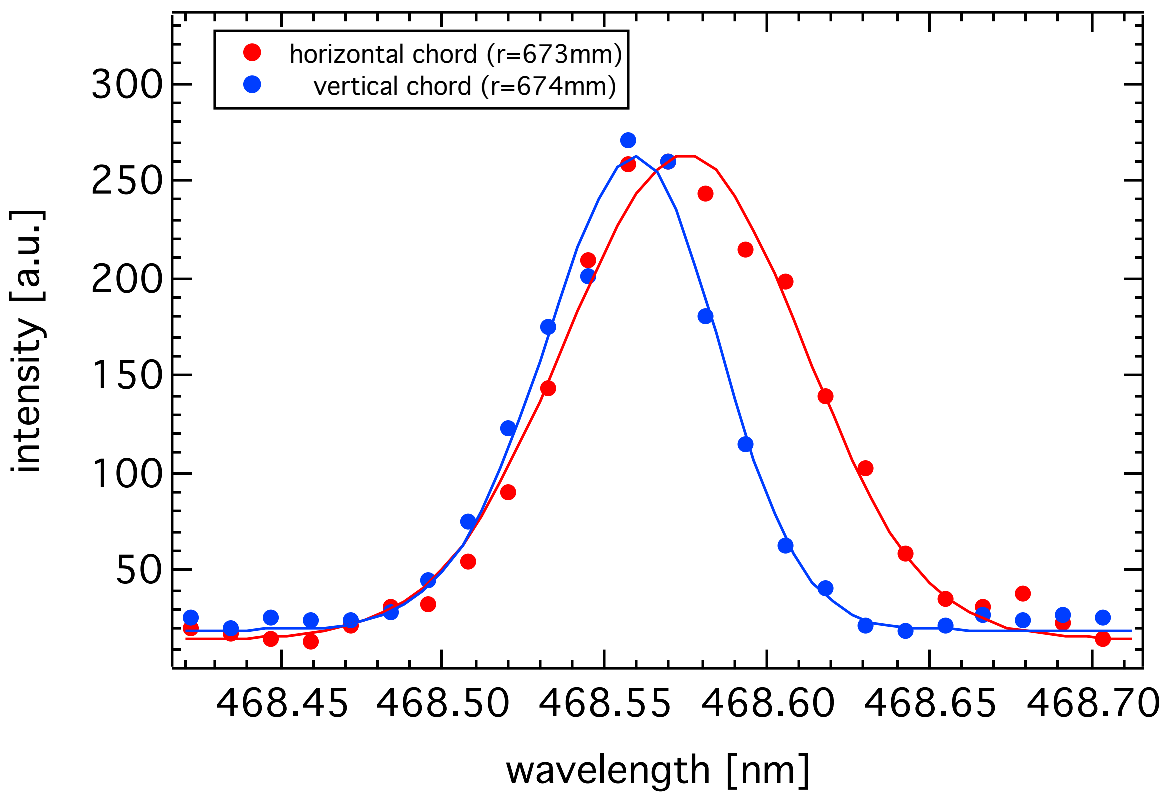

spectrum from He⁺ ion

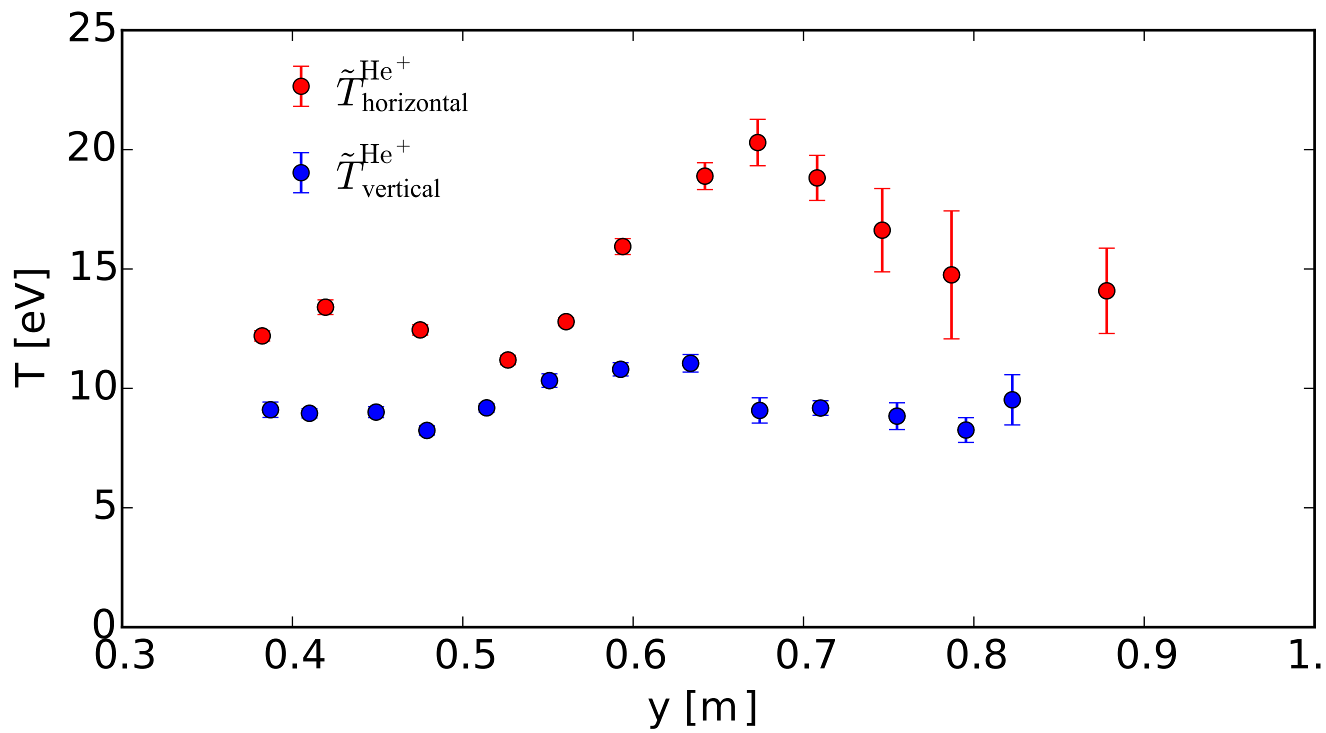

line averaged temperature profile

✓ We found ion temperature anisotropy ($T_{\perp} > T_{\|}$)

[1] Y. Kawazura, et al., Phys. Plasmas **22**, 112503 (2015).

Observation of ion temperature anisotropy

✓ Doppler broadening of He II (468.56nm) spectrum was measured to estimate $T_{\mathrm{He+}}$

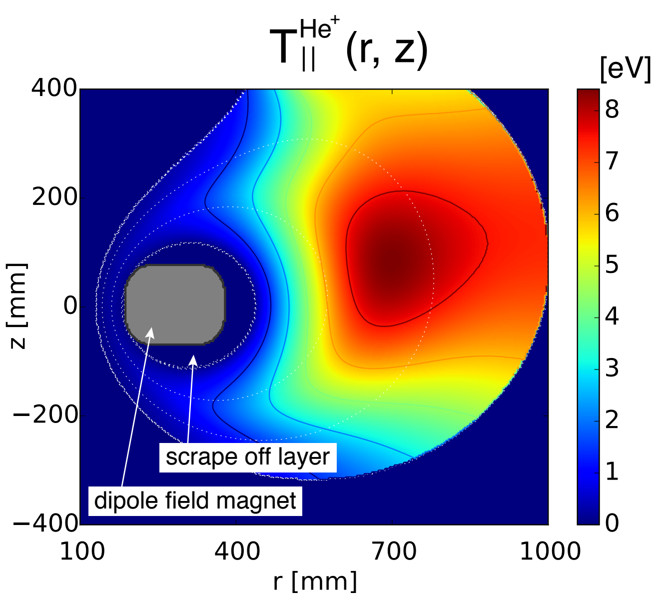

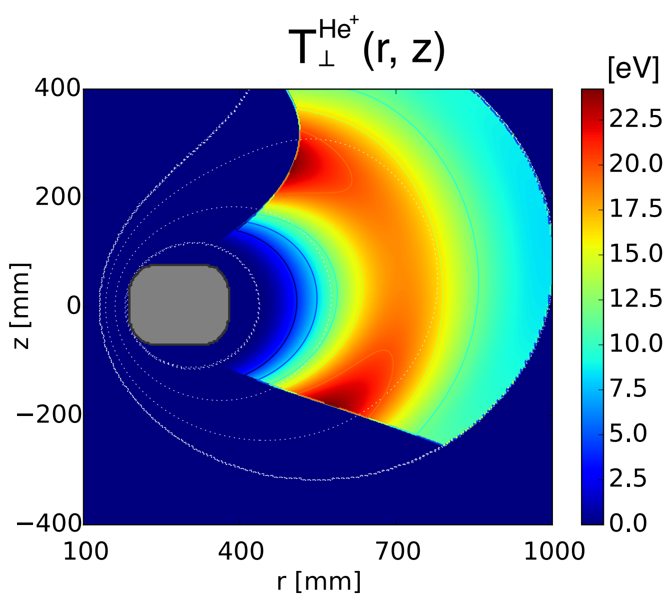

reconstructed 2D temperature profiles

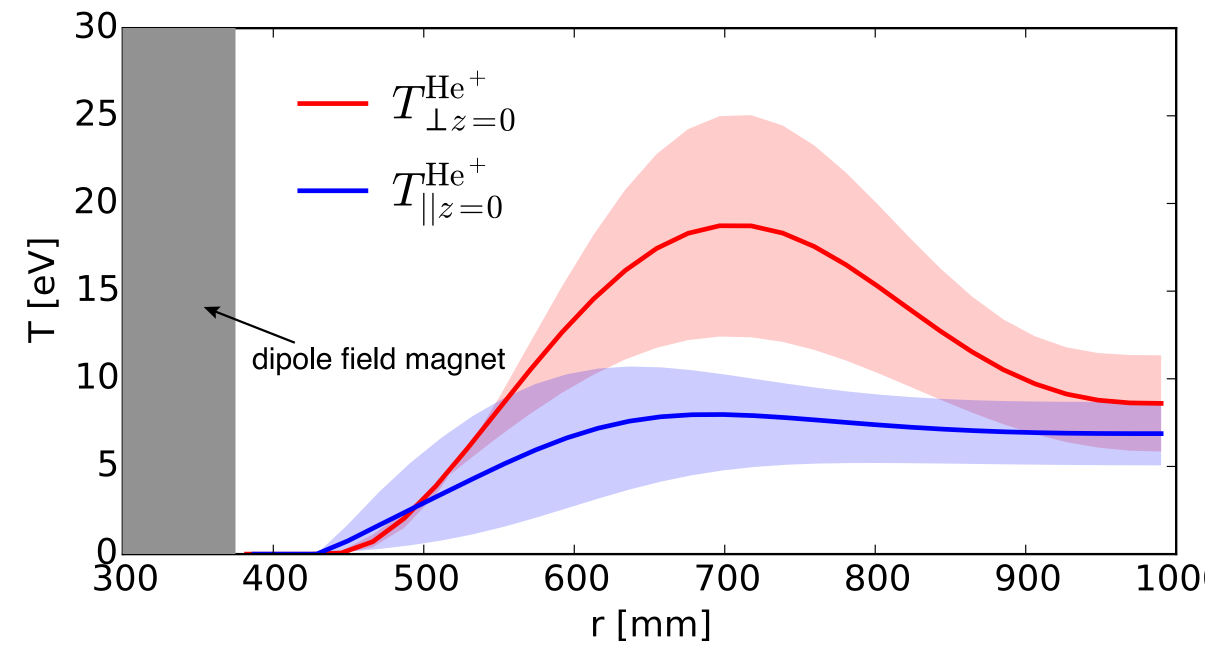

temperature on equatorial plane

✓ We found ion temperature anisotropy ($T_{\perp} > T_{||}$)

Is this anisotropy created by the adiabatic acceleration?

[1] Y. Kawazura, et al., Phys. Plasmas **22**, 112503 (2015).

Possible scenarios for anisotropy

① ~~Selective cooling of $T_{\parallel}$~~

- RT-1 is loss-cone-less

② ~~Selective heating of $T_{\perp}$ by relaxation with electrons created by ECH~~

- For the typical RT-1 parameters,

T_{ecold} = 50eV, $n_e = 1 \times 10^{17} m^{-3}$, T_i = 20eV

→ Ion/electron equipartition time $\tau^{EQ}_{He+/e-}$ ~ 600ms

Ion/ion isotropization time $\tau^{ISO}_{He+/He+}$ ~ 3ms

Although the only external injected power is ECH, the relaxation with electrons cannot explain the ions' anisotropy!

③ Selective heating of $T_{\perp}$ by betatron acceleration

Fermi acceleration

✓ As explained, for point dipole configuration,

betatron acceleration > Fermi acceration

$$B \propto r^{-3} \qquad\qquad L \text{ (bounce length)} \propto r^{1}$$

$$\downarrow \qquad\qquad \downarrow$$

$$v_\perp^2 = \frac{2\mu B}{m} \propto r^{-3} \qquad\qquad v_\parallel^2 \sim \left(\frac{J}{mL}\right)^2 \propto r^{-2}$$

✓ However, in RT-1, this is not applied

$$B \propto \rho^{-1.9} \longrightarrow v_\perp^2 \propto r^{-1.9} \qquad\qquad L \propto \rho^{1.7} \longrightarrow v_\parallel^2 \propto r^{-3.8}$$

✓ If μ and J are conserved, $T_\perp < T_\parallel$

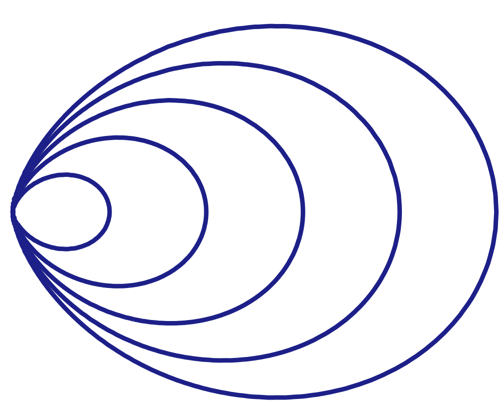

Point dipole

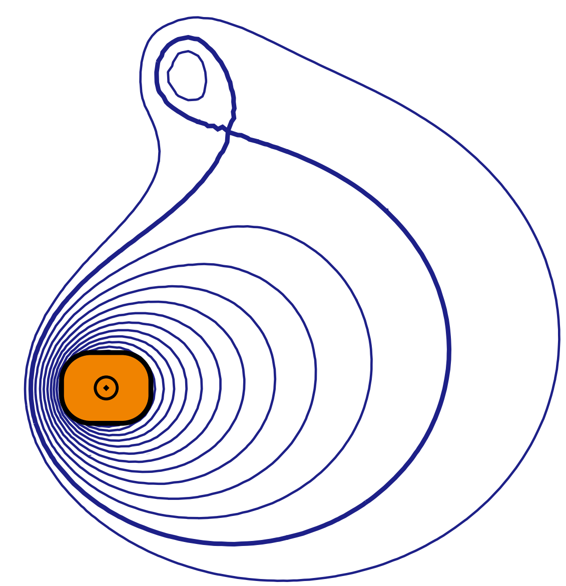

RT-1 configuration

Density fluctuation measured by a reflectometer

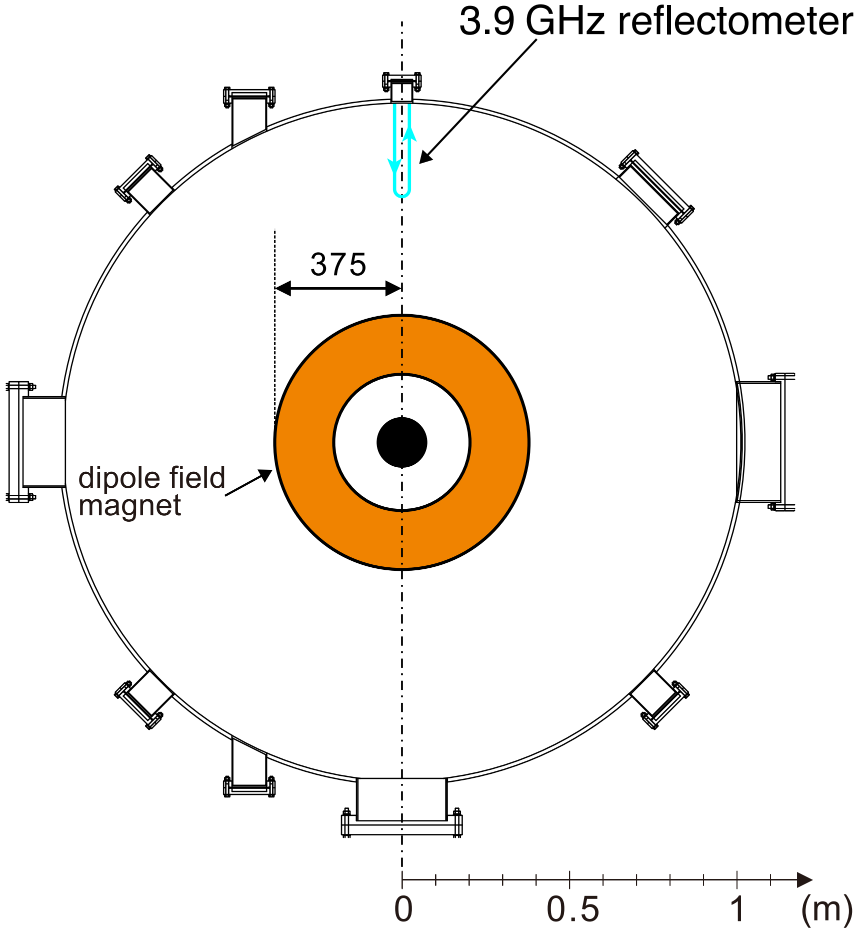

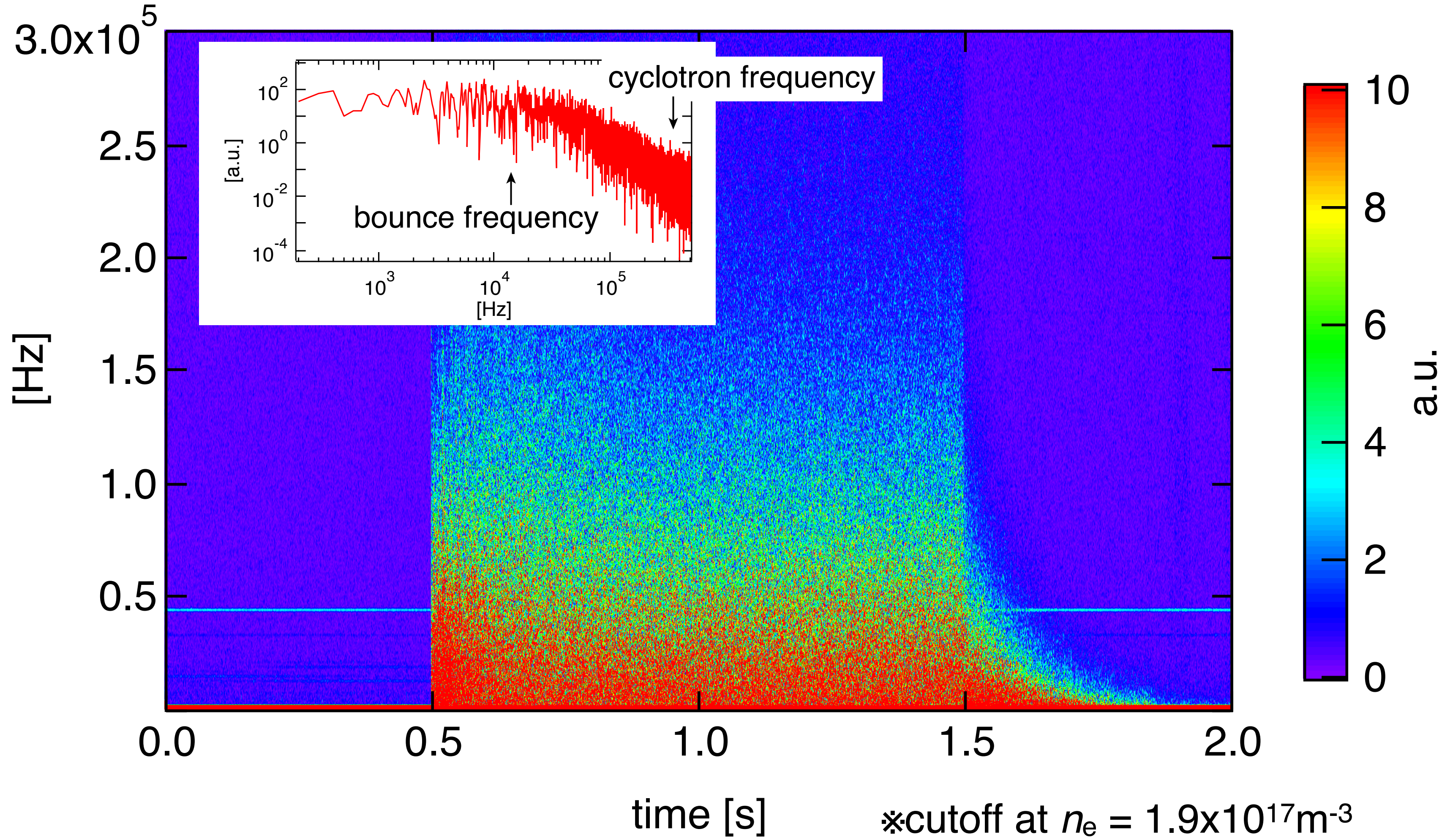

※cutoff at n_e = 1.9x10^{17}m^{-3}
r ~ 640mm for this shot

- ✓ When $T_{\parallel}$ = 10eV, bounce frequency of He is ~15kHz
  - ⇒ Existence of fluctuation near bounce frequency
    - ⇒ The second adiabatic invariant J is not conserved in RT-1
      - ⇒ Fermi acceleration is not working

We anticipate the anisotropy ($T_{\perp}$>$T_{\parallel}$) is created by a selective heating of $T_{\perp}$ through betatron acceleration

One dimensional ion energy balance model

- From Lagrangian fluid analogy, energy balance in a plasma element is modeled

$$\frac{\mathrm{d}T_\perp}{\mathrm{d}t} = \frac{T_\mathrm{e} - T_\perp}{\tau_\mathrm{ei}} - \frac{T_\perp - T_\parallel}{\tau_\mathrm{iso}} - \frac{T_\perp}{\tau_\mathrm{cx}} + P_\mathrm{betatron}$$

$$\frac{\mathrm{d}}{\mathrm{d}t}\left(\frac{T_\parallel}{2}\right) = \frac{T_\mathrm{e} - T_\parallel}{2\tau_\mathrm{ei}} + \frac{T_\perp - T_\parallel}{\tau_\mathrm{iso}} - \frac{T_\parallel}{2\tau_\mathrm{cx}}$$

$\frac{\mathrm{d}}{\mathrm{d}t} = V_r \frac{\mathrm{d}}{\mathrm{d}r}$: Lagrangian derivative given by inward diffusion speed V_r

τ_ei : electron-H^+ equipartition time

τ_iso : H^+ isotropization time

$\tau_\mathrm{cx} = \left(n_\mathrm{n} \langle \sigma v \rangle_\mathrm{cx}\right)^{-1}$: change exchange time

- Conservation of μ gives an estimate $P_\mathrm{betatron} \sim T_\perp V_r \left| \frac{\mathrm{d} \ln B}{\mathrm{d}r} \right|$

- The unknown variables are V_r and n_n which may be estimated from experimental data

Estimate of the inward diffusion speed V_r

- ✓ No direct measurement of V_r at the present stage
- ✓ Instead, we use time evolution of the interferometers at the discharge onset

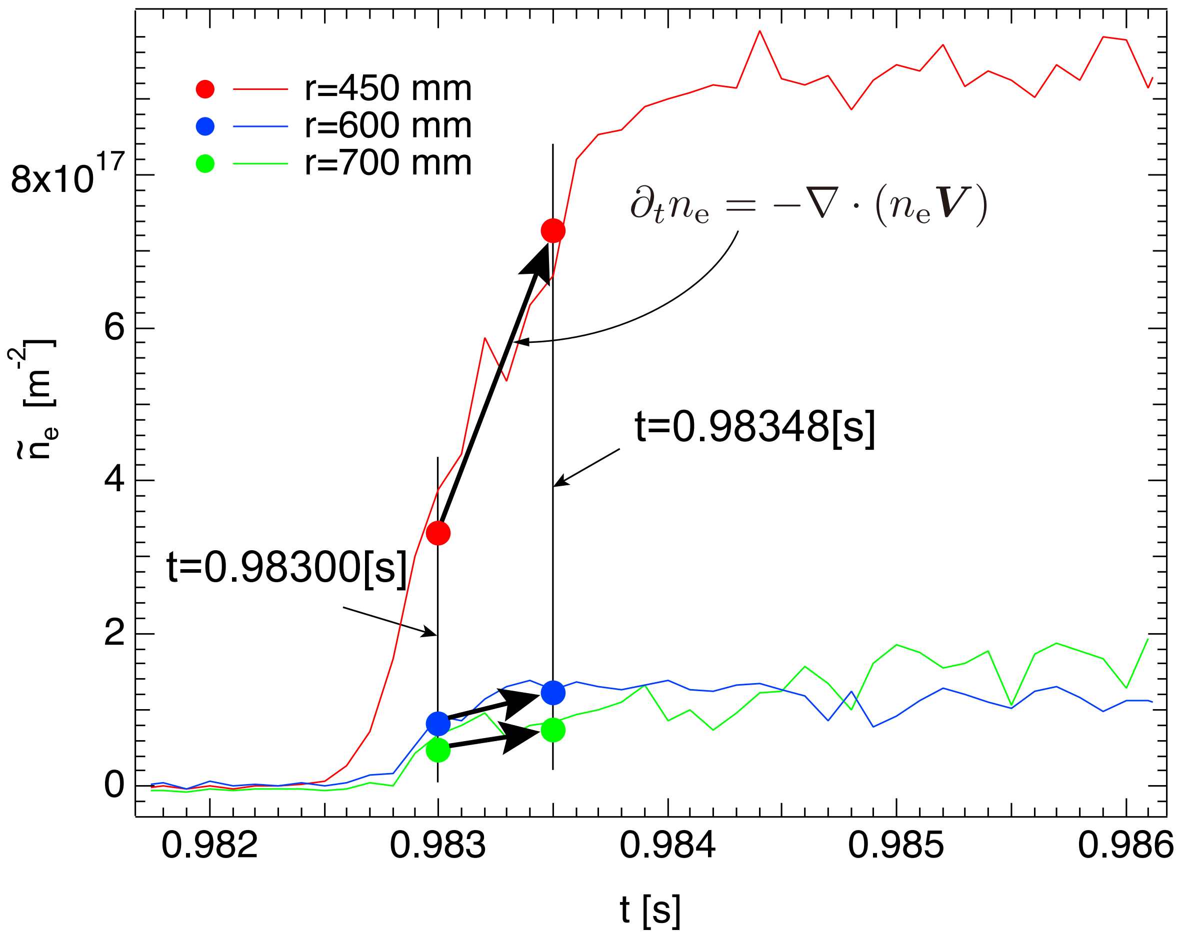

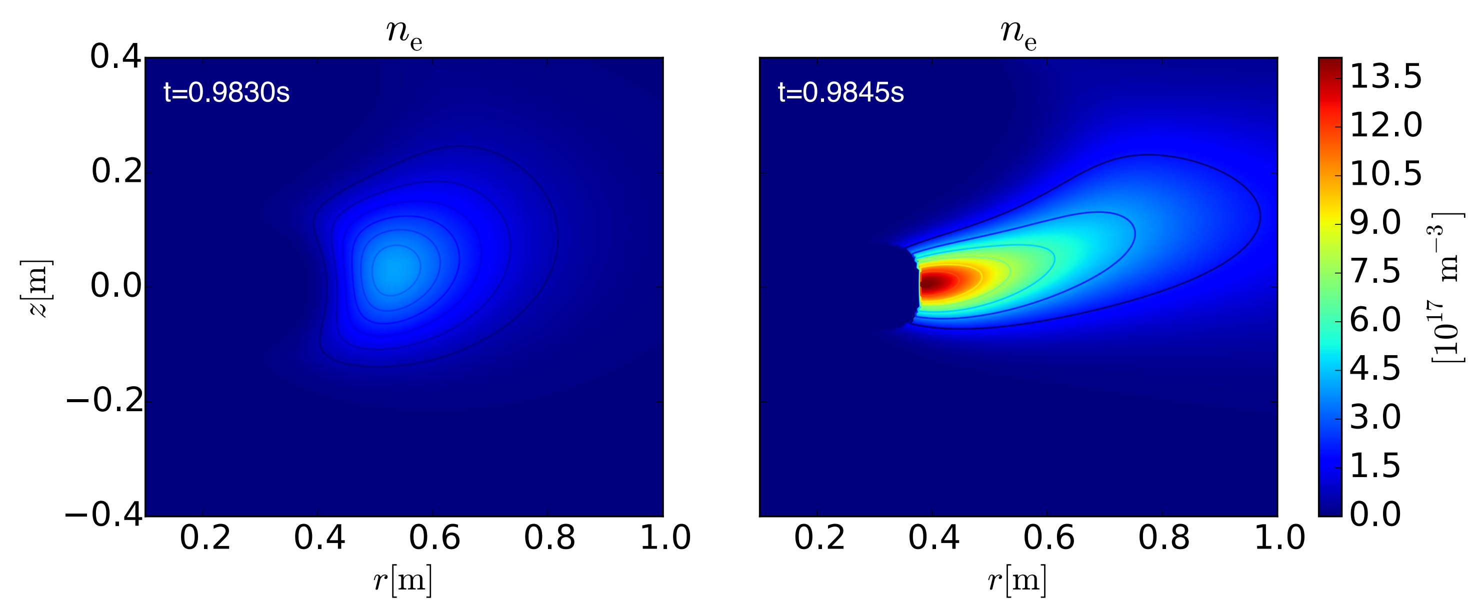

① Reconstruct 2D n_e profiles at given two instants

② Assume the two n_es are related by a continuity equation

$$\frac{n_e^1 - n_e^0}{\Delta t} = -\nabla \cdot (n_e V) \quad \longrightarrow \quad \text{Estimate } V$$

Estimate of the inward diffusion speed V_r

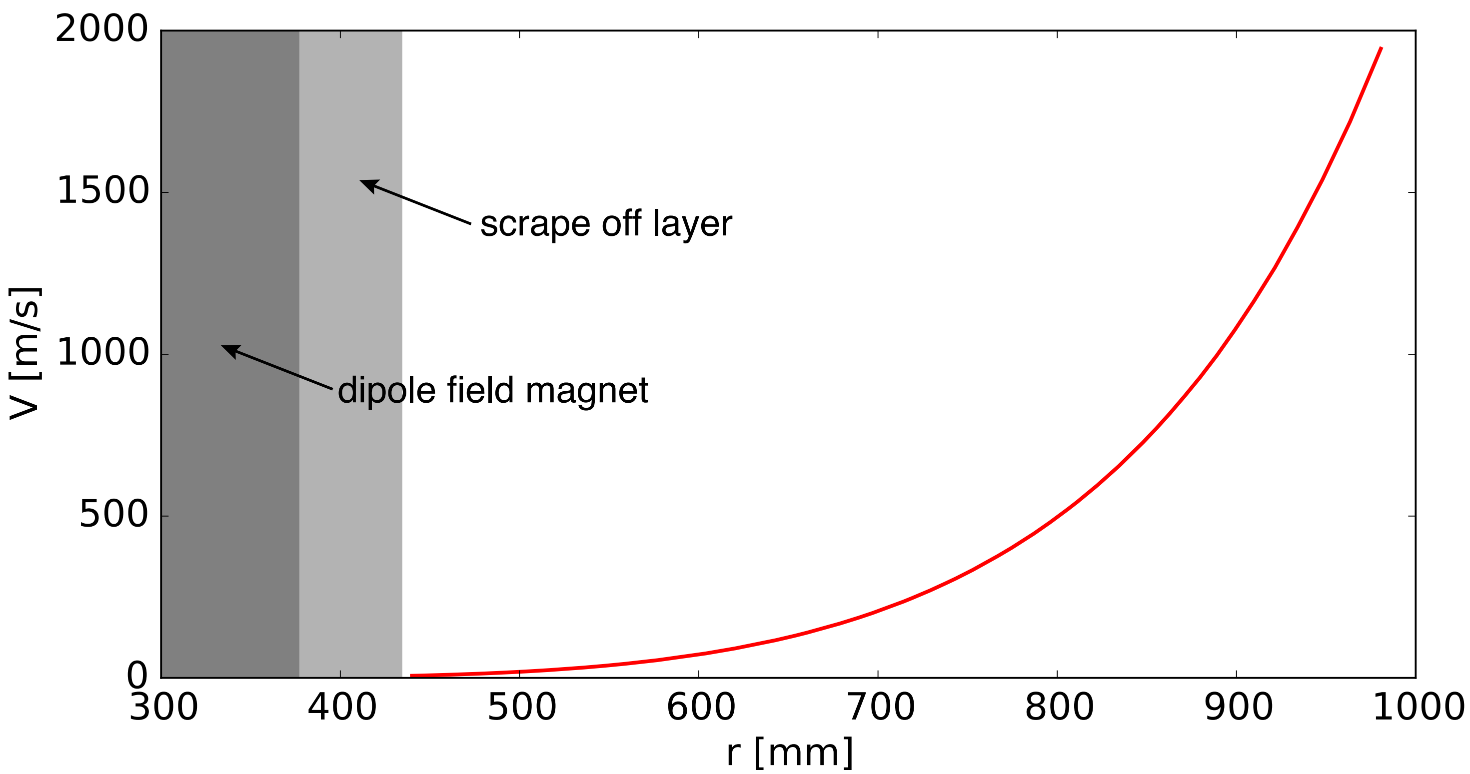

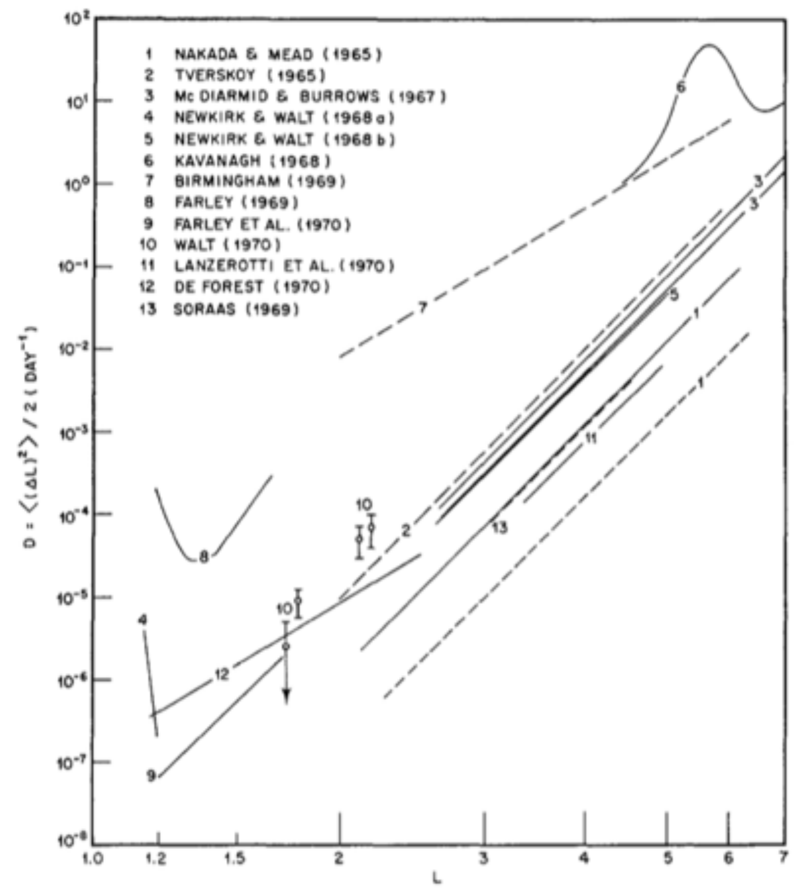

Fig. 18. Experimental (solid lines) and theoretical (dashed lines) values of the radial diffusion coefficient.

- V_r is increasing function with respect to r
- Consistent with the planetary cases (observation & simulation) [1]
- The absolute value of V_r is also consistent with the estimate by LDX experiment [2]

- We assume that V_r is the same for the rest of the discharge

[1] M. Walt, Introduction to Geomagnetically Trapped Radiation, (Cambridge Univ. Press, 1994.)
[2] A. C. Boxer, et al., Nat. Phys. **6**, 207 (2010).

Estimate of the neutral particle density n_n

- ✓ Neutral particle density
  - Mean free path of a neutral particle $\lambda = \dfrac{v_\mathrm{n}}{n_\mathrm{e}\langle\sigma v\rangle_\mathrm{ion}}$

v_n thermal speed of neutral particles

$\langle\sigma v\rangle_\mathrm{ion}$ ionization rate coefficient

- ✓ Estimate v_n from a Doppler broadening of He I spectrum (471.4nm)
- ✓ T_n ~ 0.7eV, n_e ~ $10^{17}\mathrm{m}^{-3}$, T_ecold ~ 30eV → λ > 1m > device size

  ➡ n_n = constant (neutral particles exists uniformly)

- ✓ We also estimate the absolute value of n_n by solving an ionization rate equation
- ✓ Since there are appreciable emission from He I and He II lines, n_n ~ n_e is plausible

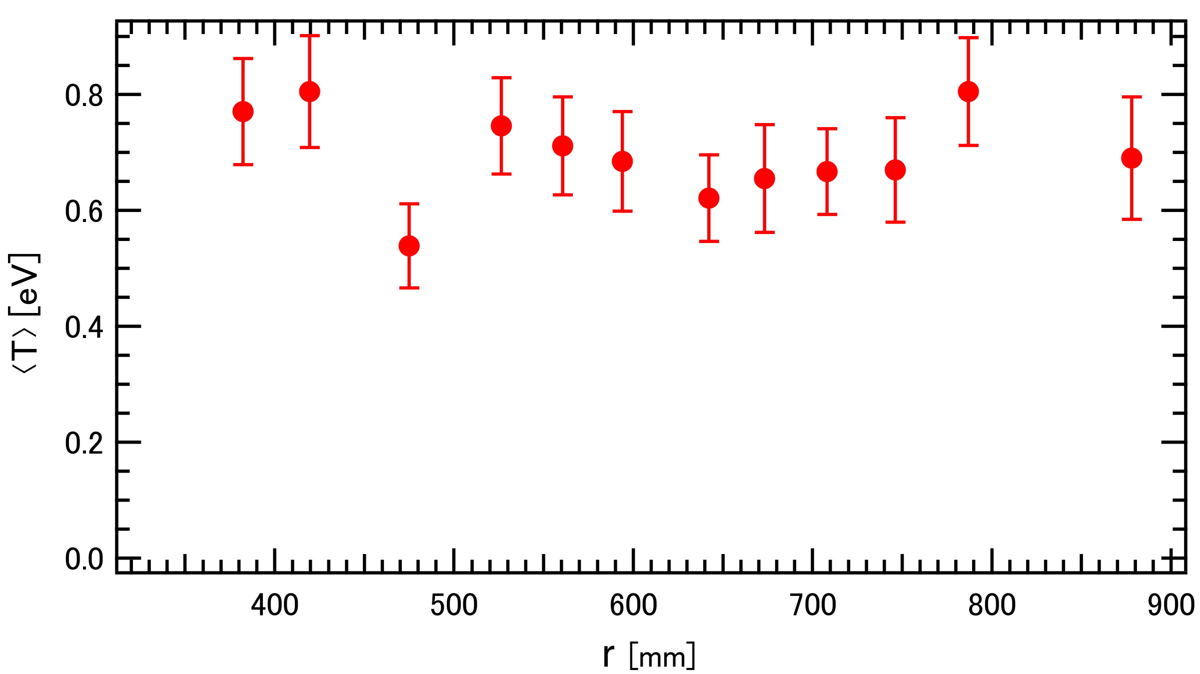

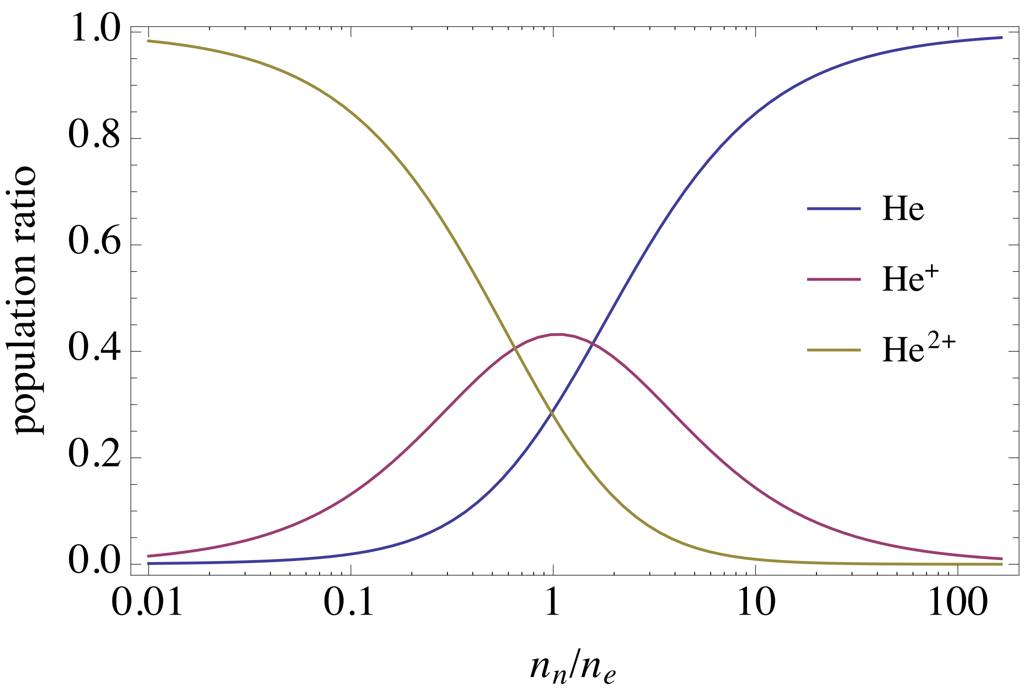

Numerical solution of the energy balance model

- Now we may solve the energy balance equation
- Numerical settings:

  neutral density : $n_n \sim n_e = 10^{17}$ m^{-3},

  initial condition (temperature at t=0, r=1000mm) : 8eV (from the observation)

Experiment

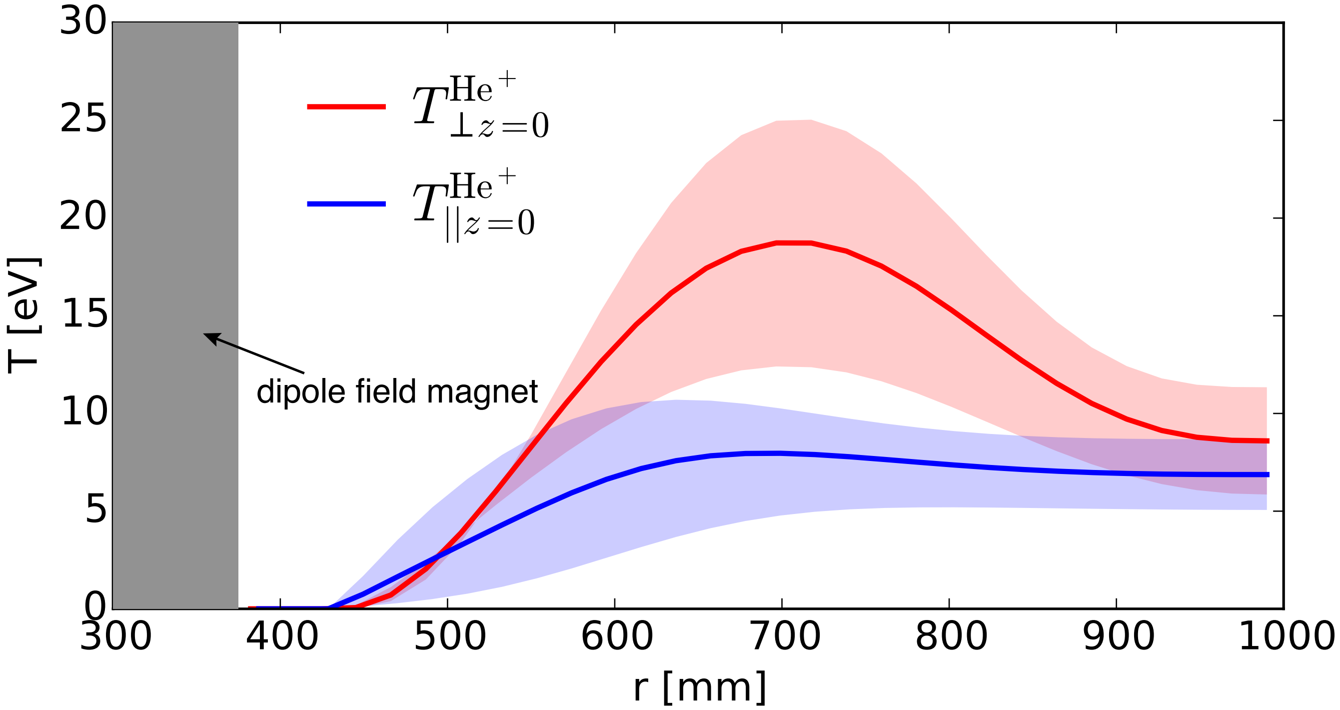

Simulation of the energy balance model

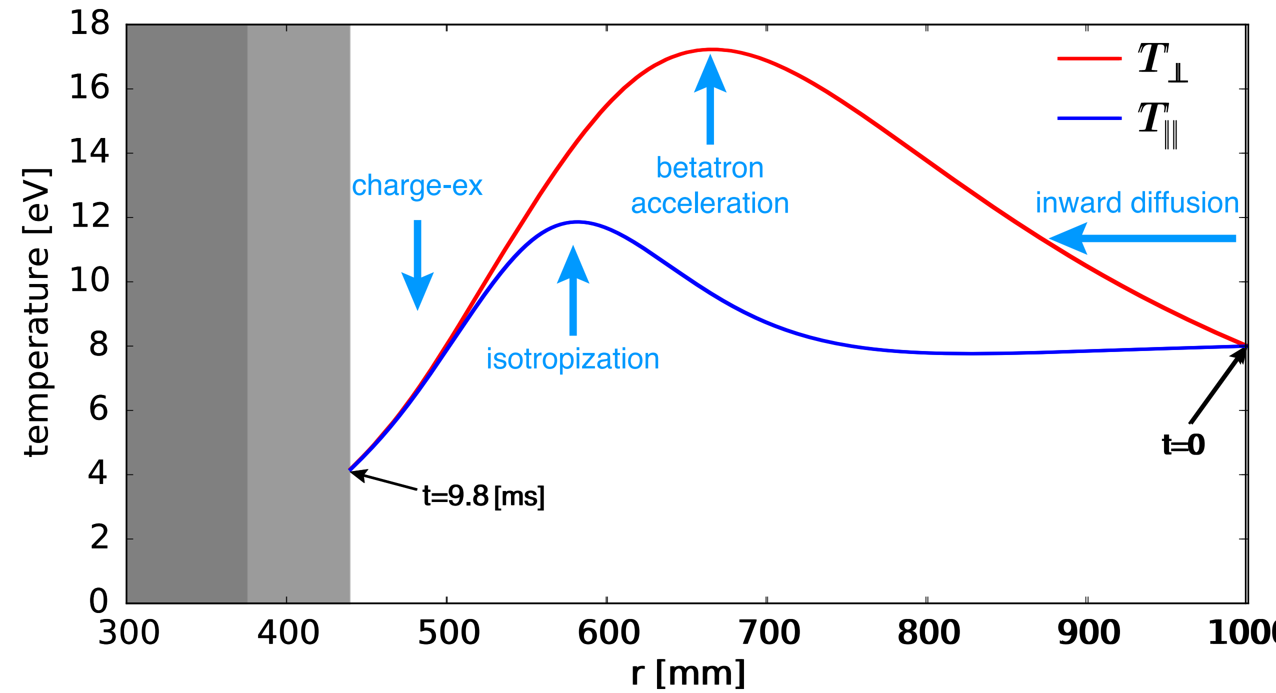

- Simulation result shows a good agreement with the experimental result
- Electron does not contribute during the inward diffusion, but determines the initial temperature

Scaling of temperature and anisotropy

	Experiment	Energy balance model	
Dependence of temperature on ECH power	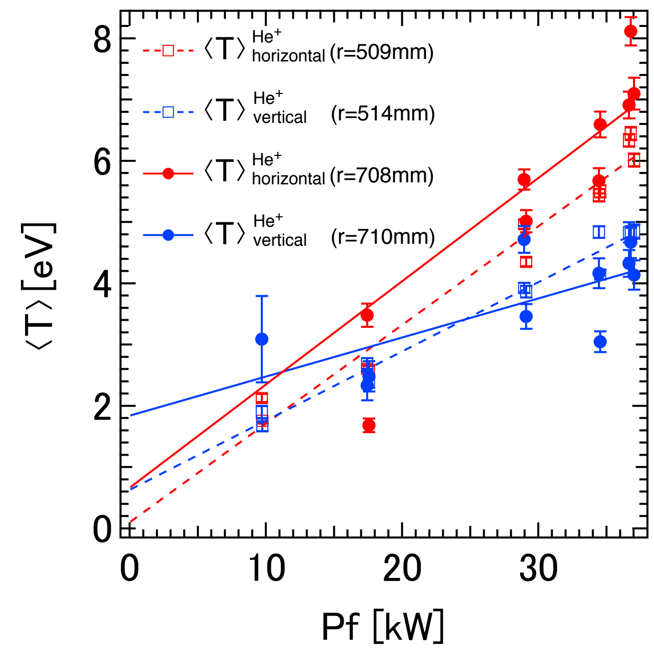	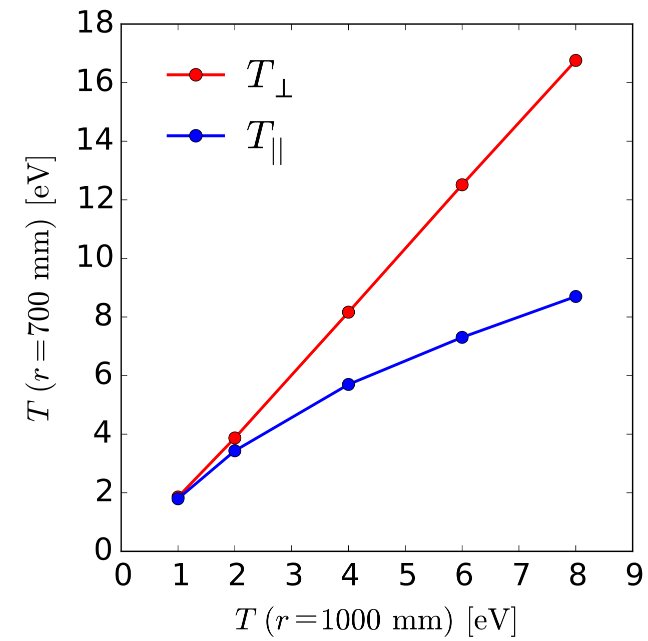	Dependence of temperature on initial temperature
Dependence of anisotropy on ECH power	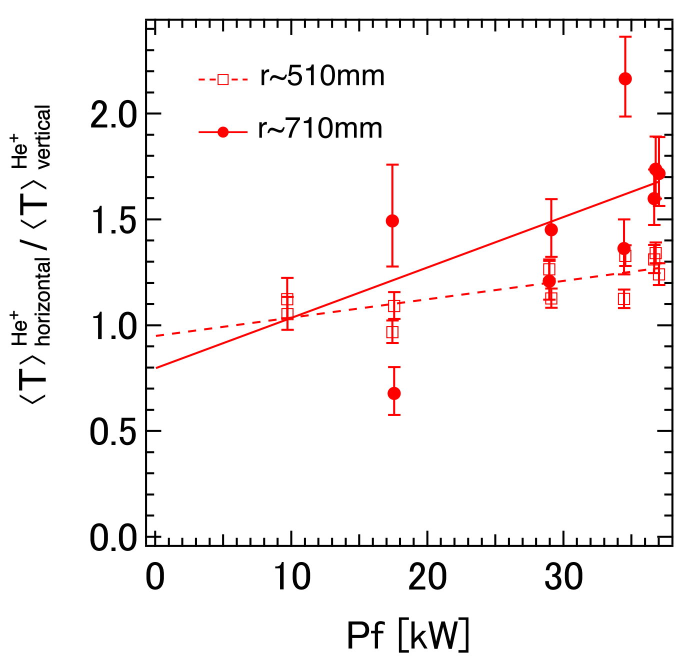	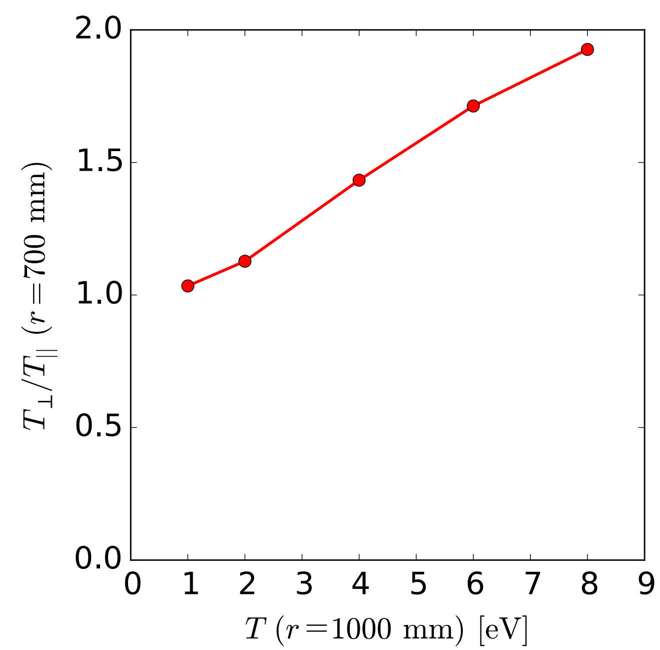	Dependence of anisotropy on ECH power

✓ ECH power ↗ ⇒ initial temperature ↗ ⇒ $P_{betatron}$ $\left(= T_\perp V_r \left|\frac{d\ln B}{dr}\right|\right)$ ↗

⇒ $T_\perp$ & anisotropy ↗ ⇒ $T_{||}$ ↗ by isotropization ↘

Scaling of temperature and anisotropy

Experiment | **Energy balance model**

Dependence of temperature on neutral density

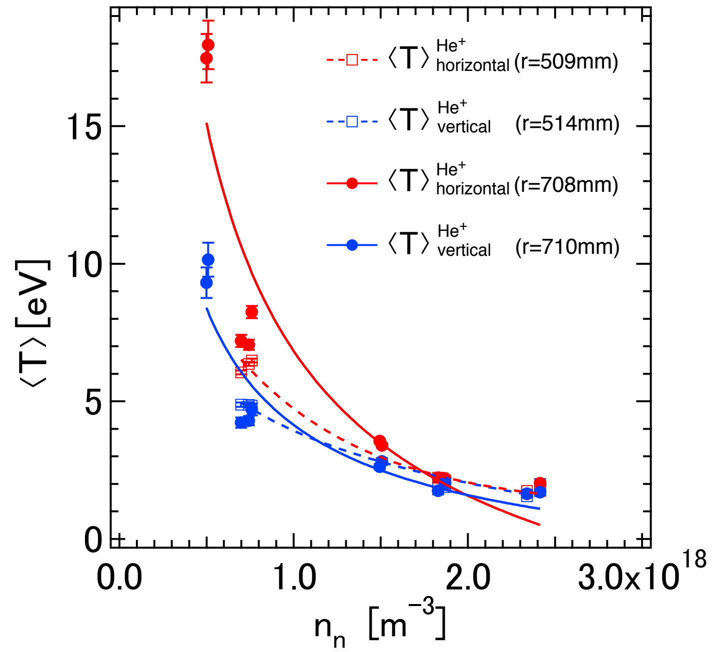

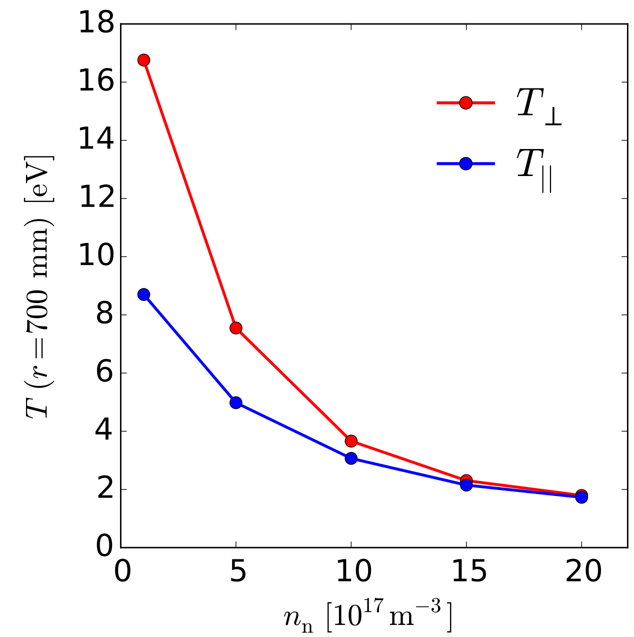

Dependence of temperature on neutral density

Dependence of anisotropy on neutral density

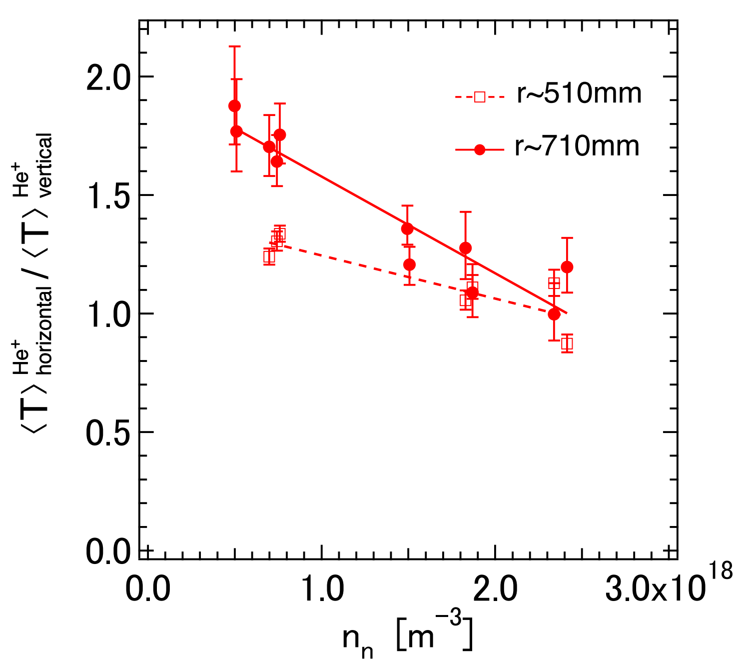

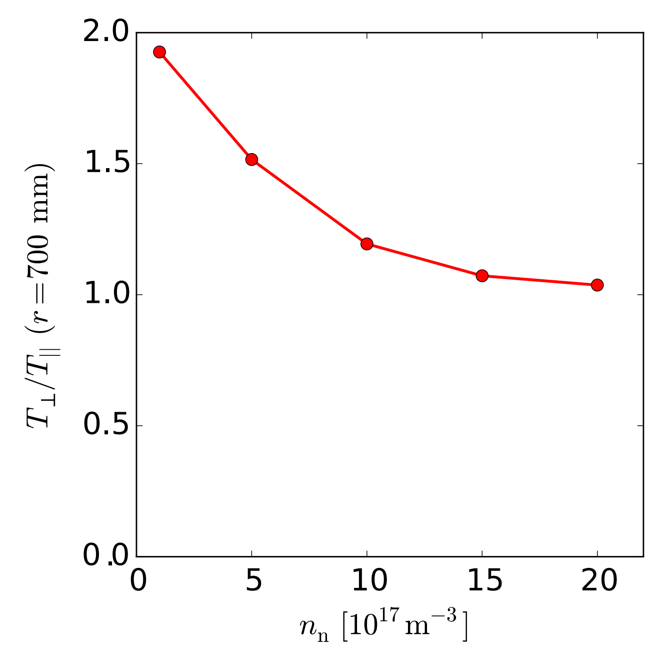

Dependence of anisotropy on neutral density

- ✓ neutral density ↗ ⇒ charge exchange loss (isotropic) ↗ ⇒ $T_\perp$ & anisotropy ↘
- ✓ Experimental scaling justify the proposed ion heating scenario

Simulation of the diffusion equation showing anisotropy

Rigorously formulated diffusion equation

$$
\begin{aligned}
\frac{\partial P}{\partial t} = & -v_{\parallel}\frac{\partial P}{\partial \ell} + \frac{\partial}{\partial v_{\parallel}}\left[\left(\frac{\langle \mu \rangle_v}{m}\frac{\partial B}{\partial \ell} + \gamma v_{\parallel}\right)P\right] \\
& -\left(\frac{1}{2}-\alpha\right)D_{\perp}\frac{\partial}{\partial \psi}\left\{\left[\left(\mathfrak{q}\frac{\partial}{\partial \ell}+\frac{\partial}{\partial \psi}\right)\ln(rB)\right]P\right\} \\
& -\left(\frac{1}{2}-\alpha\right)D_{\perp}\frac{\partial}{\partial \ell}\left\{\left[\mathfrak{q}\left(\mathfrak{q}\frac{\partial}{\partial \ell}+\frac{\partial}{\partial \psi}\right)\ln(rB)\right]P\right\} \\
& -\frac{1}{2}D_{\perp}\frac{\partial}{\partial \ell}\left\{\left[\left(\mathfrak{q}\frac{\partial}{\partial \ell}+\frac{\partial}{\partial \psi}\right)\mathfrak{q}\right]P\right\} \\
& +\frac{1}{2}D_{\perp}\frac{\partial^2}{\partial \ell^2}\left(\mathfrak{q}^2 P\right) + D_{\perp}\frac{\partial^2}{\partial \ell \partial \psi}(\mathfrak{q}P) \\
& +\frac{1}{2}D_{\perp}\frac{\partial^2 P}{\partial \psi^2} + \frac{1}{2}D_{\parallel}\frac{\partial^2 P}{\partial v_{\parallel}^2}.
\end{aligned}
$$

$\longrightarrow$

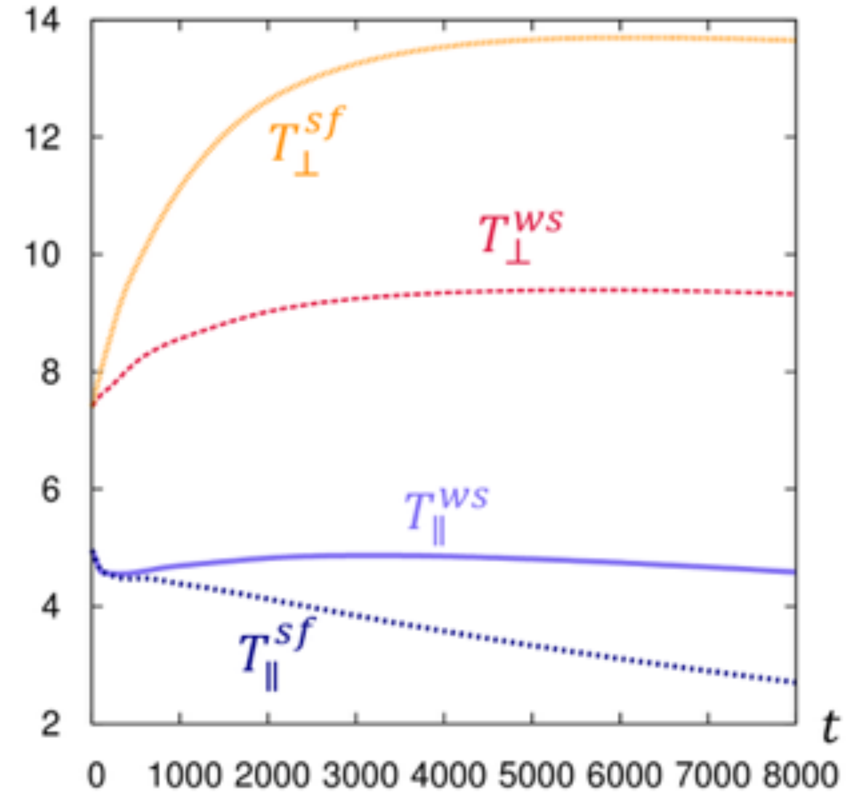

Fig. 1 Spatially averaged normal and parallel temperatures $T_{\perp}$(eV) and $T_{\parallel}$(eV) as a function of time t(a.u.). sf stands for strong and fast diffusion. ws for weak and slow diffusion. The former case has a diffusion parameter $D_{\perp}$ ten times greater than the latter.

- ✓ Enhanced anisotropy emerges via violation of $J_{\parallel}$ by short time scale fluctuation (i.e. strong $D_{\perp}$)
  - ➡ supporting the ion heating scenario in RT-1
- ✓ Moreover, it is revealed that preferential heating effect of $T_{\perp}$ increases for strong and fast diffusion

[1] N. Sato, Z. Yoshida, and Y. Kawazura, Plasma Fusion Res. **11** 2401009 (2016).

Broad component of Hα line

- ✓ Proton temperature is not measurable by a Doppler spectroscopy
- ✓ In astrophysics, proton temperature near a shock in a supernova remnant has been INDIRECTLY estimated by a **broad component** of Hα spectrum
- ✓ Broad component = hot hydrogen particles produced through charge exchange between post-shock protons
- ✓ Narrow component = cold hydrogen atoms in pre-shock interstellar medium
- ✓ Broad component of Hα has been also observed in laboratory plasma with three components (hot, warm, and cold) [2]
- ✓ However, in laboratory plasma, there is a discrepancy between proton temperature and broad component [3]
  - ➡ many competitive processes to generate hot neutrals (dissociation and reflection at a wall)

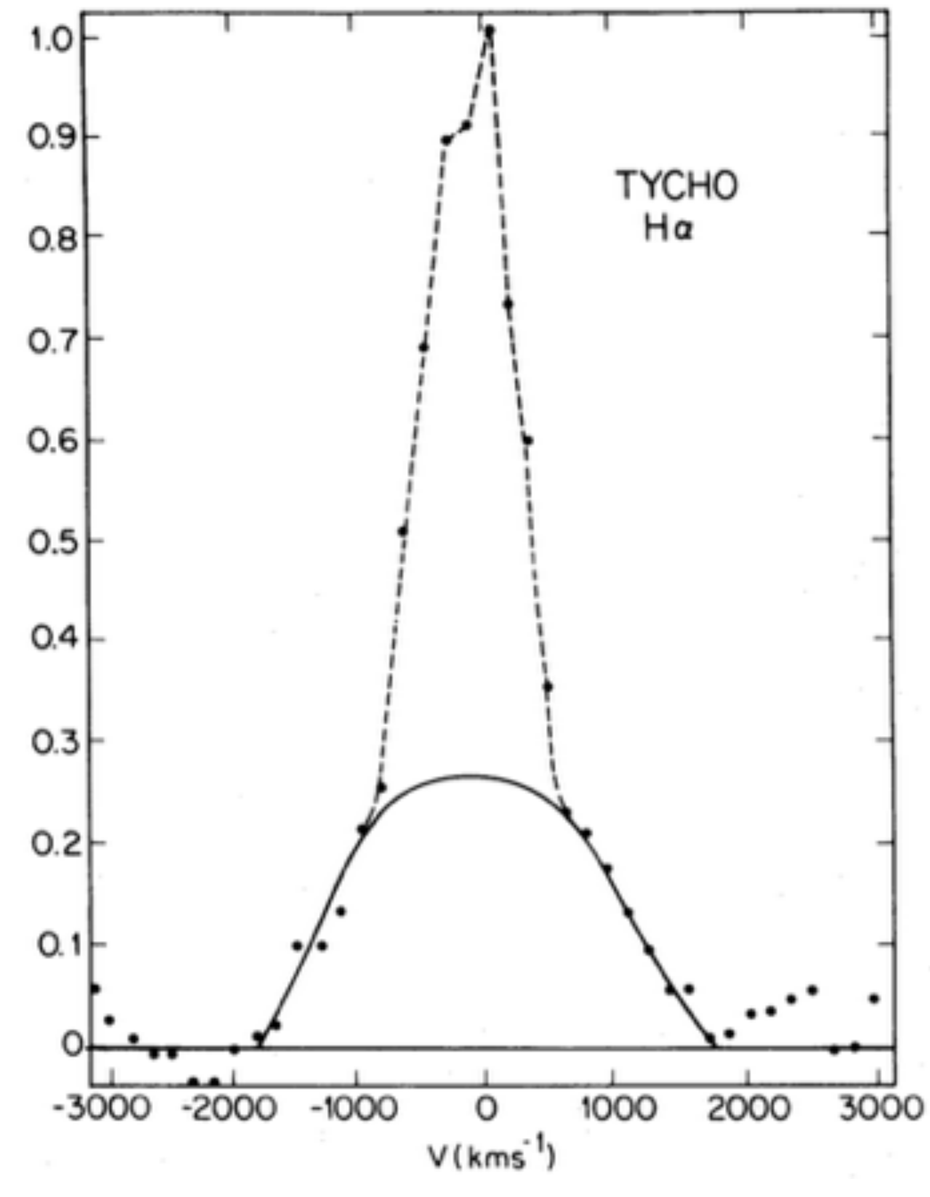

[1] R. A. Chevalier et al., ApJ, **235**, 186 (1980).
[2] S. Kasai et al., Jpn. J. Appl. Phys. **17**, 903 (1978). [3] H. Kubo et al., Plasma. Phys. Control. Fusion **40**, 1115 (1998).

Anisotropy of proton temperature

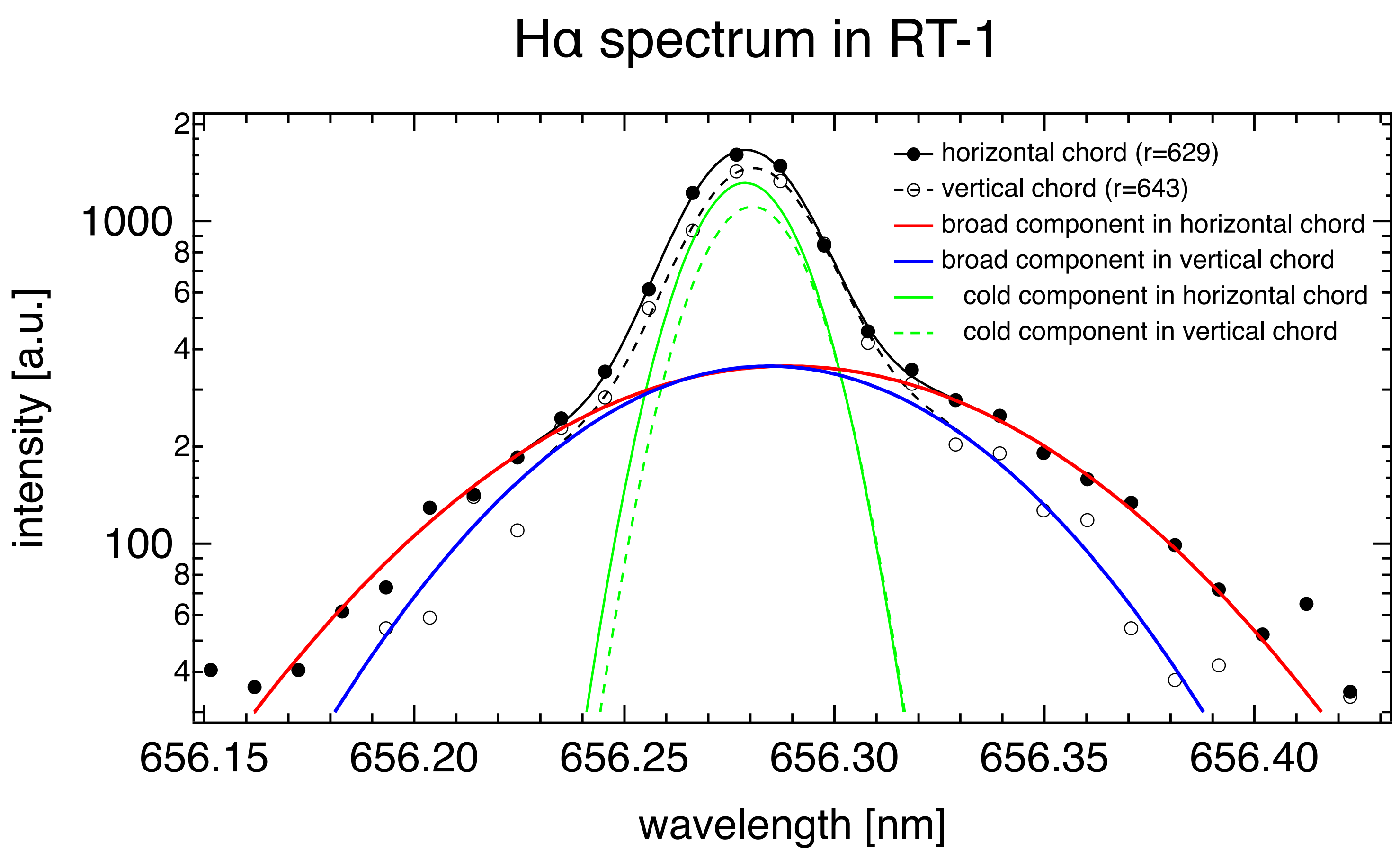

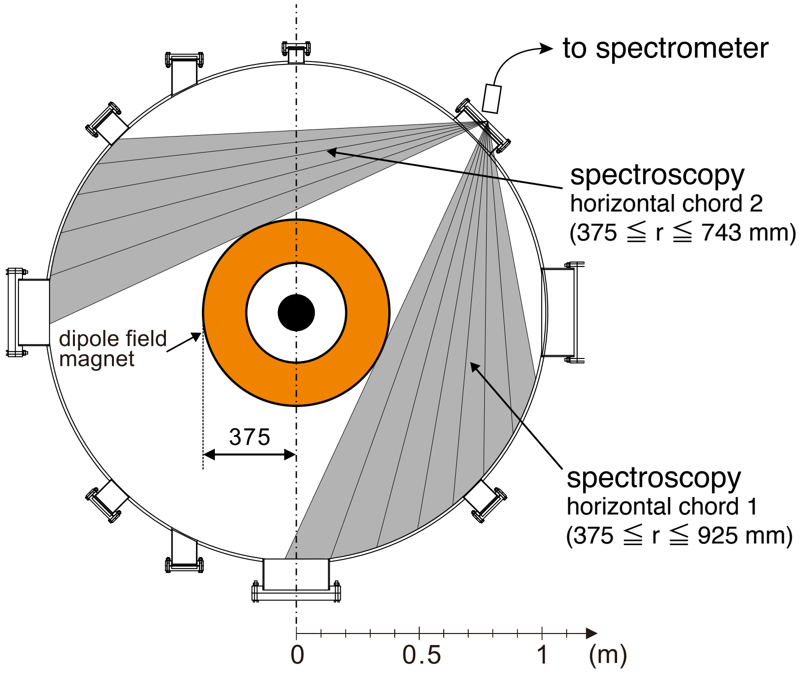

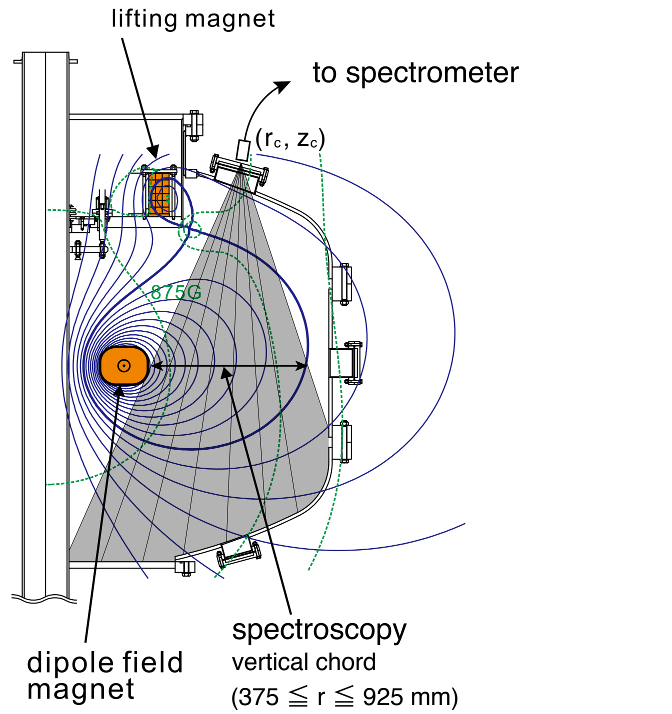

- ✓ Broad (hot) component is observed in RT-1
- ✓ Only the hot component from horizontal line of sight has Doppler shift
  - ➡ No flow of narrow (cold) component & no poloidal flow of hot component
- ✓ The hot component is anisotropic ($T_\perp > T_\parallel$) & the cold component is isotropic
  - ➡ hot component anisotropy = proton anisotropy

[1] Y. Kawazura, et al., Plasma Fusion Res. **11** 2402024 (2016).
[2] B. Wan et al., Nucl. Fusion 39, 1865 (1999).

Temperature & flow profile of hot/cold neutrals

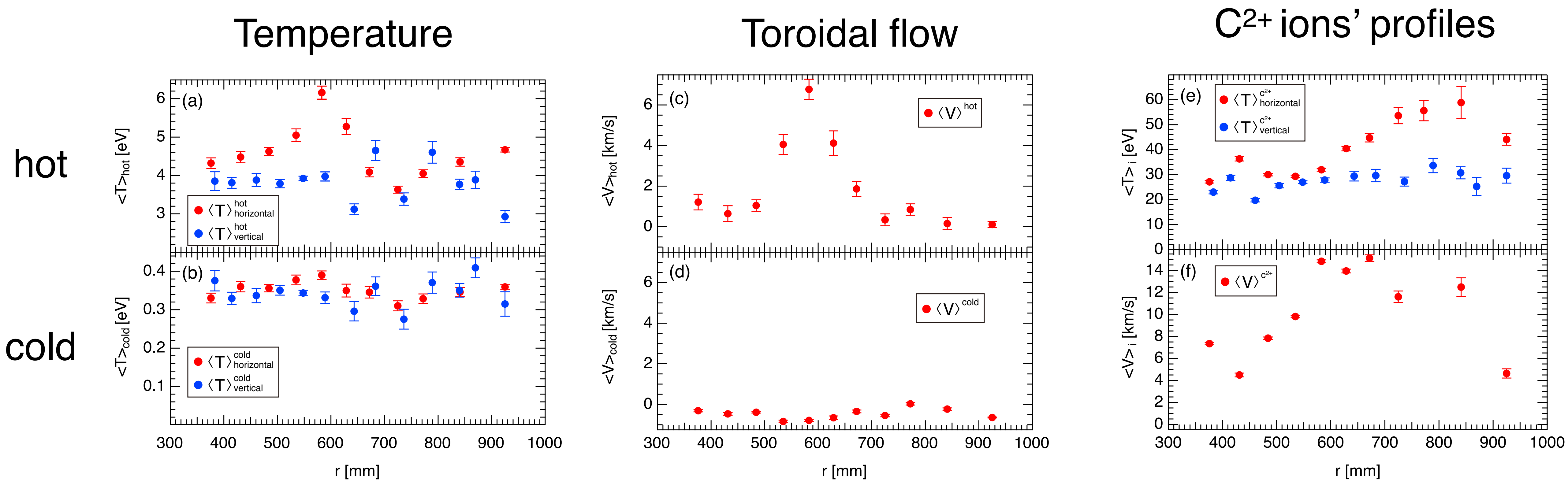

✓ The hot neutrals have non-uniform temperature & toroidal flow profile

✓ The cold neutrals are homogeneous

✓ However, the profiles are not similar to C^{2+} ions' profiles

➡ As in the preceding study, other processes to create hot neutrals are competing

➡ We may separate the competitive processes by analyzing Hα line shape [1]

[1] B. Wan et al., Nucl. Fusion 39, 1865 (1999).

Scaling of temperature and anisotropy

Temperature | **Anisotropy**

Dependence of temperature & anisotropy on ECH power

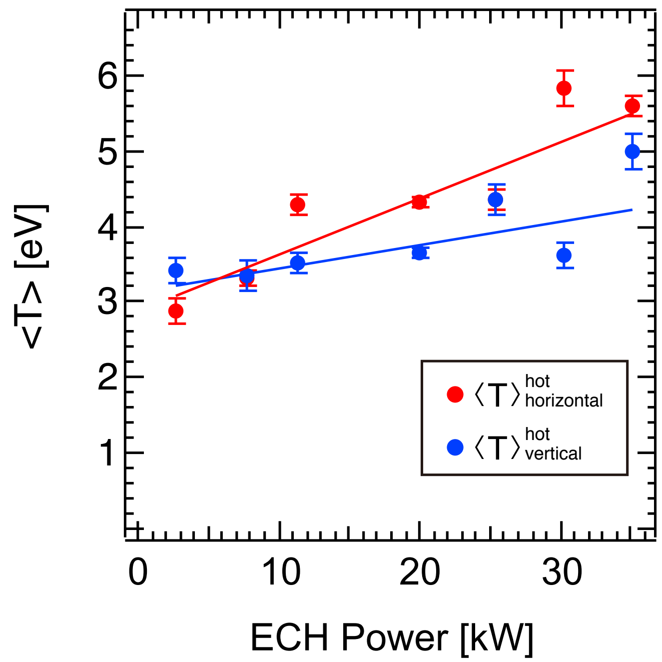

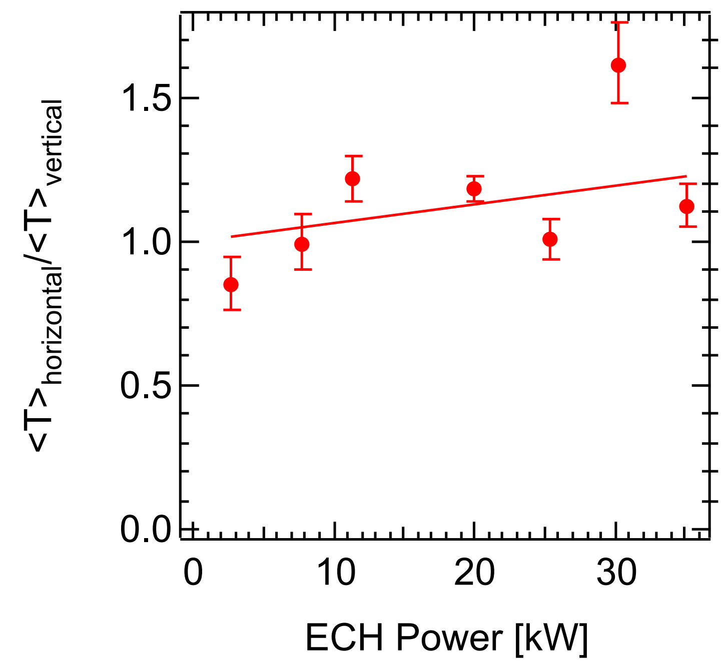

Dependence of temperature & anisotropy on filling gas pressure

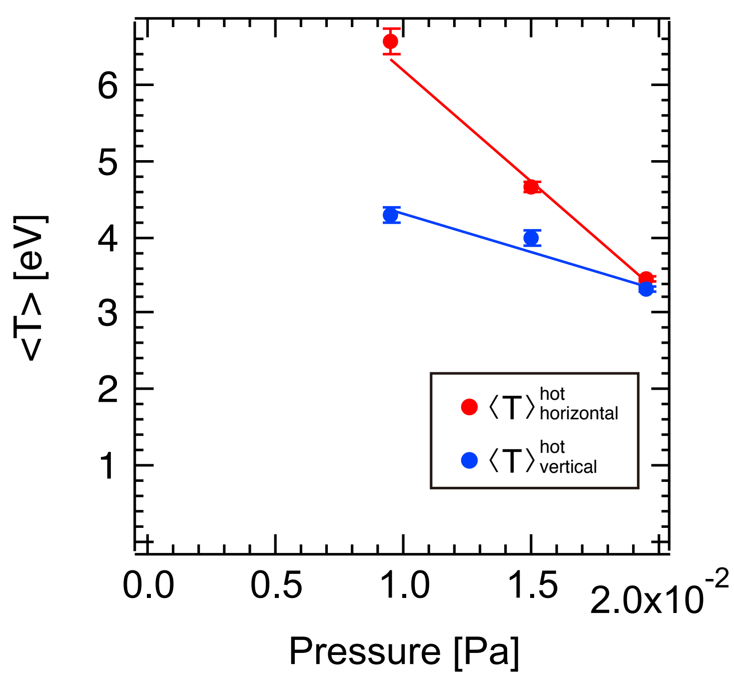

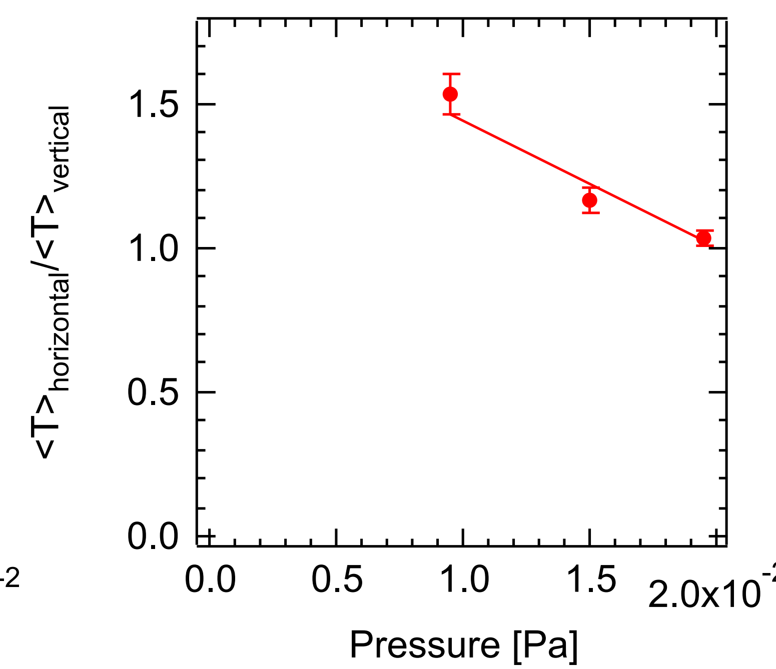

✓ The experimental scaling of hot neutral temperature & anisotropy is consistent with that of ions (and then with the ion energy balance model)

Hot neutrals are isotropic in a Tokamak

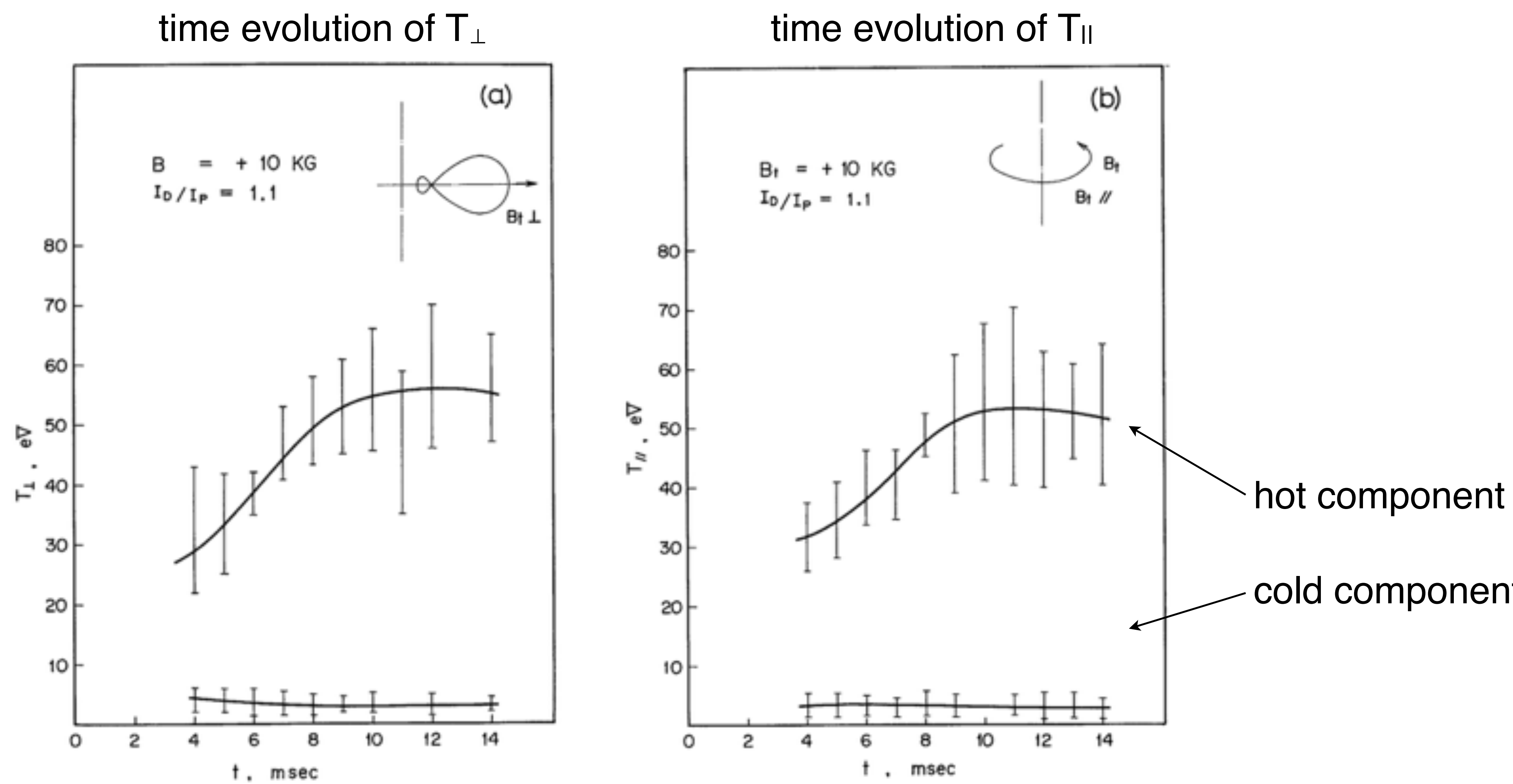

✓ In the old experiments in JFT-2a tokamak, Doppler spectroscopic measurement of Hα with tangential and perpendicular line of sight was conducted [1]

✓ The measured hot neutrals were almost isotropic

➡ Anisotropic hot neutrals are distinctive to a magnetospheric configuration

[1] S. Kasai, et al., Jpn. J. Appl. Phys. 17, 903 (1978).

Inward diffusion in non-neutral plasma

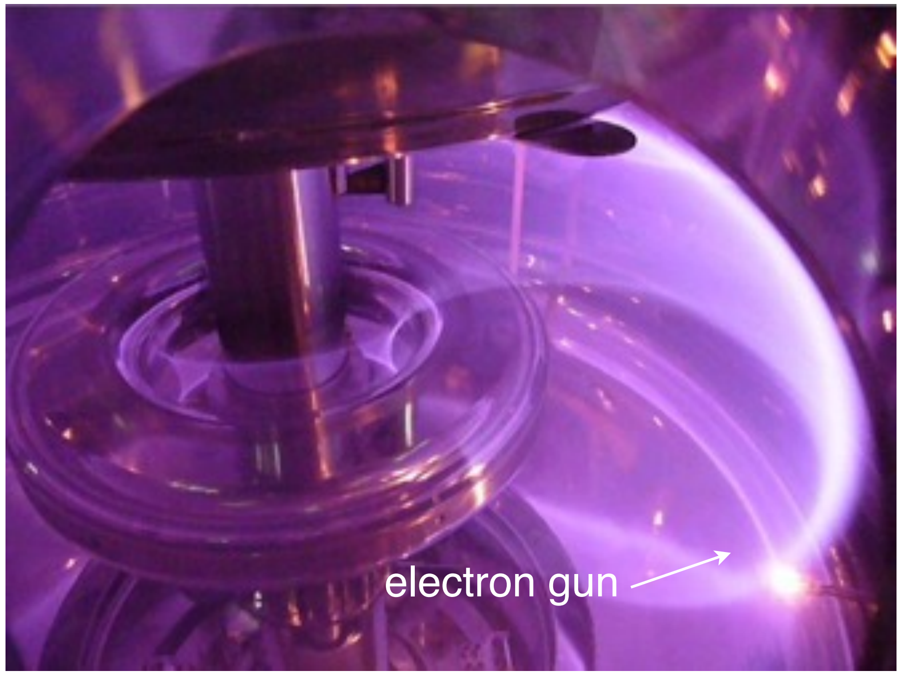

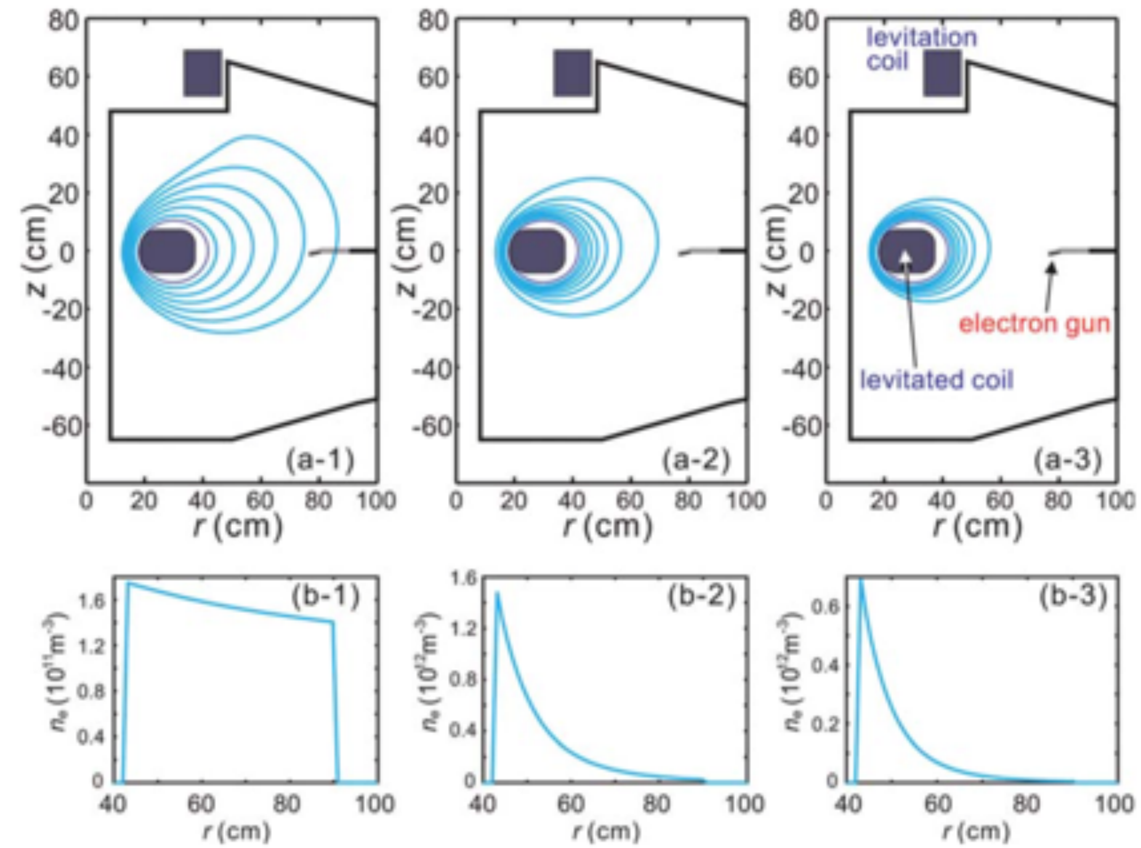

Time evolution of electron density profile

- ✓ Non-neutral plasma confinement experiments in RT-1
- ✓ Several hundred seconds confinement of pure electron plasma [1]
- ✓ Density profile was estimated from image charge measurement by wall-probes [2]
  - ➡ Inward diffusion is observed for pure electron plasma

[1] H. Saitoh et al., Plasma Fusion Res. 2, 045 (2007).
[2] H. Saitoh, et al., Plasma and Fusion Res. 4, 054 1-7 (2009); Phys. of Plasmas 18, 056102 1-9 (2011).

Inward diffusion heating in non-neutral plasma

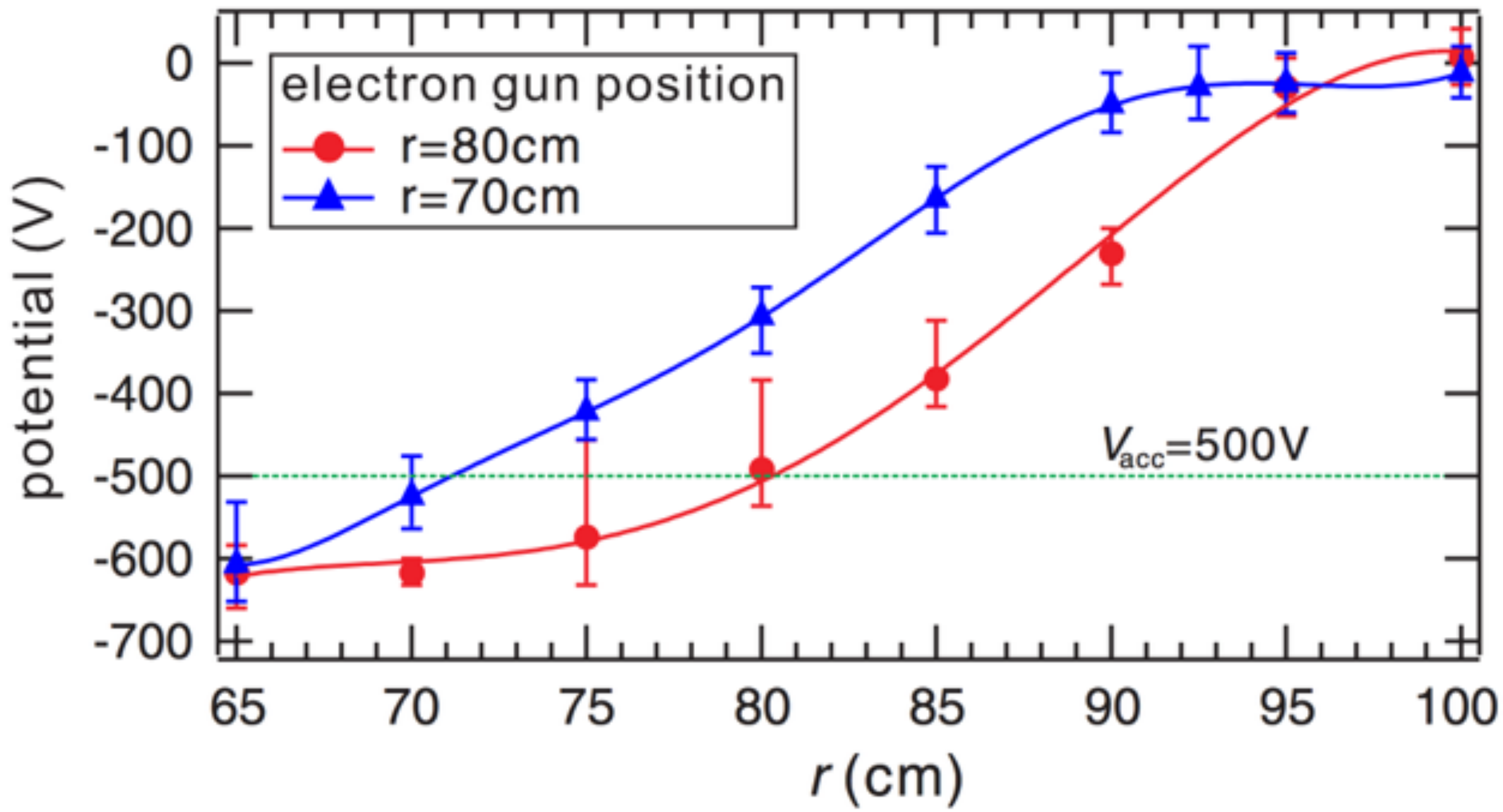

Radial profile of the space potential

✓ Measurement of the space potential by an emissive Langmuir probe

➡ Inner space potential is higher than the electron gun's acceleration voltage

➡ The electrons are accelerate together with the inward transport [1]

[1] Z. Yoshida, et al., Phys. Rev. Lett. **104**, 235004 (2010).

Summary of particle acceleration

- ✓ Inward diffusion not only creates a plasma clump but also increases particles' energy
  - Conservation of 1st AI (μ) results in increase of $T_\perp$ (betatron acceleration)
  - Conservation of 2nd AI ($J_{||}$) results in increase of $T_{||}$ (Fermi acceleration)
- ✓ These are the primary generators of planetary radiation belts
- ✓ Temperature anisotropy is key to investigating the adiabatic acceleration
- ✓ Ions and hot hydrogen atoms (created via charge exchange with protons) in RT-1 shows the temperature anisotropy.
- ✓ $J_{||}$ is not conserved in RT-1 → the anisotropy is caused by the selective heating of $T_\perp$ by the betatron acceleration
- ✓ Numerical simulation of the diffusion equation also shows temperature anisotropy
- ✓ Pure-electron plasma is also accelerated with inward diffusion

Summary of the talk

- ✓ Magnetospheres are ubiquitous in the universe showing intriguing self-organization phenomena
- ✓ Recent progress in the theoretical study has deepened our understanding of how plasma is self-organized in magnetosphere
- ✓ They have experimentally verified in the laboratory
- ✓ In addition to long-standing theory, simulations, and satellite observations, a laboratory experiment is becoming a new “platform” of astrophysics research

Selected references related to this talk

Theoretical studies

- Z. Yoshida and S.M. Mahajan, Prog. Theor. Exp. Phys. 2014, **073J01** (2014);
- N. Sato and Z. Yoshida, J. Phys. A: Math. Theor. **48** (2015) 205501.

Experimental studies

- H. Saitoh, et al., Nucler Fusion **51**, 063034 (2011).
- Y. Kawazura, et al., Phys. Plasmas **22**, 112503 (2015).